FRACTURE OF LAMINATED PANELS IN TENSION

Submitted by:

Satrio Wicaksono (G0700425G)

Supervisor:

Assoc. Prof. Chai Gin Boay

A thesis submitted to NTU
in partial fulfillment of the requirements
for the degree of Master of Engineering.

School of Mechanical and Aerospace Engineering
Nanyang Technological University
Singapore

May 2009

ABSTRACT

Composites have become very important nowadays. It has been used in many structures especially when light weight is of utmost important like in the racing car and airplane. The increased usage of composites is followed by the research on them. A lot of researchers have studied about composites and many of them studied about fracture in composites. Despite that fact, there are still numerous areas in fracture of composite that still need to be explored.

This current research focuses on fracture in composites with initial delamination. The composites that will be used here is continuous carbon fiber reinforced polymer and the only position of the delamination that will be focused on is parallel to the load. Furthermore, the load will not directly cause the initial delamination to propagate. The crack propagation will be caused by the coupling due to the existence of unsymmetric sublaminate as a direct result of delamination.

Finite element models have been developed to investigate the crack propagation and the main mode of failure. Two fracture parameters will be used here, energy release rate and stress intensity factor. The finite element results showed that some delaminations in the laminates have probability to propagate and the other have no possibility to propagate. It depends on the stacking sequence of laminates, delamination position and delamination length.

Finite element analyses and experiment validations have also been done to investigate the failure load of delaminated panels and panels without delamination. The purpose is to study the effect of initial delamination to the whole structure. One interesting result came from $(\theta//-\theta/-\theta/\theta)_t$ laminates. These laminates load dropped significantly compared to laminates without delamination. It is mainly caused by twisting in $(\theta//-\theta/-\theta/\theta)_t$ laminates. Furthermore, twisting in $(\theta//-\theta/-\theta/\theta)_t$ laminates can cause the structure to sustain stress concentration and can be followed by degradation in the structure (1^{st} failure) and will also reduce the total load that can be sustained (final failure).

Finally, it can be concluded that the effect of delamination in composite structures can be critical depends on the structures stacking sequence, the position of delamination (in which layer delamination appear) and the delamination length.

ACKNOWLEDGEMENTS

The author would like to express his gratitude to his supervisor, Associate Professor Chai Gin Boay for his kindness, patience and guidance through out this research work.

The author would also like to appreciate Mr. Athanasius Louis Commillus, for his constructive discussion and help.

A word of thanks should also go to AUN-SEED NET and JICA as organizations that provide the funds for the author.

Last but not least, the author wants to thank his parents for their never ending support.

TABLE OF CONTENTS

TABLE OF FIGURES

Chapter 1

Chapter 2

Chapter 3

Chapter 4

Chapter 5

Chapter 6

Appendix II

NOMENCLATURES

σ_{11}	Normal stress in the fiber direction
σ_{22}	Normal stress in transverse to fiber direction
σ_{33}	Out of plane normal stress
τ_{12}	In plane shear stress
ε_{11}	Normal strain in the fiber direction
ε_{22}	Normal strain in the transverse direction
γ_{12}	In plane shear strain
$[Q]$	Ply stiffness matrix
E_{11}	Modulus elasticity of the ply in the direction of the fibers
E_{22}	Modulus elasticity of the ply in the transverse direction
ν_{12}, ν_{21}	Poisson ratio in the fiber and transverse direction respectively
$\{N\}$	Given loads
$\{M\}$	Given moments
$\{\varepsilon^0\}$	Center line strains
$\{\kappa\}$	Curvatures
$\begin{bmatrix} A & B \\ B & D \end{bmatrix}$	Stiffness matrix of composite laminates
σ_{11t}, σ_{22t}	Normal tensile stress in the fiber and transverse direction
σ_{11c}, σ_{22c}	Normal compressive stress in the fiber and transverse direction
$\sigma_{11tu}, \sigma_{22tu}$	Ultimate normal tensile stress in the fiber and transverse direction
τ_{12u}	Ultimate in plane shear stress
σ_{11cu}, σ_{22cu}	Ultimate normal compressive stress in the fiber and transverse direction
$\varepsilon_{11t}, \varepsilon_{22t}$	Normal tensile strain in the fiber and transverse direction
$\varepsilon_{11c}, \varepsilon_{22c}$	Normal compressive strain in the fiber and transverse direction
$\varepsilon_{11tu}, \varepsilon_{22tu}$	Ultimate normal tensile strain in the fiber and transverse direction
γ_{12u}	Ultimate in plane shear strain

ε_{11cu} , ε_{22cu}	Ultimate normal compressive strain in the fiber and transverse direction
τ_{23} , τ_{13}	Out of plane shear stress
τ_{23u} , τ_{13u}	Ultimate out of plane shear stress
a	Half crack length
a_c	Critical half crack length
σ	Far away stress
σ_c	Critical stress
E	Isotropic modulus elasticity
γ	Surface energy per unit area
G_I , G_{II} , G_{III}	Mode I, mode II, mode III energy release rates, respectively
G_{IC} , G_{IIC} , G_{IIIC}	Mode I, mode II, mode III critical energy release rates, respectively
C	Compliance
B	Width of the DCB specimen
K_I , K_{II} , K_{III}	Mode I, mode II, mode III stress intensity factor, respectively

Chapter One

INTRODUCTION

1.1 Background

There are four commonly known engineering materials in this world. They are metals, ceramics, polymers (plastics), and composites. The first three materials are already well known and have been very well researched into. The last material is still at its infancy stage. Composites are the cluster of two or more materials. One material has a function as reinforcement and the other as matrix. Actually composites have already existed in this world long time a go. Figure 1.1 clearly shows from 10,000 BC composites were already been used in the shape of straw brick and paper.

Based on the reinforcement type, composites can be divided into two: fiber reinforced composites and particle reinforced composites. Figure 1.2 shows the classification of composite materials. Furthermore, the use of fiber reinforced composites nowadays is more common than particle reinforced composites. For clarity, several types of fiber reinforced composites can be seen in Figure 1.3.

The use of fiber reinforced composites has been increasing nowadays. Furthermore, in the last two decades several new materials are starting to be used as reinforcement in fiber reinforced composites like glass fiber, carbon fiber and kevlar fiber. This rapid growth is mainly because the advantages of fiber reinforced composites over the three other materials. One of the main advantage is fiber reinforced composites can give higher strength in certain direction and lower mass compared to even high strength steel. As the result, structures with high specific strength can be made by using fiber reinforced composites.

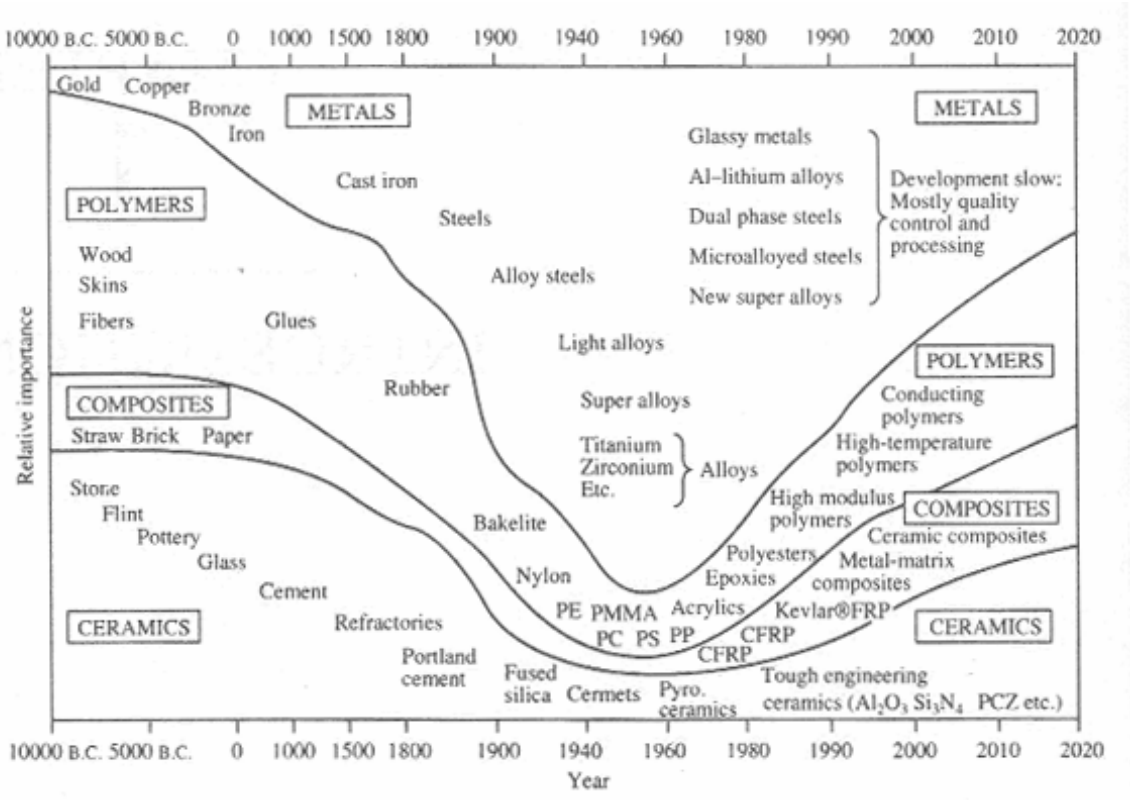

Figure 1. 1: The relative importance of metals, polymers, composites, and ceramics as a function of time [1].

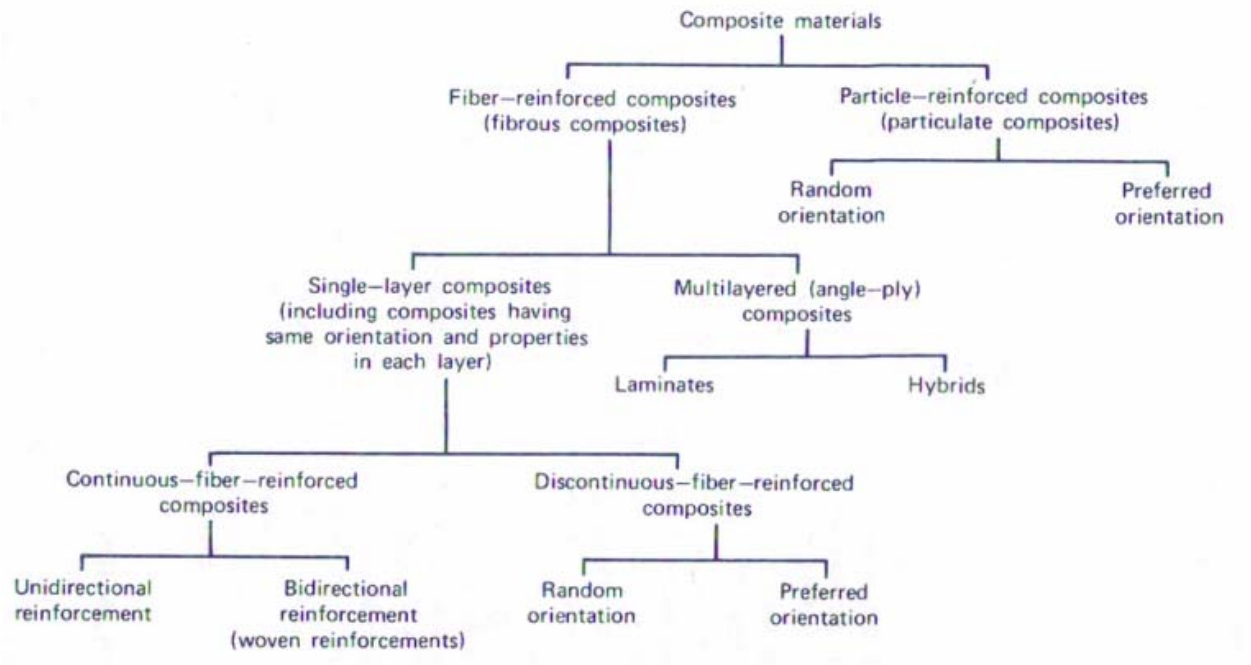

Figure 1. 2: Classification of composite materials [2].

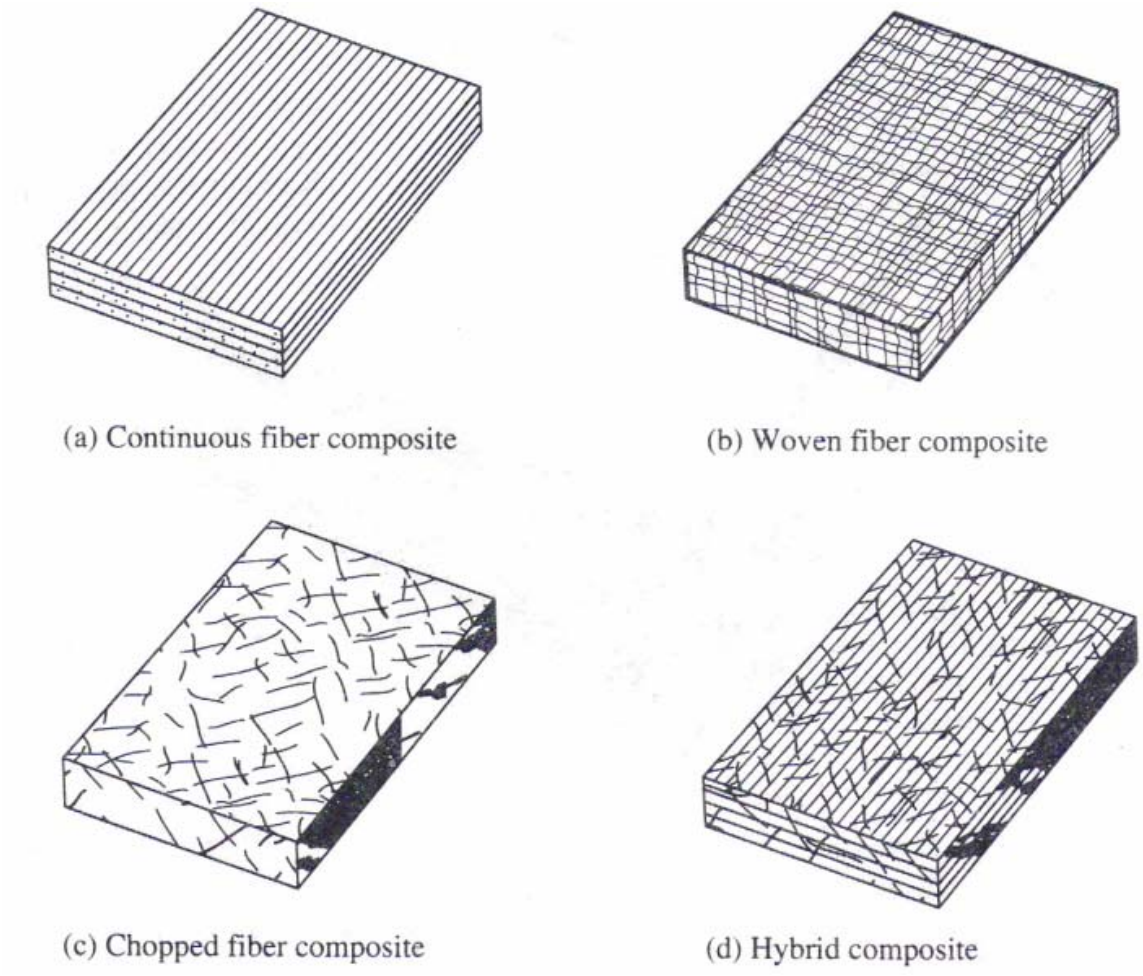

Figure 1. 3: Types of fiber reinforced composites [3].

Fiber reinforced composites have a lot of advantages compared to the other three materials, but knowledge of fracture mechanics in fiber reinforced composites has not been built well as the other three materials. A lot of people have studied fracture in metal, plastic and ceramic in the last 50 years. As the result unpredictable failure for these three materials can be avoided. These things have not been happen in fiber reinforced composites especially fiber reinforced plastics, because the use of fiber reinforced plastics are still new. Therefore, not a lot of studies have been done in fracture of fiber reinforced plastics. Consequently, there are still a lot of areas in fracture of fiber reinforced plastics to have research on.

In the last two decades, many researchers have made contribution in the development of fracture mechanics and failure analysis in composites material. Some of them have concerned about failure mode [4-6], buckling [7-9], impact failure [10-12] and a lot of them have studied on compressive failure. For instance, post impact

compressive strength [13-15], post buckling compressive strength [16, 17] and compressive failure in composites with initial hole [18-21]. Additionally, several researchers have shown their concern about delamination problem in fiber reinforced composites. Those researchers mainly concerned about free edge delamination [22-24] and fiber reinforced composites with initial delamination under compressive load [25-28]. In contrast only few of them focused on failure in fiber reinforced composites with initial delamination under tensile load [29]. It is logical, because the effect of compressive load in fiber reinforced composites with initial delamination is more catastrophic than tensile load, therefore the impact of findings in failure under compressive load will be higher. However, tensile load in fiber reinforced composites structures with initial delamination still can cause degradation like strength and stiffness reduction. The existence of initial delamination will cause additional coupling in the fiber reinforced composites, especially in the initial delamination area. This coupling can appear because initial delamination divides fiber reinforced composites that initially bond together into upper part and lower part. These upper and lower parts act differently compared to when those two have not been separated. Additional coupling that appear depends on both composite lamination angle and delamination position. When the load is given to the structure, the additional coupling can cause the structure to bend or twist depend on the additional coupling it self. Furthermore, it can cause the initial delamination to propagate and stress concentration to happen. As a result, it can reduce the structures performance. Because of that, study in this special research field is very important and can give quite good impact.

In the current research, fracture behavior of fiber reinforced plastics especially continuous fiber reinforced plastics with initial delamination under tensile load will be studied. The relation between size, location and kind of delamination with fracture propagation and failure load will be formulated. This research is very important because a lot of structures that use fiber reinforced plastics are very prone to initial delamination. Moreover, after initial delamination these structures will react differently compared to structures without delamination, therefore the fracture behavior will be different. Examples of these kinds of structures are aircraft body and pressure vessel. Initial delamination can appear in both structures after impact load such as bird attacks for aircraft structure and dropping tools for pressure vessel.

1.2 Objectives

Under tensile load, initial delamination in fiber reinforced plastics can induce stress concentration in the vicinity of initial delamination itself. Furthermore it can also become starting point of crack propagation. The first objective of this thesis is to find out whether the crack will propagate or not with variation in initial delamination size and position. The other objective is to determine the relationship between twisting and failure load in $(\theta°/\!/-\theta°/-\theta°/\theta°)_t$ laminates with respect to initial delamination size.

1.3 Scope

This thesis covers the following:

1. The effect of thickness variation in composite laminates fracture parameters.
   Fracture parameters for several composites thicknesses and angles were studied. The initial delamination size was remain the same, and all of composites have been used here were symmetric.
2. The effect of delamination position in composites laminates fracture parameters.
   Delamination positions were varied for several composite laminates with certain stacking sequence and thickness. Furthermore fracture parameters for those composite laminates were studied.
3. The effect of delamination size in composites laminates fracture parameters.
   The delamination size was varied and the effect to the fracture parameters of the composite laminates was studied.
4. Twisting in $(\theta°/\!/-\theta°/-\theta°/\theta°)_t$ laminates and relationship with its failure load.
   The delamination size was varied and the relationship between twisting and failure load in $(\theta°/\!/-\theta°/-\theta°/\theta°)_t$ laminates was found.

1.4 Outline

This report is organized into the following structure:

- **Chapter 1 – Introduction**
  Chapter one explains the background, objectives of the research and the scope of the work. Furthermore, the outline of this report will be presented.
- **Chapter 2 – Literature Review**

Literature review covers all information relevance to the current study, including the theories and findings from previous work. The basic theories and equations used in this study are also presented in this chapter.

- **Chapter 3 – Finite Element Modeling**

  This chapter consists of the development of finite element model to measure the energy release rate and stress intensity factor in the vicinity of the crack and finite element model to measure the twisting angle and the failure load of composite laminates.

- **Chapter 4 – Experimental Set Up**

  The preparation of the specimen and the set up for the experiment are presented in this chapter.

- **Chapter 5 – Delamination Propagation**

  This chapter mainly talks about whether the delamination will propagate or not for certain type of laminates.

- **Chapter 6 – Twisting Effect in $(\theta°//-\theta°/-\theta°/\theta°)_t$ Laminates**

  The results from finite element simulation and experiment related to twisting effect in $(\theta°//-\theta°/-\theta°/\theta°)_t$ laminates are presented in this chapter along with the discussion about those results.

- **Chapter 7 – Conclusion and Future Works**

  Conclusions can be deduced from the results that were obtained and presented in chapter 5 and 6 are presented here. Additionally, future works that can be done in this area are also presented in this chapter.

Chapter Two

LITERATURE REVIEW AND THEORY

2.1 A Review on Composites

Compared to other engineering materials, the stress strain relationship of composites is quite different because composite is not isotropic. So, it is important to know about the behavior of composite before go through to the next step. There are two things that will be discussed in this review. They are composite laminates stress strain relationship and strength of orthotropic lamina.

2.1.1 Composite laminates stress strain relationship

As stated before, composite laminates can not be modeled as isotropic like the other materials. It is mainly because composite laminates consist of several laminas. Furthermore, those laminas also can not be modeled as isotropic, because they have orthotropic properties, which mean they have three symmetries of properties. Moreover, lamina is very thin, so it can be modeled as 2D orthotropic and its stress strain relationship can be written as following.

$$\begin{Bmatrix} \sigma_{11} \\ \sigma_{22} \\ \tau_{12} \end{Bmatrix} = \begin{bmatrix} Q_{11} & Q_{12} & 0 \\ Q_{12} & Q_{22} & 0 \\ 0 & 0 & 2Q_{66} \end{bmatrix} \begin{Bmatrix} \varepsilon_{11} \\ \varepsilon_{22} \\ \gamma_{12}/2 \end{Bmatrix} \tag{2.1}$$

where

$$Q_{11} = \frac{E_{11}}{1-\nu_{12}\nu_{21}}$$

$$Q_{12} = \frac{\nu_{12}E_{22}}{1-\nu_{12}\nu_{21}} \tag{2.2}$$

$$Q_{22} = \frac{E_{22}}{1-\nu_{12}\nu_{21}}$$

The stiffness matrix of laminates depends on the stiffness matrix of laminas that assemble those laminates. It is important to know how to derive the stiffness matrix of laminates form stiffness matrix of laminas, but it will be very long. The

final equation is presented here and the derivation is presented in the appendix. The relationship between force and moment with strain and curvature are in the form.

$$\begin{Bmatrix} N \\ M \end{Bmatrix} = \begin{bmatrix} A & B \\ B & D \end{bmatrix} \begin{Bmatrix} \varepsilon^0 \\ \kappa \end{Bmatrix} \tag{2.3},$$

where (the definition of N , h_k and h_{k-1} can be seen in Figure 2.1)

$$A_{ij} = \sum_{k=1}^{N} \left(\overline{Q_{ij}}\right)_k (h_k - h_{k-1})$$

$$B_{ij} = \sum_{k=1}^{N} \left(\overline{Q_{ij}}\right)_k \frac{h_k^2 - h_{k-1}^2}{2} \tag{2.4}.$$

$$D_{ij} = \sum_{k=1}^{N} \left(\overline{Q_{ij}}\right)_k \frac{h_k^3 - h_{k-1}^3}{3}$$

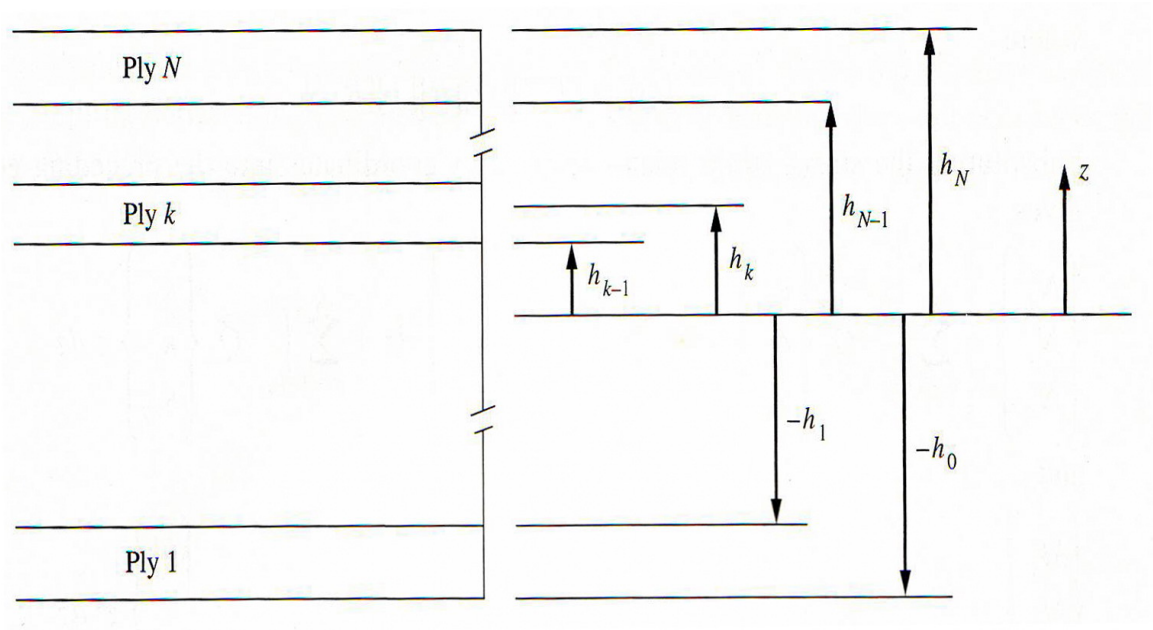

Figure 2. 1: Notation for location of ply interfaces [30].

2.1.2 Strength of orthotropic lamina

Before moving on to another topic, it is needed to discuss about the failure theory of orthotropic lamina. There are a lot of failure theories for orthotropic lamina, but only five are commonly used :

- Maximum stress theory

  Maximum stress theory states that failure in orthotropic lamina will not occur if all of these following conditions are satisfied.

$$\sigma_{11t} < \sigma_{11tu}$$

$$\sigma_{22t} < \sigma_{22tu}$$

$$\tau_{12} < \tau_{12u} \qquad (2.5)$$

$$\sigma_{11c} < \sigma_{11cu}$$

$$\sigma_{22c} < \sigma_{22cu}$$

Thus it means, the failure will be happen if one of these conditions is not fulfilled.

- Maximum strain theory

Maximum strain theory is using almost the same as maximum stress theory, but it based on strain not stress. In order to prevent orthotropic lamina from failure, these following conditions must not be violated.

$$\varepsilon_{11t} < \varepsilon_{11tu}$$

$$\varepsilon_{22t} < \varepsilon_{22tu}$$

$$\gamma_{12} < \gamma_{12u} \qquad (2.6)$$

$$\varepsilon_{11c} < \varepsilon_{11cu}$$

$$\varepsilon_{22c} < \varepsilon_{22cu}$$

- Tsai-Hill theory

This theory was proposed by Tsai [31] using a yield criterion for anisotropic materials that had been proposed by Hill [32], that is why this theory is known as Tsai-Hill theory. Based on this theory, orthotropic lamina will be failed if the following inequality is violated.

$$\left(\frac{\sigma_{11}}{\sigma_{11u}}\right)^2 - \left(\frac{\sigma_{11}}{\sigma_{11u}}\right)\left(\frac{\sigma_{22}}{\sigma_{22u}}\right) + \left(\frac{\sigma_{22}}{\sigma_{22u}}\right)^2 + \left(\frac{\tau_{12}}{\tau_{12u}}\right)^2 < 1 \qquad (2.7)$$

- Tsai-Wu theory

Tsai and Wu [33] have derived a quadratic stress polynomial to predict failure in composites. As the result, now this theory is known as Tsai-Wu theory. Tsai-Wu theory states that orthotropic lamina will not fail if it fulfills the inequality mentioned below.

$$F_1\sigma_{11} + F_{11}{\sigma_{11}}^2 + F_2\sigma_{22} + F_{22}{\sigma_{22}}^2 + 2F_{12}\sigma_{11}\sigma_{22} + F_{66}{\tau_{12}}^2 \qquad (2.8),$$

where

$$F_1 = \frac{1}{\sigma_{11tu}} + \frac{1}{\sigma_{11cu}}$$

$$F_2 = \frac{1}{\sigma_{22tu}} + \frac{1}{\sigma_{22cu}}$$

$$F_{11} = -\frac{1}{\sigma_{11tu}\sigma_{11cu}} \qquad (2.9).$$

$$F_{22} = -\frac{1}{\sigma_{22tu}\sigma_{22cu}}$$

$$F_{66} = \frac{1}{{\sigma_{12u}}^2}$$

- Hashin theory

The last failure theory that will be discussed here is Hashin [34, 35]. This theory can be divided into four damage mechanism: fiber tension, fiber compression, matrix tension and matrix compression. This criteria states that orthotropic lamina will not fail if it fulfill these following inequality.

- Fiber tension ($\sigma_{11} \geq 0$)

$$\left(\frac{\sigma_{11}}{\sigma_{11tu}}\right)^2 + \alpha\left(\frac{\tau_{12}}{\tau_{12u}}\right)^2 \leq 1 \qquad (2.10)$$

- Fiber compression ($\sigma_{11} \leq 0$)

$$\left(\frac{\sigma_{11}}{\sigma_{11cu}}\right)^2 \leq 1 \qquad (2.11)$$

- Matrix tension ($\sigma_{22} \geq 0$)

$$\left(\frac{\sigma_{22}}{\sigma_{22tu}}\right)^2 + \left(\frac{\tau_{12}}{\tau_{12u}}\right)^2 \leq 1 \qquad (2.12)$$

- Matrix compression ($\sigma_2 \leq 0$)

$$\left(\frac{\sigma_{22}}{2\tau_{23u}}\right)^2 + \left[\left(\frac{\sigma_{22}}{2\tau_{23u}}\right)^2 - 1\right]\frac{\sigma_{22}}{\sigma_{22cu}} + \left(\frac{\tau_{12}}{\tau_{12u}}\right)^2 \leq 1 \qquad (2.13)$$

2.2 A Review on Fracture Mechanics in Isotropic Materials

Fracture mechanics is a discipline that mainly concern about whether a crack will grow under certain load condition. The fracture mechanisms are already well established for isotropic materials but not so for composite materials. The

development of fracture mechanics was started very long time ago by Leonardo da Vinci (1452-1519), but the first significant contribution was given by Griffith [36, 37] in 1920s when he found out about energy requirement to move a crack. Unfortunately Griffith work was not taken seriously at that time. The turning point was happen in World War II. At that time industrial production was increasing very fast. One of those products is cargo ship. At first cargo ship had been made by riveting method, but to reduce the production time, the method was changed to welding method. These cargo ships were known as liberty ships. Astonishing fact was happen later. Many of liberty ships broke into two parts when they exposed to the cold temperature of North Atlantic Ocean. As a result, examination about the cause of that failure was made, and it accelerated the development of fracture mechanics. One of the main contributors at that time was George Irwin [38]. In 1948, Irwin formulated energy release rate and stress intensity factor.

Every material would act differently against certain kind and magnitude of load. It depends on the material properties especially resistance to fracture properties. They are three modes of fracture failure (Figure 2.2), opening mode (mode I), sliding mode (mode II) and tearing mode (mode III).

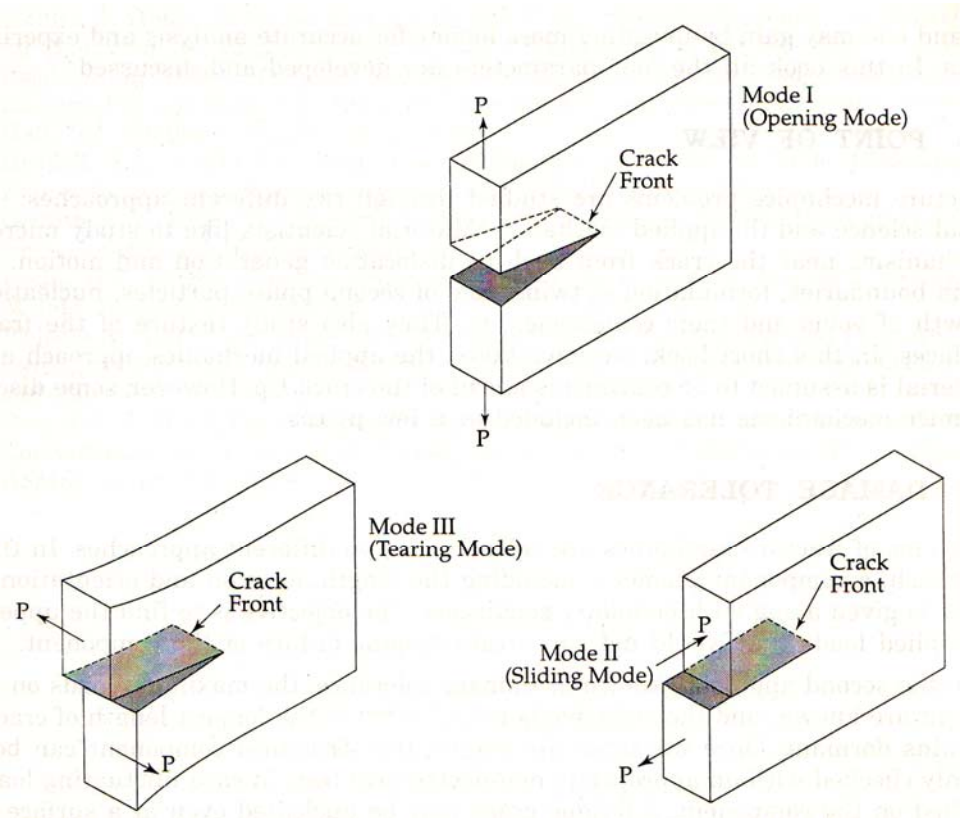

Figure 2. 2: The three modes of fracture [39].

The predominant fracture mode for certain structure depends on the given load. Despite that fact, mode I is the most predominant mode in all of the structures.

A lot of researchers have studied about fracture mechanics, and they used several different approach. As a result several parameters to measure crack potency have been developed. Four of those parameters have been well accepted

- Energy release rate (*G*),
- Stress intensity factor (*K*),
- J integral (*J*) and
- Crack tip opening displacement (CTOD).

Energy release rate and stress intensity factor were made based on linear elastic fracture mechanics theorem, so they only can be used for brittle materials. On the contrary, J integral and crack tip opening displacement is based on elastic plastic fracture mechanics, so those parameters suit well for ductile materials. Those four fracture parameters will be discussed in the following subchapter and Prashant Kumar's [39] book will be used as guidance.

2.2.1 Energy release rate

One of parameter has been developed to measure potency of crack is energy release rate. This parameter was discovered for the first time by Griffith. Griffith realized that crack in a structure can not extend if the magnitude of the energy that is released in the process is below the magnitude of the energy to form two new surfaces. As the crack length is increasing, the total energy released and the surface energy required also increase. The variation of the total energy released (E_R) and the total surface energy required (E_s) to make the crack to propagate can be seen in the Figure 2.3.

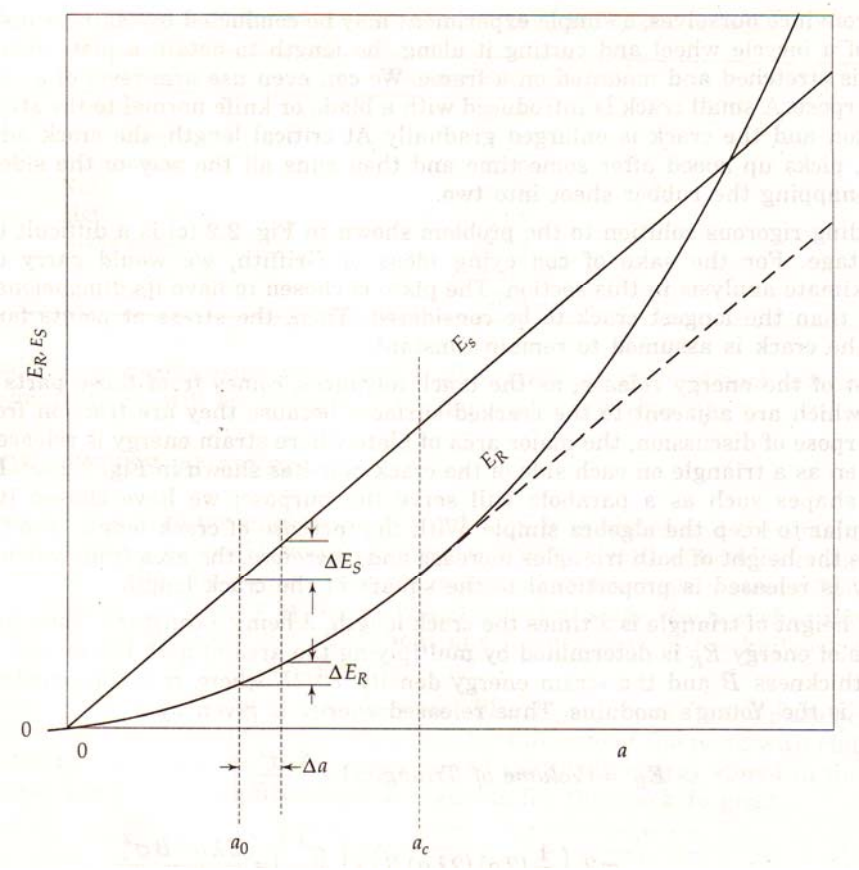

Figure 2. 3: Variation of energy release and required surface energy with crack length [39].

When the crack length is equal to $2a_0$ and the virtual crack extension is equal to Δa, the slope of total surface energy required is smaller than the slope of total surface energy required. It makes the energy released smaller than the energy to make new surfaces. As a result, the crack can not expand unless external energy is added into the system. Assume, external energy is added into the system so the crack can grow until its length reaches $2a_c$. At that time the magnitude of energy release is the same as energy to make new surfaces. As a result, the crack can grow and in this case the system will fail. Thus, the crack will become critical if

$$\frac{dE_R}{da} \geq \frac{dE_S}{da} \qquad (2.14).$$

For certain load magnitude, the crack will become critical if the length of the crack is in the form

$$a_c = \frac{2E\gamma}{\pi\sigma^2} \qquad (2.15).$$

Conversely, for certain crack length, the crack will become critical if the far away stress reach

$$\sigma_c = \left[\frac{2E\gamma}{\pi a}\right]^{1/2} \tag{2.16}$$

for plane stress case and

$$\sigma_c = \left[\frac{2E\gamma}{\pi(1-\nu^2)a}\right]^{1/2} \tag{2.17}$$

for plane strain case.

Next step is to formulate the energy release rate itself. For this problem conservation of energy will be used. Imagine the crack is expand virtually by ΔA and to get this crack expansion external force is applied so external work will increase by ΔW_{ext}. Furthermore, strain energy will also increase by ΔU. Consequently, energy balance for this problem can be stated as

$$G\Delta A = \Delta W_{ext} - \Delta U \tag{2.18}$$

where $G\Delta A$ is the available energy to expand the crack. Moreover, by assuming ΔA is very small, equation (2.18) can be modified to

$$G = -\frac{d}{dA}(\Delta U - W_{ext}) \tag{2.19}.$$

In addition, $\Delta U - W_{ext}$ can also be expressed as potential energy (Π), so the equation can be rewritten as

$$G = -\frac{d\Pi}{dA} \tag{2.20}.$$

It can be seen from equation (2.20) that energy will be available for crack propagation if the potential energy is decreasing.

The most well known way to measure fracture toughness in the first direction for certain materials is double cantilever beam test (DCB test) because it can be done easily to certain materials using normal tensile machine (Figure 2.4).

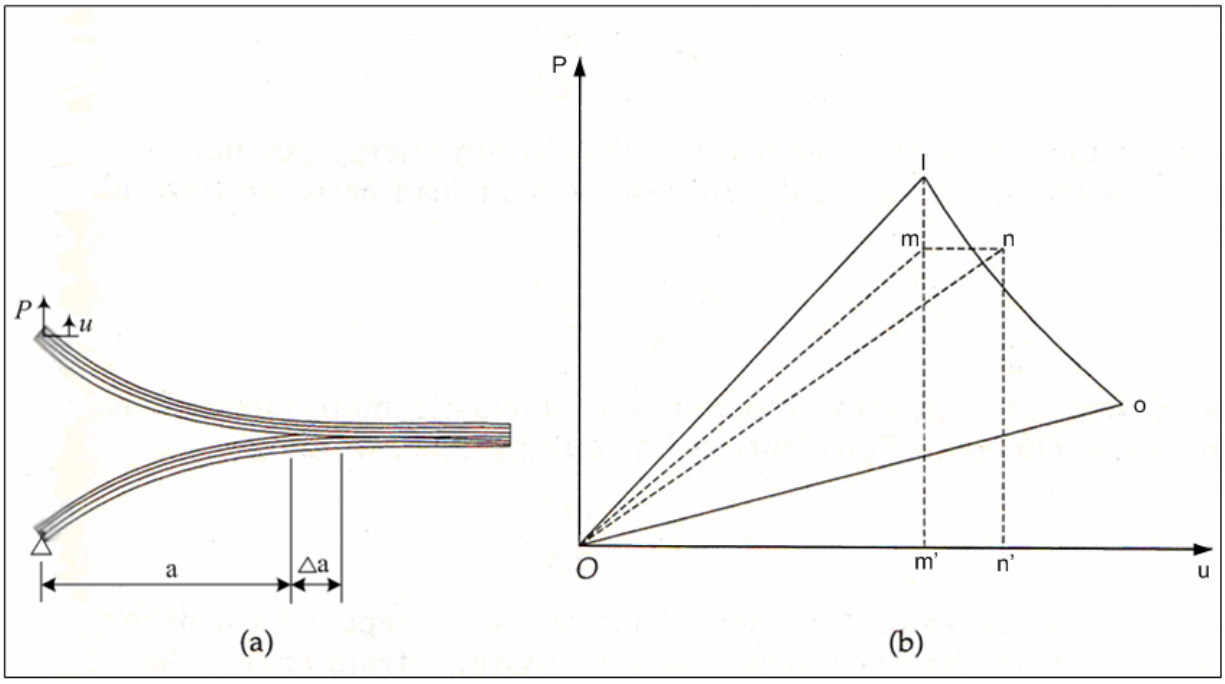

Figure 2. 4: DCB specimen [39].

Therefore, it is very important to understand how to get energy release rate value in DCB test. There are two extreme cases on this problem, constant load and constant displacement. Both cases will be solved separately.

For constant load problem, works is given to the specimen by tensile machine

$$W_{ext} = Pu \tag{2.21}$$

and the specimen will deflect and absorb certain amount of energy

$$U = \frac{1}{2}Pu \tag{2.22},$$

so the decrease in potential energy to propagate the crack is equal to

$$\Pi = U - W_{ext} = \frac{1}{2}Pu - Pu = -\frac{1}{2}Pu \tag{2.23}.$$

Employ equation (2.23) into equation (2.20), we can get

$$G_I = \frac{P}{2}\frac{du}{dA} \tag{2.24}.$$

ΔA can be expressed as $B\Delta a$, so do dA can be expressed as Bda. As a result, equation (2.24) can be written as

$$G_I = \frac{P}{2B}\frac{du}{da} \tag{2.25}.$$

Where u is in the form

$$u = CP \tag{2.26}$$

In the end, equation (2.25) can be rewritten as

$$G_I = \frac{P^2}{2B}\frac{dC}{da} \tag{2.27}$$

Next one is the constant displacement problem. For constant displacement problem, no external works is being done to the system, so the only term in the potential energy is the strain energy term. As a result, the potential energy can be written as

$$\Pi = U = \frac{1}{2}Pu \tag{2.28}$$

Substitute this value to equation (2.20),

$$G_I = -\frac{u}{2B}\frac{dP}{da} \tag{2.29}$$

Substitute the value of *P* from equation (2.26), equation (2.29) can be rewritten as

$$G_I = \frac{u^2}{2BC^2}\frac{dC}{da} \tag{2.30}$$

Furthermore, because *u* is constant, it can be eliminated and as a result

$$G_I = \frac{P^2}{2B}\frac{dC}{da} \tag{2.31}$$

The result of constant load problem and constant displacement problem are just the same.

After both constant load problem and constant displacement problem have been solved, the next step is to relate the parameters that can be got from experimental result with equations have been derived. The load (*P*), the width of the specimen (*B*) and the crack length (*a*) can be got from the DCB specimen and experiment result data, only the compliance (*C*) that not directly related to the DCB specimen and experimental result data. Consequently, the relation between the compliance (*C*) and parameters form experimental result must be found.

It is well known that the deflection of a cantilever beam at the free end because of load *P* at the same spot is in the form

$$\delta = \frac{1}{3}\frac{Pl^3}{EI} \tag{2.32}$$

where *l* and *I* are the length of the beam and moment inertia area of the beam's cross section, respectively. Using the same way, the displacement (*u*) can be written as

$$u = \frac{2}{3}\frac{Pa^3}{EI} \quad (2.33),$$

because this problem can be simplified as two cantilever beam that have the same length (a) which move away from each other. Using equation (2.26) and relate it with equation (2.33), we obtain

$$C = \frac{u}{P} = \frac{2a^3}{3EI} \quad (2.34),$$

where moment inertia area (I) for rectangular cross section of cantilever is in the form

$$I = \frac{Bh^3}{12} \quad (2.35).$$

Equation (2.34) can be rewritten as

$$C = 8\frac{a^3}{EBh^3} \quad (2.36).$$

In the end, differentiate and substitute equation (2.36) into equation (2.31), we can get

$$G_I = 12\frac{a^2P^2}{EB^2h^3} \quad (2.37).$$

The last thing needs to be understood in relation to energy release rate is the crack resistance. The crack resistance (R) is the energy required by the crack to propagate per unit increase area. Crack resistance is depends much on the plastic zone size, larger the plastic zone size makes crack harder to propagate which means higher crack resistance. Crack resistance in relation to crack length for ductile materials can be seen in the R-curve in Figure 2.5.

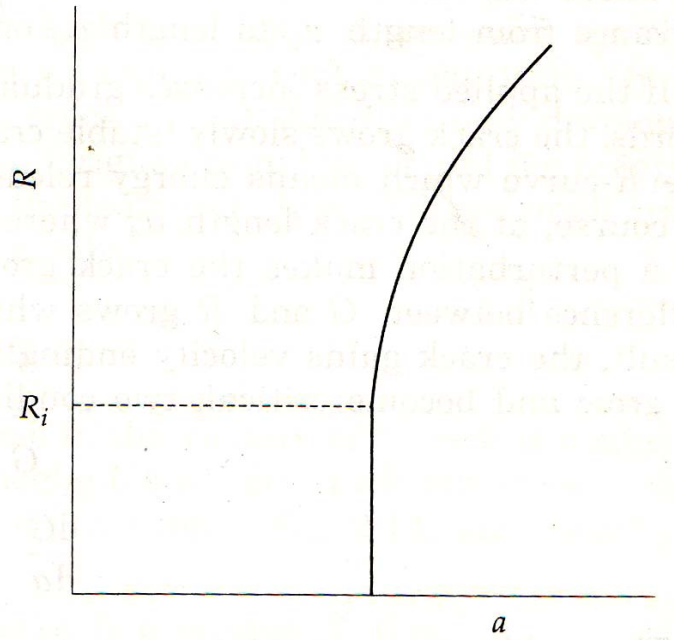

Figure 2. 5: R-curve of ductile materials [39].

The crack will propagate if strain energy release rate (G) is larger than crack resistance (R). One simple example is center cracked plate problem. For this problem energy release rate depend linearly on the crack length and energy release rate for several far away stress in comparison with crack resistance can be seen in Figure 2.6.

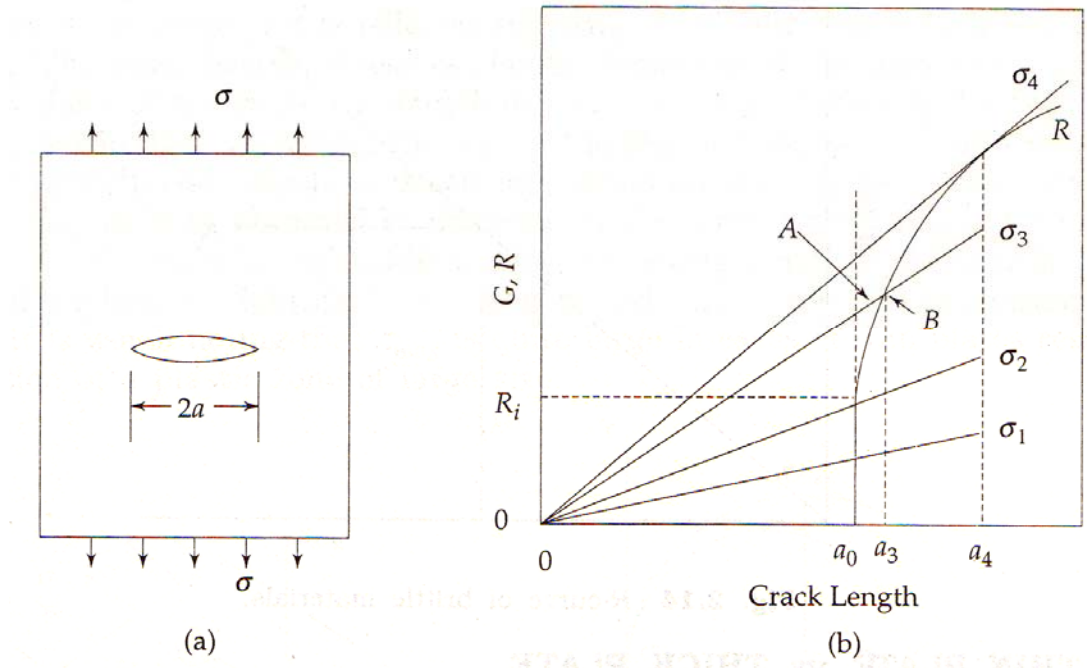

Figure 2. 6: (a) Center cracked plate, and (b) crack growth [39].

When far away stress reach σ_1 and σ_2, at crack length equal to a_0 the energy release rate is below the minimum value to make the crack grow (R_i), so the crack will not propagate. Furthermore, if far away stress is increased until it reach σ_3, the energy release rate is higher than R_i so the crack can propagate till the crack length reach a_3 and the crack will be stable after that. In the end, if far away stress reach σ_4, the crack will propagate till the crack length reach a_4 when strain energy release rate are equal to crack resistance. If the far away stress is slightly increased from σ_4, the whole system will fail catastrophically. As a result, we can conclude that crack will become critical if the following conditions are satisfied.

$$G \geq R$$

$$\frac{dG}{da} \geq \frac{dR}{da} \tag{2.38}$$

Brittle materials have different *R*-curve from ductile materials (Figure 2.7), because the size of plastic zone in the vicinity of the crack is negligible.

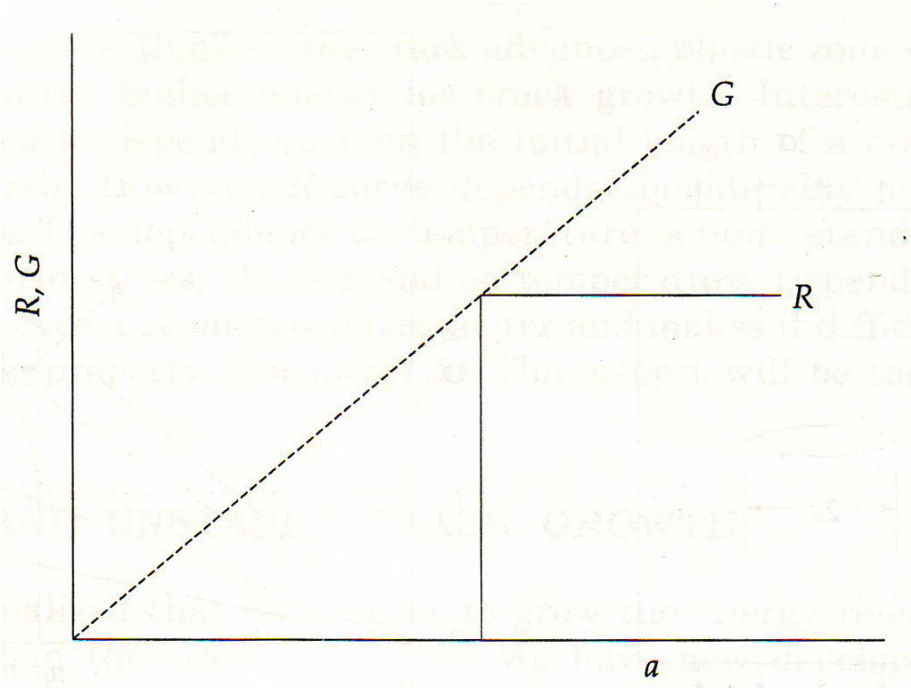

Figure 2. 7: R-curve of brittle materials [39].

Thus, for brittle material, crack will become critical when strain energy release rate overcome crack resistance.

2.2.2 Stress intensity factor

Analysis of stress or displacement in the vicinity of the crack sometimes is very useful. One of the results is stress intensity factor, parameter to measure crack propagation. Compared to strain energy release rate, stress intensity factor is an easier parameter for an analyst to use. In this part, only stress intensity factor in the first direction that will be discussed. Imagine infinite plate with a crack of length 2a (Figure 2.8) and it is needed to find the relationship between stress intensity factor and the stress, displacement field in the vicinity of the crack.

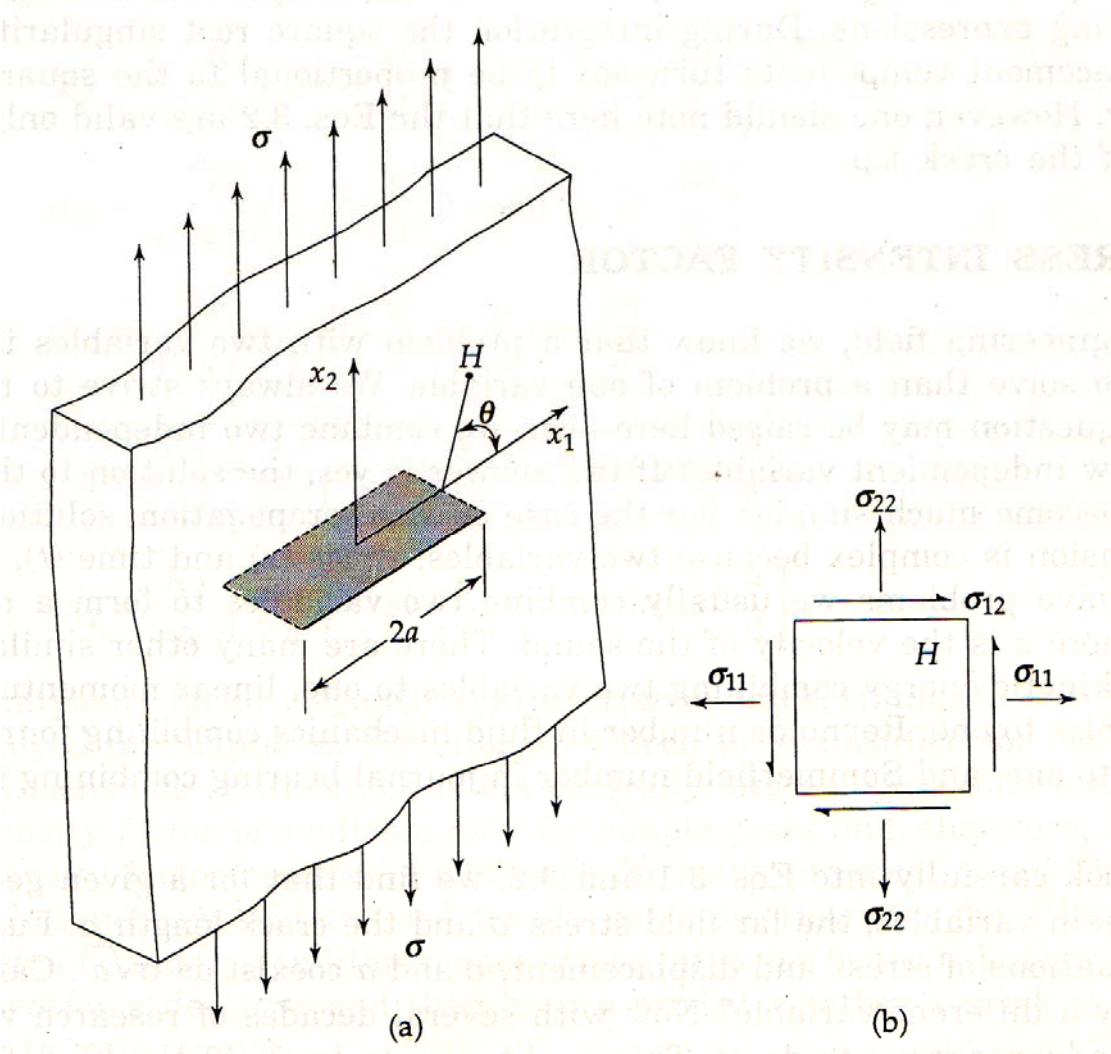

Figure 2. 8: (a) Infinite plate with a crack of length 2a with far away field stress , and (b) definition of stress components at point H [39].

First, the stress and displacement field in the vicinity of the crack in relation with crack length (a), far away stress (σ) and position (r, θ) are determined. It is well

known that the stress field in this problem for a thin plate (plane stress) can be expressed as the following.

$$\sigma_{11} = \frac{\sigma(\pi a)^{1/2}}{(2\pi r)^{1/2}} \cos\frac{\theta}{2}\left[1 - \sin\frac{\theta}{2}\sin\frac{3\theta}{2}\right]$$

$$\sigma_{22} = \frac{\sigma(\pi a)^{1/2}}{(2\pi r)^{1/2}} \cos\frac{\theta}{2}\left[1 + \sin\frac{\theta}{2}\sin\frac{3\theta}{2}\right] \qquad (2.39)$$

$$\sigma_{12} = \frac{\sigma(\pi a)^{1/2}}{(2\pi r)^{1/2}} \sin\frac{\theta}{2}\cos\frac{\theta}{2}\cos\frac{3\theta}{2}$$

Furthermore, the other stress components are negligible. For thick plate (plane strain), the value for σ_{11}, σ_{22} and σ_{12} are the same as thin plate problem, in addition the value of σ_{33} is of the form

$$\sigma_{33} = \nu(\sigma_{11} + \sigma_{22}) \qquad (2.40),$$

and the value of σ_{13} and σ_{23} are negligible. Moreover, the displacement field for plane strain problem can be written as

$$u_1 = \frac{\sigma(\pi a)^{1/2}}{\mu}\left(\frac{r}{2\pi}\right)^{1/2} \cos\frac{\theta}{2}\left(1 - 2\nu + \sin^2\frac{\theta}{2}\right)$$

$$u_2 = \frac{\sigma(\pi a)^{1/2}}{\mu}\left(\frac{r}{2\pi}\right)^{1/2} \sin\frac{\theta}{2}\left(2 - 2\nu + \cos^2\frac{\theta}{2}\right) \qquad (2.41).$$

$$u_3 = 0$$

It can be seen that every non zero stress and displacement field in the vicinity of the crack has $\sigma(\pi a)^{1/2}$ term. Thanks to Irwin, who defined this term as stress intensity factor :

$$K_I = \sigma(\pi a)^{1/2} \qquad (2.42).$$

As the result, every stress field in the vicinity of the crack can be rewritten in relation to stress intensity factor as

$$\sigma_{11} = \frac{K_I}{(2\pi r)^{1/2}} \cos\frac{\theta}{2}\left[1 - \sin\frac{\theta}{2}\sin\frac{3\theta}{2}\right]$$

$$\sigma_{22} = \frac{K_I}{(2\pi r)^{1/2}} \cos\frac{\theta}{2}\left[1 + \sin\frac{\theta}{2}\sin\frac{3\theta}{2}\right] \qquad (2.43)$$

$$\sigma_{12} = \frac{K_I}{(2\pi r)^{1/2}} \sin\frac{\theta}{2}\cos\frac{\theta}{2}\cos\frac{3\theta}{2}$$

and displacement field also can be rewritten as

$$u_1 = \frac{K_I}{\mu}\left(\frac{r}{2\pi}\right)^{1/2} \cos\frac{\theta}{2}\left(1 - 2\nu + \sin^2\frac{\theta}{2}\right)$$

$$u_2 = \frac{K_I}{\mu}\left(\frac{r}{2\pi}\right)^{1/2} \sin\frac{\theta}{2}\left(2 - 2\nu + \cos^2\frac{\theta}{2}\right) \qquad (2.44).$$

2.2.3 J integral

J Integral is another parameter beside stress intensity factor (K) and energy release rate (G) but in can be used not only for linear and non linear elastic materials. Furthermore, need to be known that energy release rate is a special case of J Integral for linear elastic materials. To determine the value of J Integral, first the integral path Γ must be chosen around the crack tip which starts from any point of a crack face and ends on any point on the other crack face (Figure 2.9).

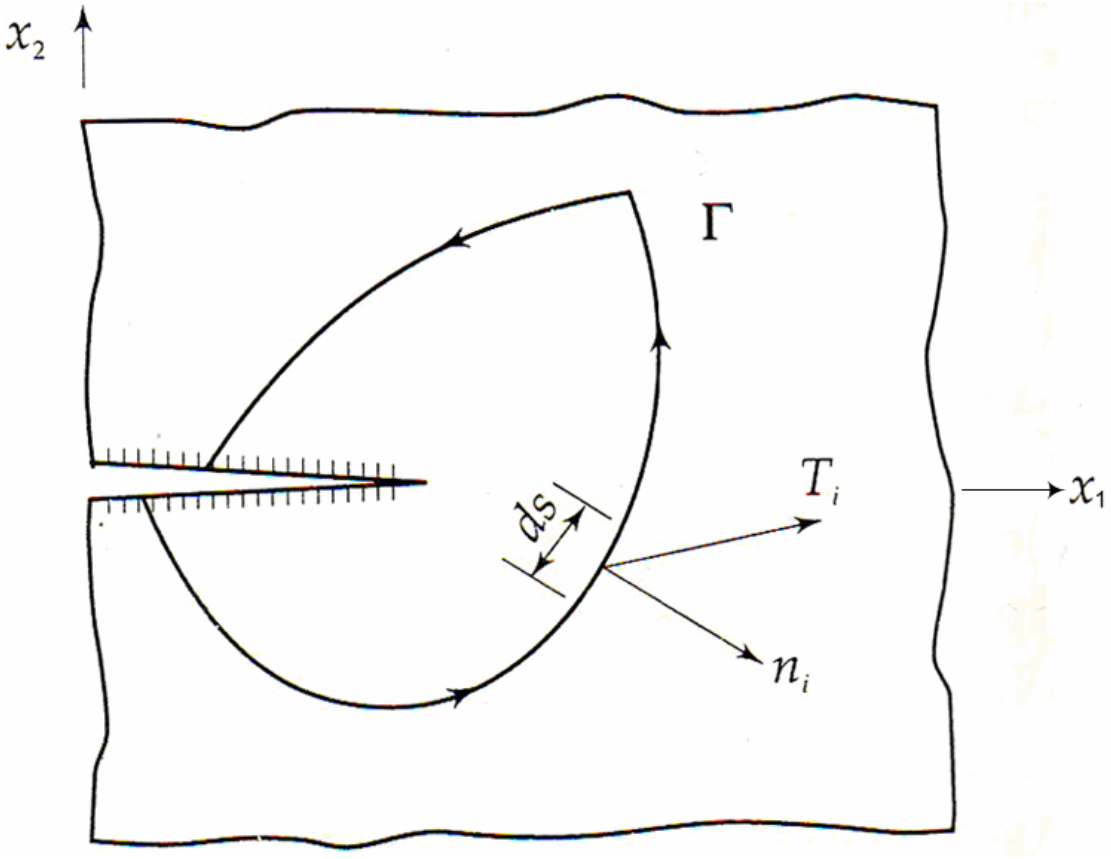

Figure 2. 9: Path Γ around the crack tip with outward normal and traction [39].

To be noted, the integral path Γ can be chosen arbitrarily as long as the path is continuous because J Integral is path independent. J Integral was defined by Rice [40] as

$$J = \int_{\Gamma} \left(W dx_2 - T_i \frac{\partial u_i}{\partial x_1} ds \right) \quad (2.45),$$

where

$$W = \int \sigma_{ij} d\varepsilon_{ij} \quad (2.46),$$

or in the full form, it can be written as

$$W = \int_0^{\varepsilon_{11}} \sigma_{11} d\varepsilon_{11} + 2 \int_0^{\varepsilon_{12}} \sigma_{12} d\varepsilon_{12} + \int_0^{\varepsilon_{22}} \sigma_{22} d\varepsilon_{22} \quad (2.47).$$

Expanded form of the second term in equation (2.45) can be expressed as

$$\int_{\Gamma} T_i \frac{\partial u_i}{\partial x_1} ds = \int_{\Gamma} \left[T_1 \frac{\partial u_1}{\partial x_1} + T_2 \frac{\partial u_2}{\partial x_1} \right] ds \quad (2.48),$$

where

$$T_1 = \sigma_{11} n_1 + \sigma_{12} n_2$$

$$T_2 = \sigma_{12} n_1 + \sigma_{22} n_2 \quad (2.49).$$

2.2.4 Crack tip opening displacement

Crack Tip Opening Displacement (CTOD) is the last parameter that can be used to characterize a crack. The same as J Integral, CTOD can be used for both linear elastic fracture mechanics and elastic plastic fracture mechanics. To define CTOD, imagine a crack which has plastic deformation in the vicinity of the crack tip (Figure 2.10), and assume that plastic deformation can not be neglected.

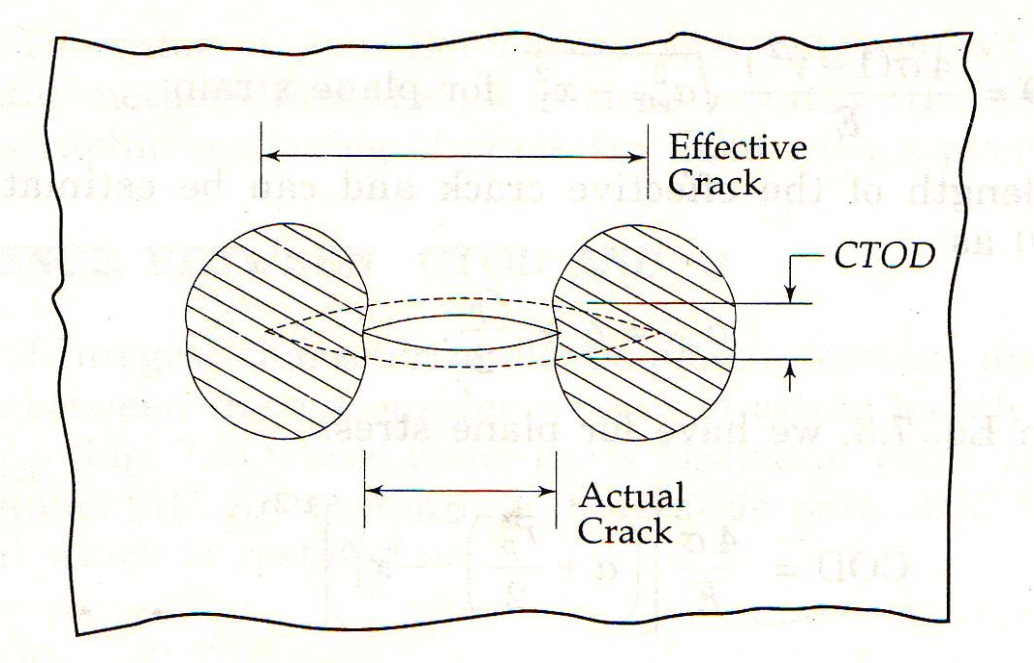

Figure 2. 10: The effective crack and CTOD [35].

In the plastic zone, the stress singularity no longer exists because the materials near the crack will yield, which result in rearrangement of the stress, and it can be accounted by an effective crack that is located in the plastic zone. The effective crack has certain opening at the same location as the crack tip of actual crack. That opening is defined as crack tip opening displacement (CTOD).

Another important thing that needs to be known is relations between CTOD with the other fracture parameters. CTOD in relation with stress intensity factor can be written as

$$CTOD = \frac{K_I^2}{\lambda E \sigma_{ys}} \qquad (2.50),$$

where λ is a constant that depends on plastic zone size and has value near to unity. Furthermore, the relation between CTOD and strain energy release rate can be expressed as

$$CTOD = \frac{G}{\lambda \sigma_{ys}} \qquad (2.51).$$

In the end, CTOD in relation with J Integral is of the form

$$CTOD = \frac{J}{\alpha \sigma_{ys}} \qquad (2.52)$$

where α is a dimensionless factor that depends on work hardening factor (n).

2.2.5 Mixed mode crack propagation criteria

Fracture mechanic parameters have been discussed in previous subchapter and derivations for simple mode I case have been shown. For several decades, researchers have been concentrating in mode I failure because in many cases, mode I is the predominant failure mode. Despite that fact, many structures in the world are undergoing mixed mode loading. The analysis for mixed mode loading is quite different from single mode loading. They are three well known criteria focusing on mixed mode crack propagation: maximum energy release rates, maximum tangential stress and strain energy density. These three criteria will be explained here and example on plate subjected to mode I and II loading (Figure 2.11) will be shown.

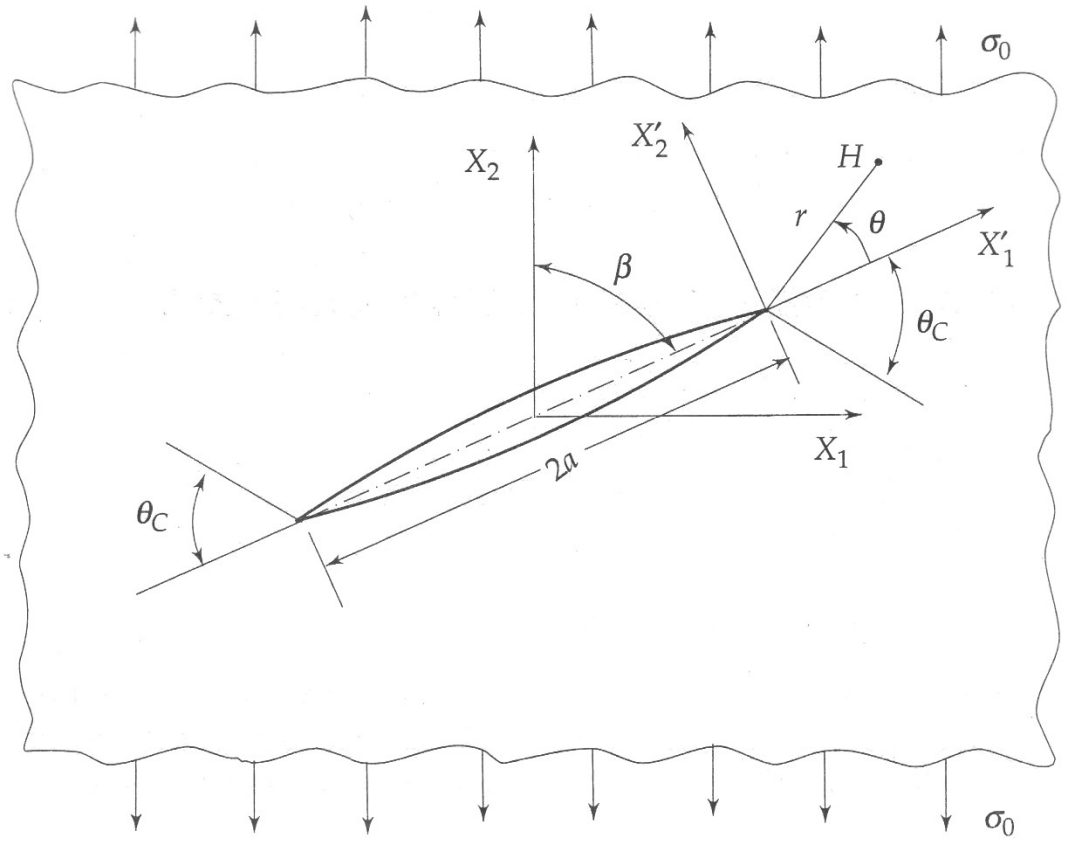

Figure 2. 11: Mixed mode crack subjected to remote loading [39].

- Maximum energy release rates criterion

  Total energy release rate for a crack undergo mode I and II loading can be expressed as

  $$G = G_I + G_{II} \tag{2.53}$$

  where

  $$G_I = \alpha \frac{K_I^2}{E}$$

  $$G_{II} = \alpha \frac{K_{II}^2}{E} \tag{2.54}$$

  and $\alpha = 1$ for plane stress and $\alpha = 1 - \nu^2$ for plane strain. This criterion stated crack propagation direction (θ_C) in the direction where total energy release rate (G_θ) reaches maximum ($G_\theta^{\max}$) and will occur when the maximum total energy release rate ($G_\theta^{\max}$) reaches the critical value (G_C), as can be seen in

Figure 2.12. Using the same way, $G_\theta^{\max}$ can be obtained when G_θ satisfy the following equation

$$\frac{\partial G_\theta}{\partial \theta} = 0 \text{ and } \frac{\partial^2 G_\theta}{\partial \theta^2} < 0 \qquad (2.55)$$

and crack propagate when

$$G_\theta^{\max} \geq G_C \qquad (2.56),$$

where G_C can be obtained from

$$G_C = \alpha \frac{K_{IC}^2}{E} \qquad (2.57),$$

which is pure mode I loading.

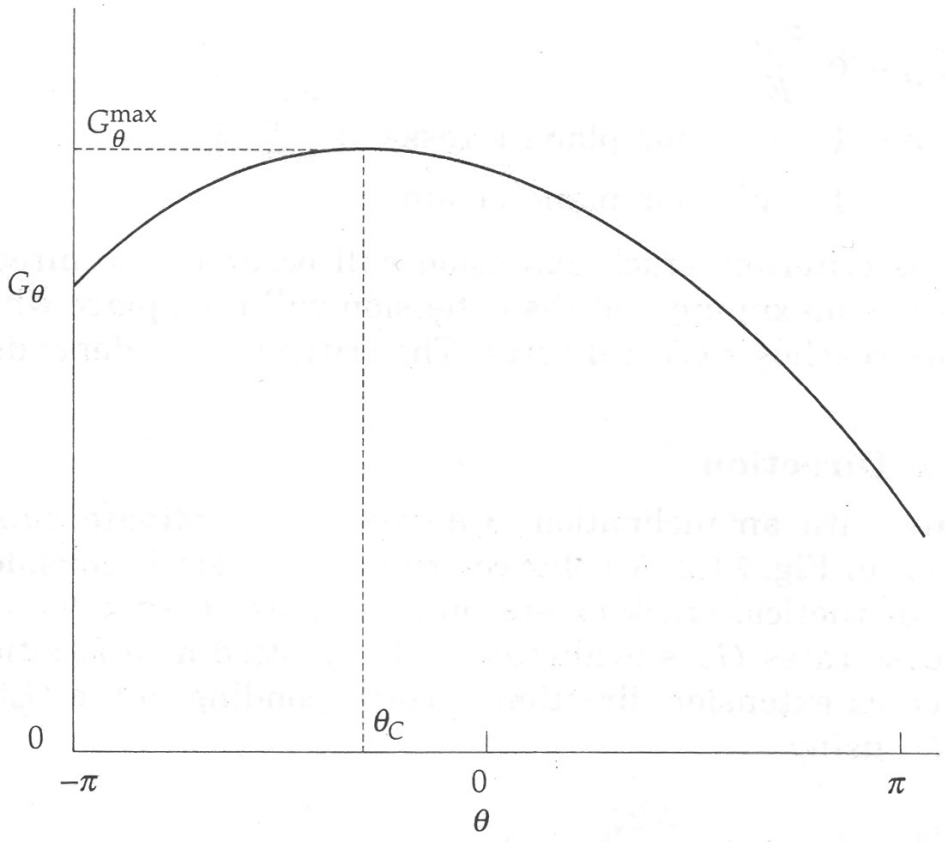

Figure 2. 12: Variation of energy release rate with crack extension direction [39].

- Maximum tangential stress criterion

Different from maximum energy release rates criterion that based on energy, maximum tangential stress criterion is based on one of stress

component in the vicinity of the crack tip. This criterion was proposed by Erdorgan and Sih [41]. Furthermore, in the loading condition as can be seen in Figure 2.11, stress component in the vicinity of the crack tip can be stated as

$$\sigma_{rr} = K_I f_{11}(r,\theta) + K_{II} f_{12}(r,\theta) \tag{2.58a}$$

$$\sigma_{\theta\theta} = K_I f_{21}(r,\theta) + K_{II} f_{22}(r,\theta) \tag{2.58b}$$

$$\sigma_{r\theta} = K_I f_{31}(r,\theta) + K_{II} f_{32}(r,\theta) \tag{2.58c}$$

where $f_{ij}(r,\theta)$ are the coordinate dependent function, that can be expressed as

$$f_{11}(r,\theta) = \frac{1}{\sqrt{2\pi r}}\left(\frac{5}{4}\cos\frac{\theta}{2} - \frac{1}{4}\cos\frac{3\theta}{2}\right) \tag{2.59a}$$

$$f_{12}(r,\theta) = \frac{1}{\sqrt{2\pi r}}\left(-\frac{5}{4}\sin\frac{\theta}{2} + \frac{3}{4}\sin\frac{3\theta}{2}\right) \tag{2.59b}$$

$$f_{21}(r,\theta) = \frac{1}{\sqrt{2\pi r}}\left(\frac{3}{4}\cos\frac{\theta}{2} + \frac{1}{4}\cos\frac{3\theta}{2}\right) \tag{2.59c}$$

$$f_{22}(r,\theta) = \frac{1}{\sqrt{2\pi r}}\left(-\frac{3}{4}\sin\frac{\theta}{2} - \frac{3}{4}\sin\frac{3\theta}{2}\right) \tag{2.59d}$$

$$f_{31}(r,\theta) = \frac{1}{\sqrt{2\pi r}}\left(\frac{1}{4}\sin\frac{\theta}{2} + \frac{1}{4}\sin\frac{3\theta}{2}\right) \tag{2.59e}$$

$$f_{32}(r,\theta) = \frac{1}{\sqrt{2\pi r}}\left(\frac{1}{4}\cos\frac{\theta}{2} + \frac{3}{4}\cos\frac{3\theta}{2}\right) \tag{2.59f}$$

Figure 2.13 shows the direction of these stresses at the vicinity of the crack tip.

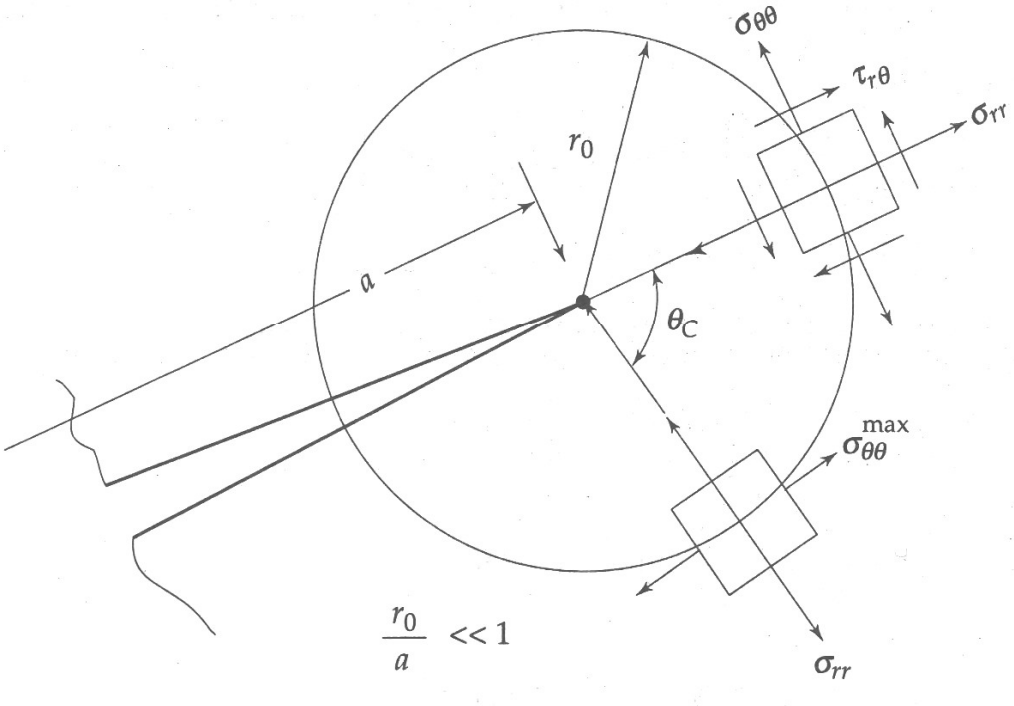

Figure 2. 13: Stress direction at the vicinity of the crack tip [35].

Furthermore, maximum tangential stress criterion stated that crack will occur in the direction where tangential stress ($\sigma_{\theta\theta}$) at r_o (infinitesimal radius around the crack tip) reaches maximum and crack will propagate when $\sigma_{\theta\theta}$ reaches the critical value (σ_C). The maximum tangential stress ($\sigma_{\theta\theta}^{\max}$) can be found using the following equation.

$$\frac{\partial \sigma_{\theta\theta}}{\partial \theta} = 0 \qquad (2.60a)$$

$$\frac{\partial^2 \sigma_{\theta\theta}}{\partial \theta^2} < 0 \qquad (2.60b)$$

Substituting equation (2.59c) and (2.59d) into equation (2.58b), after that applying equation (2.60a) and simplifying using trigonometric manipulation, yields :

$$K_I \sin\theta_C + K_{II}(3\cos\theta_C - 1) = 0 \qquad (2.61).$$

In addition, $\sigma_{\theta\theta}^{\max}$ can be written as :

$$\sigma_{\theta\theta}^{\max} = \frac{K_I}{\sqrt{2\pi r_o}} \cos^3 \frac{\theta_C}{2} - \frac{3}{2} \frac{K_{II}}{\sqrt{2\pi r_o}} \cos\frac{\theta_C}{2} \sin\theta_C \qquad (2.62)$$

As explained previously, the crack will propagate when $\sigma_{\theta\theta}^{\max}$ reaches σ_C and normally pure mode I loading is used to determine the value of σ_C, which is :

$$\sigma_C = \frac{K_{IC}}{\sqrt{2\pi r_o}} \tag{2.63}$$

- Strain energy density criterion

Strain energy density criterion was proposed by Sih [42-44] based on energy principles. When a plate undergo loading condition as can be seen in Figure 2.11, the total strain energy can be expressed as

$$U = \int_V \left[\int_0^{\varepsilon_{ij}} \sigma_{ij} d\varepsilon_{ij} \right] dV \tag{2.64}$$

where V is the total volume. Furthermore, the strain energy density can be stated as

$$W = \frac{dU}{dV} = \int_0^{\varepsilon_{ij}} \sigma_{ij} d\varepsilon_{ij} \tag{2.65}.$$

For linear elastic problem and with help from algebraic manipulation, we can rewrite equation (2.65) become

$$W = \frac{1}{\pi r}\left[g_{11}K_1^2 + 2g_{12}K_I K_{II} + g_{22}K_{II}^2 \right] \tag{2.66}$$

where,

$$g_{11} = \frac{1}{16\mu}(1+\cos\theta)(\kappa - \cos\theta)$$

$$g_{12} = \frac{1}{16\mu}\sin\theta\left[2\cos\theta - (\kappa - 1)\right] \tag{2.67}$$

$$g_{22} = \frac{1}{16\mu}\left[(\kappa+1)(1-\cos\theta) + (1+\cos\theta)(3\cos\theta - 1)\right]$$

and

$$\mu = \frac{E}{2(1+\nu)} \tag{2.68}$$

Strain energy density still depends on the radius (r), and it will be singular if the value of the radius near to zero. So, it is more comfortable to make a new parameter, strain energy density factor (S) which is independent of r.

$$S(\theta) = \frac{1}{\pi}(g_{11}K_I^2 + 2g_{12}K_I K_{II} + g_{22}K_{II}^2) \tag{2.69}$$

This criterion stated that crack will propagate to the direction where the θ fulfill the following conditions.

$$\frac{\partial S}{\partial \theta} = 0 \text{ and } \frac{\partial^2 S}{\partial \theta^2} > 0 \qquad (2.70)$$

Moreover, the crack will propagate when $S_{\min} \geq S_C$, where $S_{\min}$ is the minimum value of strain energy density and S_C is critical strain energy density factor which depend on the material. Additionally, the value of S_C normally can be got from pure mode I loading, where $\theta_C = 0$ and $K_I = K_{IC}$. The end result of S_C can be stated as

$$S_C = \frac{(1+\nu)(\kappa-1)}{4\pi E} K_{IC}^2 \qquad (2.71).$$

2.3 A Review on Fracture Mechanics in Composite Materials

Fracture mechanics approach is already well established for isotropic materials, but not so for composite materials. The response of composites may not be the same as the response of the isotropic materials that undergo the same loading condition. Meaning the expression of fracture mechanics parameters for isotropic materials may not be used directly to the composites. Here, two fracture mechanics parameters for composite materials are presented and discussed.

2.3.1 Energy release rates

Energy release rate for isotropic double cantilever beam specimen can be seen in equation (2.27). For the critical condition, this equation can be rewritten as :

$$G_{IC} = \frac{P_C^2}{2B}\left(\frac{dC}{da}\right)_C \qquad (2.72)$$

This equation also can be used for composite materials, because we do not need to know about the material properties and the crack stress distribution, which means all the needed parameters can be determined from the measurements on the specimen. Beside that, critical energy release rate for laminate also can be determined from the corresponding laminas energy release rates as expressed in the following.

$$G_{IC} = \frac{\sum_{i=1}^{N} G_{ICi} t_i}{t} \qquad (2.73)$$

where G_{IC} is the critical strain energy release rate for the laminate, G_{ICi} is the critical strain energy release rate for the i th angle-ply component, t is the total laminate thickness and t_i is the thickness of the i th angle-ply component.

2.3.2 Stress intensity factors

Equation (2.43) shows the expression of the stress in the vicinity of the crack tip for pure mode I loading in isotropic plate. Those equations can be rewritten as :

$$\sigma_{11} = \frac{K_I}{(2\pi r)^{1/2}} f_1(\theta)$$

$$\sigma_{22} = \frac{K_I}{(2\pi r)^{1/2}} f_2(\theta) \qquad (2.74)$$

$$\sigma_{12} = \frac{K_I}{(2\pi r)^{1/2}} f_3(\theta)$$

It can be seen that stresses at certain r and certain θ for isotropic materials only depend on K_I . But in composite materials, stresses at certain point in the vicinity of the crack, also depends on s_1 and s_2, which are complex roots of the characteristic equation corresponding to a differential equation in the stress function. In the end, the stresses in the vicinity of the crack tip for composite materials can be expressed as :

$$\sigma_{11} = \frac{K_I}{(2\pi r)^{1/2}} F_1(\theta, s_1, s_2)$$

$$\sigma_{22} = \frac{K_I}{(2\pi r)^{1/2}} F_2(\theta, s_1, s_2) \qquad (2.75).$$

$$\sigma_{12} = \frac{K_I}{(2\pi r)^{1/2}} F_3(\theta, s_1, s_2)$$

2.4 Delamination in Composites

There are a lot of possibilities of damage mode in composite laminate [45, 46], the main ones are intra ply cracking, interlaminar delamination and fiber failure. First of all, the cause of interlaminar delamination will be discussed and later we will discuss about prediction and modeling delamination.

2.4.1 Causes of delamination

Before moving on to the further discussion about delamination, it is better to discuss about the causes of delamination. They are three causes of delamination will be discussed here: free edge stress, impact and matrix cracks [47].

- Free edge stresses

  At the free edge of laminated composites, normally interlaminar stress will appear. This interlaminar stress is happen due to the mismatch between layers in Poisson's ratio (ν_{xy}) and coefficient of mutual influence ($\eta_{xy,x}$) [48]. Many people assume that interlaminar stress will also appear if there is a mismatch in elastic and shear modulus between layers. It was wrong assumption. Interlaminar stress will not appear in those conditions [48], but it does not means that interlaminar stress will not appear between layers with the same orientation. Interlaminar stress can occur in these kinds of conditions if the interface moment exists [47].

  The interlaminar normal (σ_z) and shear stresses (τ_{yz}) are caused by the mismatch in ν_{xy} and the rise in interlaminar shear stress (τ_{zx}) near the free edge is caused by mismatch in $\eta_{xy,x}$ [47]. The rise of those stresses is affected by three causes: stacking sequence [48-52], ply thickness [53] and residual thermal stresses [54-60]. For stacking sequence problem, Herakovich's [48] has found that the largest value of σ_z, τ_{yz} and τ_{zx} respectively occur for (11.5°/-11.5°) and (22°/90°) layups. Related to the effect of ply thickness, O'Brien [53] has found that thicker ply will cause the rise in interlaminar stresses or decrease in critical strain (ε_c). This result can be seen in Figure 2.14.

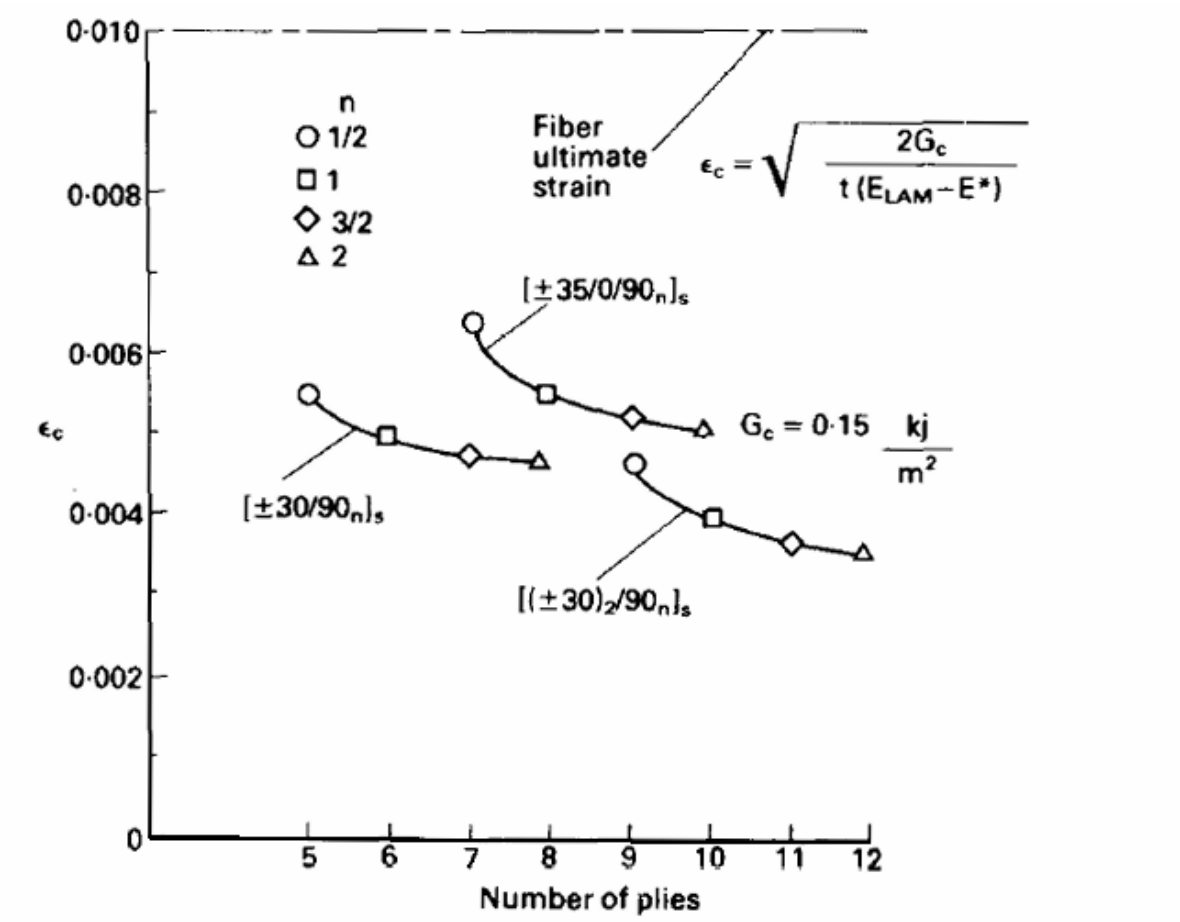

Figure 2. 14: Parametric study of variation in delamination onset strains with thickness [53].

- Impact

  Under impact load, laminate composites will suffer highly deformation gradient (Figure 2.15 [61]). This deformation can cause transverse shear and out of plane normal stresses which can cause damage in laminated composites. Damage that is caused by impact in laminated composites can be either visible or not visible, depends on impact velocities. Moreover, damage can only be seen if the impact velocities higher than 80-100 m/s [47, 62]. Thus, it can be very dangerous, because invisible damage still can cause degradation in composite laminates properties.

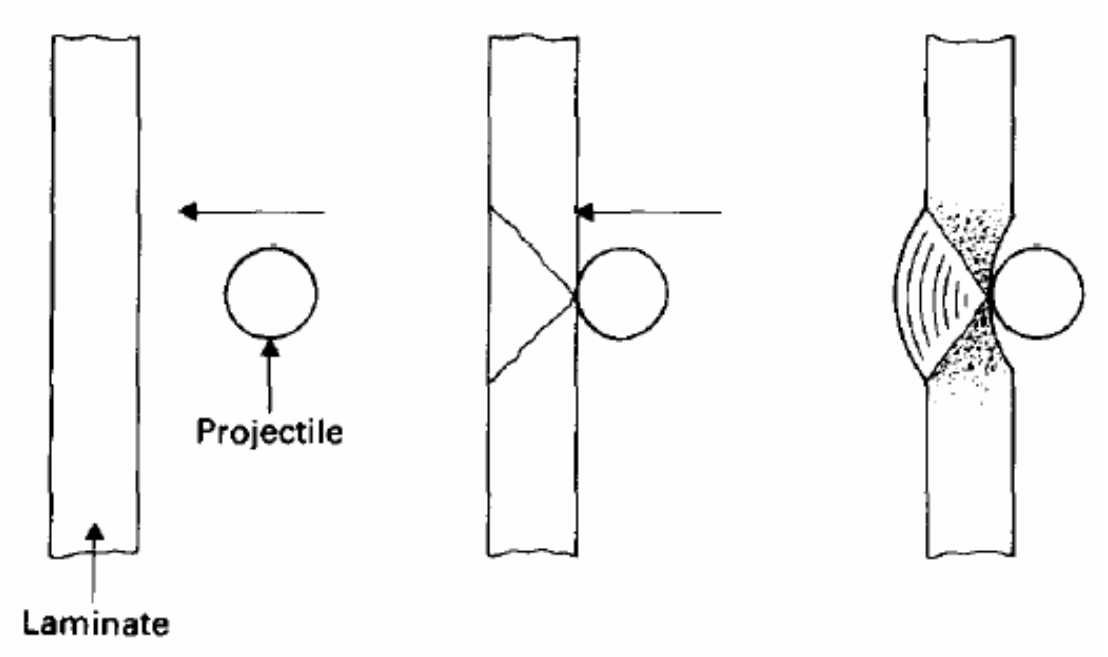

Figure 2. 15: Deformation by projectile hitting a laminate [61].

- Matrix cracks

  The last major damage mode is matrix cracking in off axis plies. Under tensile load, this off axis plies can cause interlaminar stresses as shown in Figure 2.16 [47]. Several publications have concerned about this problem in quasi isotropic laminated composites (0°,±45°,90°)s [45, 52, 63], and Ref [52] provided the distribution of interlaminar stresses near a crack in between 90° plies (Figure 2.17).

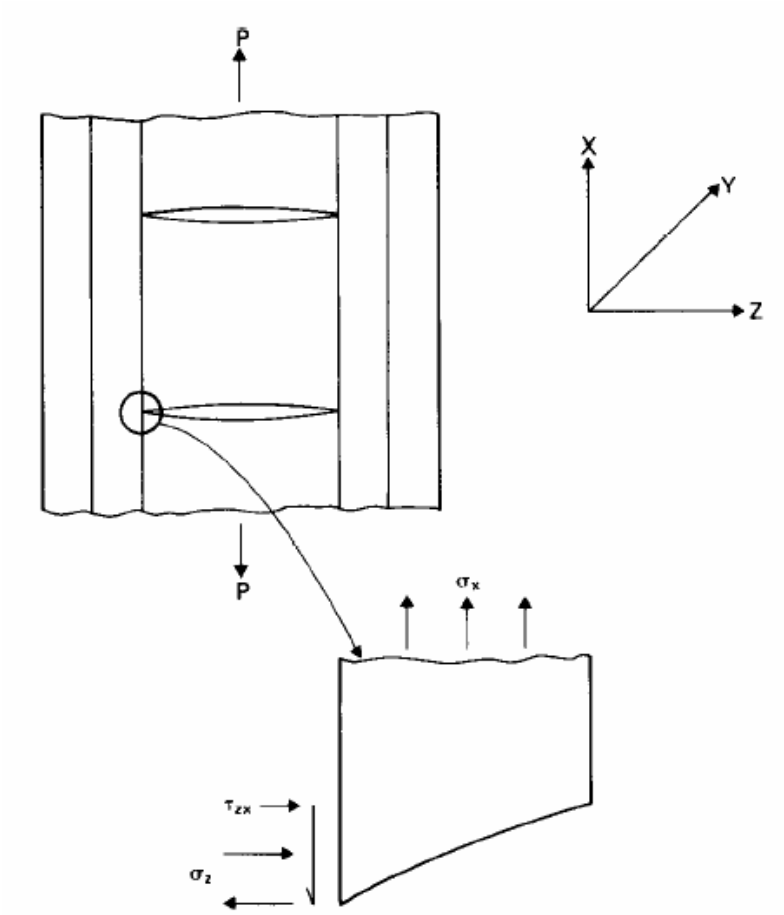

Figure 2. 16: Interlaminar stresses due to matrix crack in off axis plies [47].

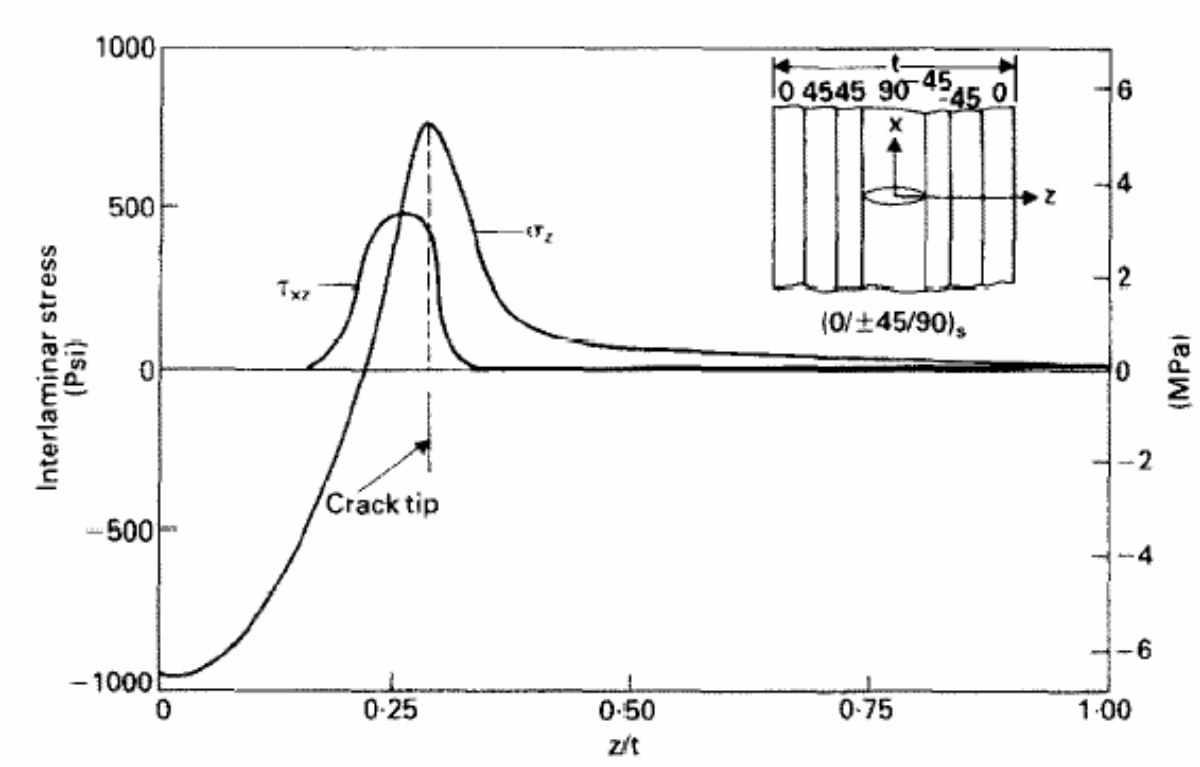

Figure 2. 17: Distribution of interlaminar stresses near a crack in the 90° plies of a (0°,±45°,90°)s laminated composites [52].

2.4.2 Delamination propagation

Delamination propagation in laminated composites normally is a combination of all three modes of fracture. Furthermore, the fraction of each mode depends on the given loading. As a result, for general delamination problem, it is important to know the fracture toughness for every mode. It is widely known that fracture toughness in the first mode is the lowest one [64]. Consequently, a lot of researchers have concerned about it [65-67]. Despite that fact, the second and third fracture mode are utmost important in certain loading condition. A number of finding related to these modes of failure have already been found too [68-70]. Those researches have discussed fracture mode in the delamination problem separately. Eventually, quite a few research have fulfilled the need to mix it together in the mixed mode failure [71, 72].

In general, there are several things that can affect the delamination fracture toughness of laminated composites. They are:

- Resin toughness

The use of tougher resin will cause in the rise of fracture toughness [73, 74], because it will makes initial delamination harder propagate.

- The direction of plies above and below the delamination

  Delamination in between 0° plies will have lower fracture toughness than delamination in between 90° plies or in between 0° ply and 90° ply [75], because delamination in between 0° plies tends to propagate only in one crack propagation plane and delamination in between 90° plies and 0° ply and 90° ply tend to propagate in two crack propagation plane. Thus, it causes the energy dissipates during the crack propagation is lower for delamination in between 0° plies. Consequently, the fracture toughness for delamination in between 0° plies becomes lower. In the case of delamination in ±θ interface with pure mode I loading, G_{IC} tends to decrease when θ increases [76]. On the other hand, for delamination in ±θ interface with pure mode II loading, G_{IIC} tends to increase when θ increases [77]. Moreover, in the case of delamination in ±θ interface with mixed mode loading, G_C tends to increase when θ increases or G_I / G_{II} decreases [78, 79]. Furthermore, the interaction between fracture toughness with crack path instabilities also discussed in several literatures [80-82] along with the interaction with imperfect fiber alignments. The later gives considerable effect of suppressing the delamination [82].

- Temperature and humidity

  Beside resin toughness and adjacent plies direction, delamination fracture toughness also depends on temperature and humidity [83].

  Delamination in between 0° plies will have lower fracture toughness than delamination in between 90° plies or in between 0° ply and 90° ply [75],

By modifying these parameters, it is possible to fabricate laminated composites that have very high delamination fracture toughness.

2.4.3 Coupling after delamination appearance

Generally, composite maker try to make their composite structures symmetrical and balanced in order to prevent the appearance of coupling. Furthermore, after the emergence of delamination, some parts of the structure may not be symmetrical and balanced anymore, especially areas above and below

delamination. Figure 2.18 shows an example of symmetric angle ply composite before and after delamination appearance.

In the case of Figure 2.18, the structure initially symmetric and balanced. Moreover, after delamination emerges at the mid plane, some of the parts (areas I and IV) still in symmetric and balanced condition but other parts (areas II and III) become antisymmetric. As a result, couplings B_{16} and B_{26} appear in those areas. Couplings that emerge after delamination appearance are affected by lamination angle and the position where delamination appears. Another example, cross ply laminates with delamination at the mid plane will cause couplings B_{11} and B_{22} to emerge.

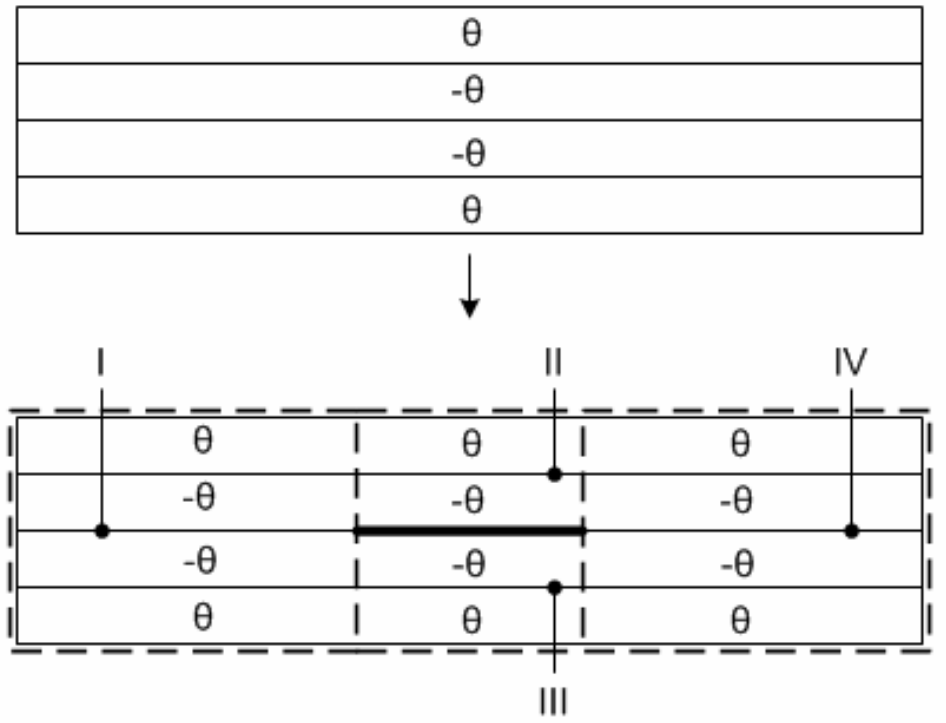

Figure 2. 188: Symmetric angle ply composite before and after delamination appearance, which can be divided into 4 areas (I, II, III and IV).

Chapter Three

FINITE ELEMENT MODELING

One of the aims of current research is to predict the direction of crack propagation. Fracture mechanics parameters (energy release rate, stress intensity factor, J integral and crack tip opening displacement) can be used to predict crack propagation direction. Here, the fracture mechanics parameter used to predict crack propagation direction is the energy release rate (G). In this chapter, the making of the model to measure energy release rate distribution will be discussed in details, but before going through to the model development, it would be better to define the problem first.

3.1 Problem Definitions

To reduce the costs and time to perform actual tests, the finite element method is used. For that reason, the finite element model is geometrically identical to the experimental specimen (Figure 3.1). The experimental specimens are constrained by several things such as the loading capacity of the tensile machine that limit the maximum cross section area of the specimen and the space of the tensile machine that restrict the maximum length of the specimen. Figure 3.2 shows important dimensions of the specimen. The width of the specimen (w) is fixed at 20 mm and the end tab length (e) is also fixed at 50 mm. Furthermore, the total length of the specimen (L+2e) is 240mm. Furthermore, the thickness (t) depends on the number of the layers and the crack length (2a) will be varied.

As explained in chapter 1, the specimen is subjected to tensile load. Unfortunately, the specimen used here are continuous carbon fiber reinforced polymer. It is commonly known that carbon fiber reinforced polymer can not be tested without end tab, because the tensile machine holder can tear the specimen. As can be seen in Figure 3.2, the specimen is divided into two sections: green section (the gauge length section) and red section (the section where end tab need to be installed on the top and bottom surfaces). Furthermore, only the green section that needs to be modeled.

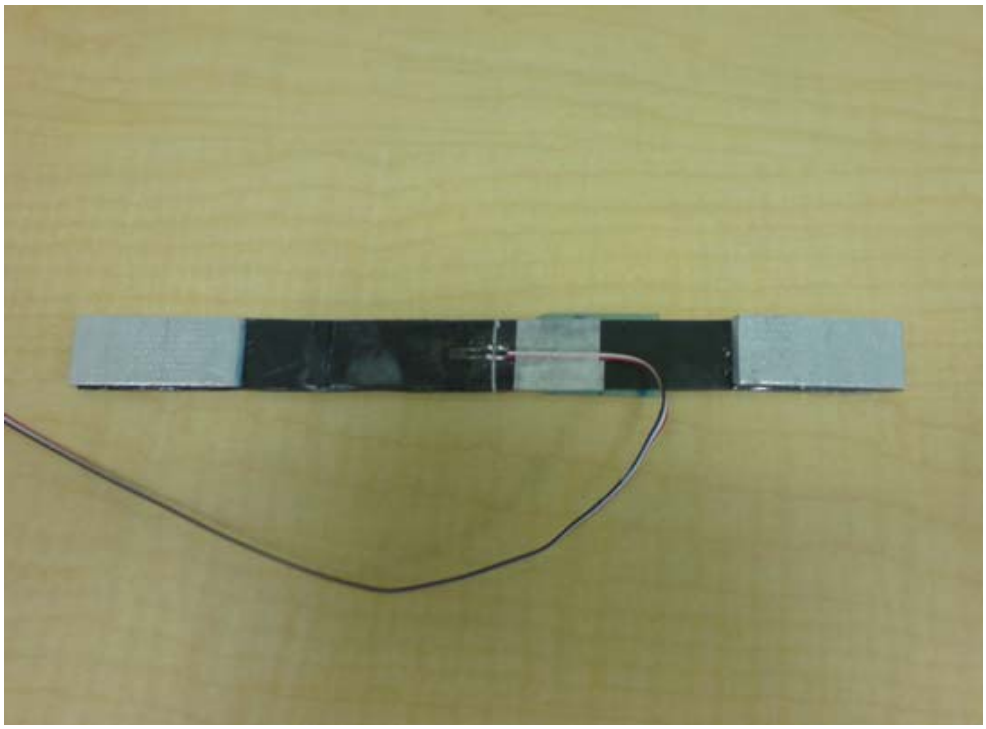

Figure 3. 1 : Experimental specimen.

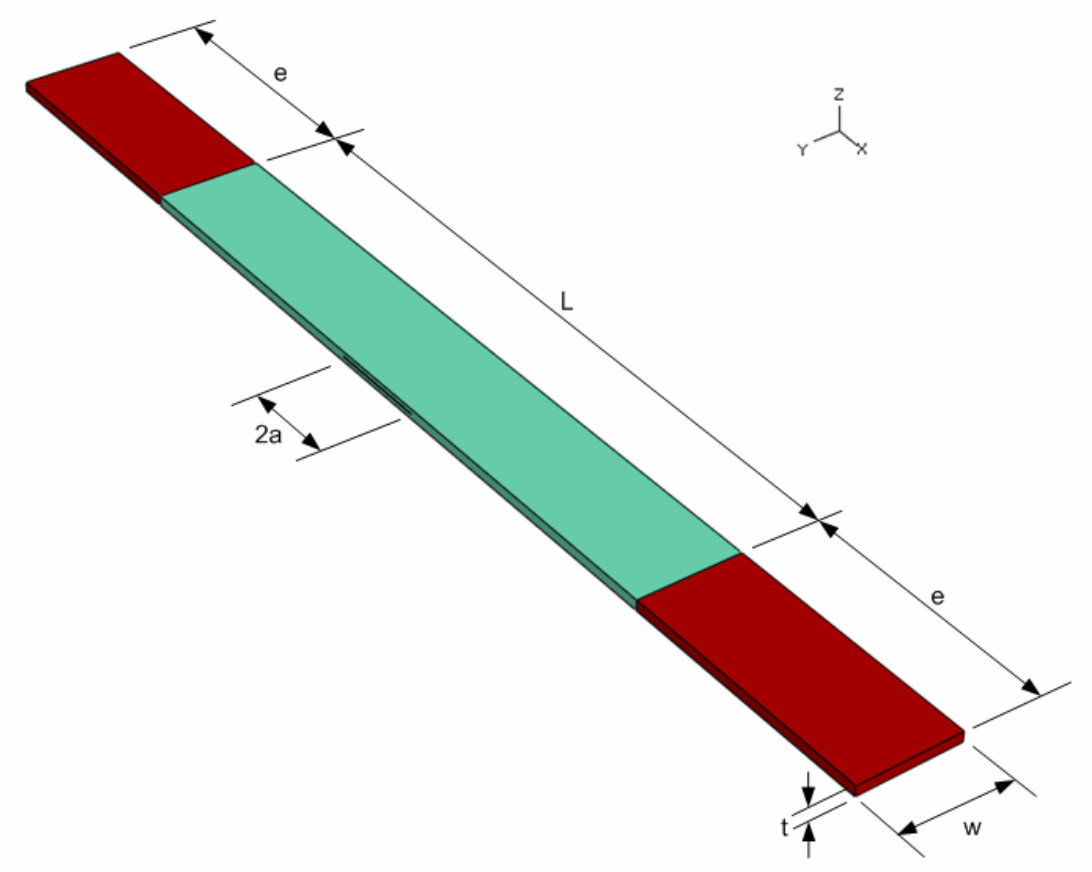

Figure 3. 2 : Problem definitions.

3.2 Model Development for Measuring Energy Release Rate and Stress Intensity Factor

The model development for the simulation will be discussed in details. Starting from properties definition, and followed by part modeling, mesh refinement and at the end constraint modeling.

3.2.1 3D orthotropic properties

Laminated composites can be modeled either as 2D orthotropic or 3D orthotropic. To measure energy release rate 3D orthotropic model is chosen. The composite used in the finite element model and experiment is Fiberdux 913C-HTA carbon epoxy. The properties of this composite are given in Table 3.1.

Table 3.1 Properties of Fiberdux 913C-HTA carbon epoxy

Properties	Magnitude	Unit
E_{11}	150	GPa
E_{22}	9.5	GPa
E_{33}	9.5	GPa
ν_{12} and ν_{13}	0.263	-
ν_{23}	0.458	-
G_{12} and G_{13}	5.43	GPa
G_{23}	3.26	GPa
σ_{1tu}	2167	MPa
σ_{1cu}	1550	MPa
σ_{2tu}	35.97	MPa
σ_{2cu}	140	MPa
σ_{3cu}	35.97	MPa
τ_{12u} , τ_{13u} and τ_{23u}	101.2	MPa
ρ	1100	kg/m^3

One problem appears, in the current version of ABAQUS the properties of Fiberdux 913C-HTA carbon epoxy above has to be converted to the properties of 3D orthotropic. Based on Hooke's Law, the relation between these properties are:

$$
\begin{aligned}
D_{1111} &= E_1(1-\nu_{23}\nu_{32})\gamma \\
D_{2222} &= E_2(1-\nu_{13}\nu_{31})\gamma \\
D_{3333} &= E_3(1-\nu_{12}\nu_{21})\gamma \\
D_{1122} &= E_1(\nu_{21}+\nu_{31}\nu_{23})\gamma \\
D_{1133} &= E_1(\nu_{31}+\nu_{21}\nu_{32})\gamma \\
D_{2233} &= E_2(\nu_{32}+\nu_{12}\nu_{31})\gamma \\
D_{1212} &= G_{12} \\
D_{1313} &= G_{13} \\
D_{2323} &= G_{23}
\end{aligned}
\qquad (3.1),
$$

where

$$\gamma = \frac{1}{1-\nu_{12}\nu_{21}-\nu_{23}\nu_{32}-\nu_{31}\nu_{13}-2\nu_{21}\nu_{32}\nu_{13}} \qquad (3.2).$$

Using above equation, we can get 3D orthotropic properties as in Table 3.2.

Table 3.2 3D orthotropic properties of Fiberdux 913C-HTA carbon epoxy

Properties	Magnitude	Unit
D_{1111}	152456.4927	MPa
D_{2222} and D_{3333}	12165.0443	MPa
D_{1122} and D_{1133}	4687.896507	MPa
D_{2233}	5649.675017	MPa
D_{1212} and D_{1313}	5430	MPa
D_{2323}	3260	MPa

3.2.2 Part modeling with seam

They are several ways to make a model to measure energy release rate, for instance full model, half model and quarter model. Half model and quarter model are less expensive than full model, but those models can not be used for stacking sequences that have no symmetry. Therefore, only full model that will be used here. Figure 3.3 shows the full model dimensions. Those dimensions are fixed except the thickness (t). The thickness of the specimen depends on number of layers that are used. The area covered by 20 mm and 2a dimensions is the area

that initial delamination will be modeled. To model initial delamination in finite element, we have to make a seam. The purpose of seam is to separate the node between upper and lower surface where the seam is made. Figure 3.4 shows an example of seam that is made at mid plane (the area that covered by dark blue and red lines) to model specimen with initial delamination at mid plane.

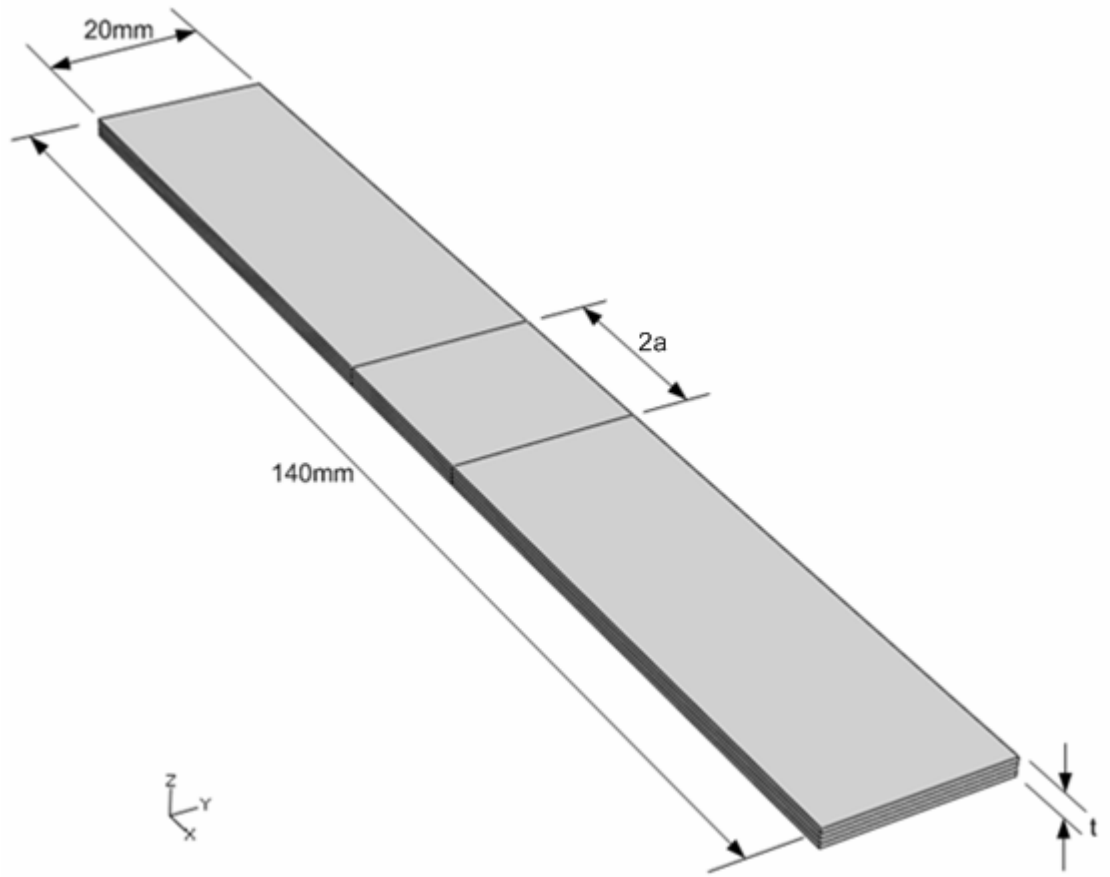

Figure 3. 3 : Full model dimensions.

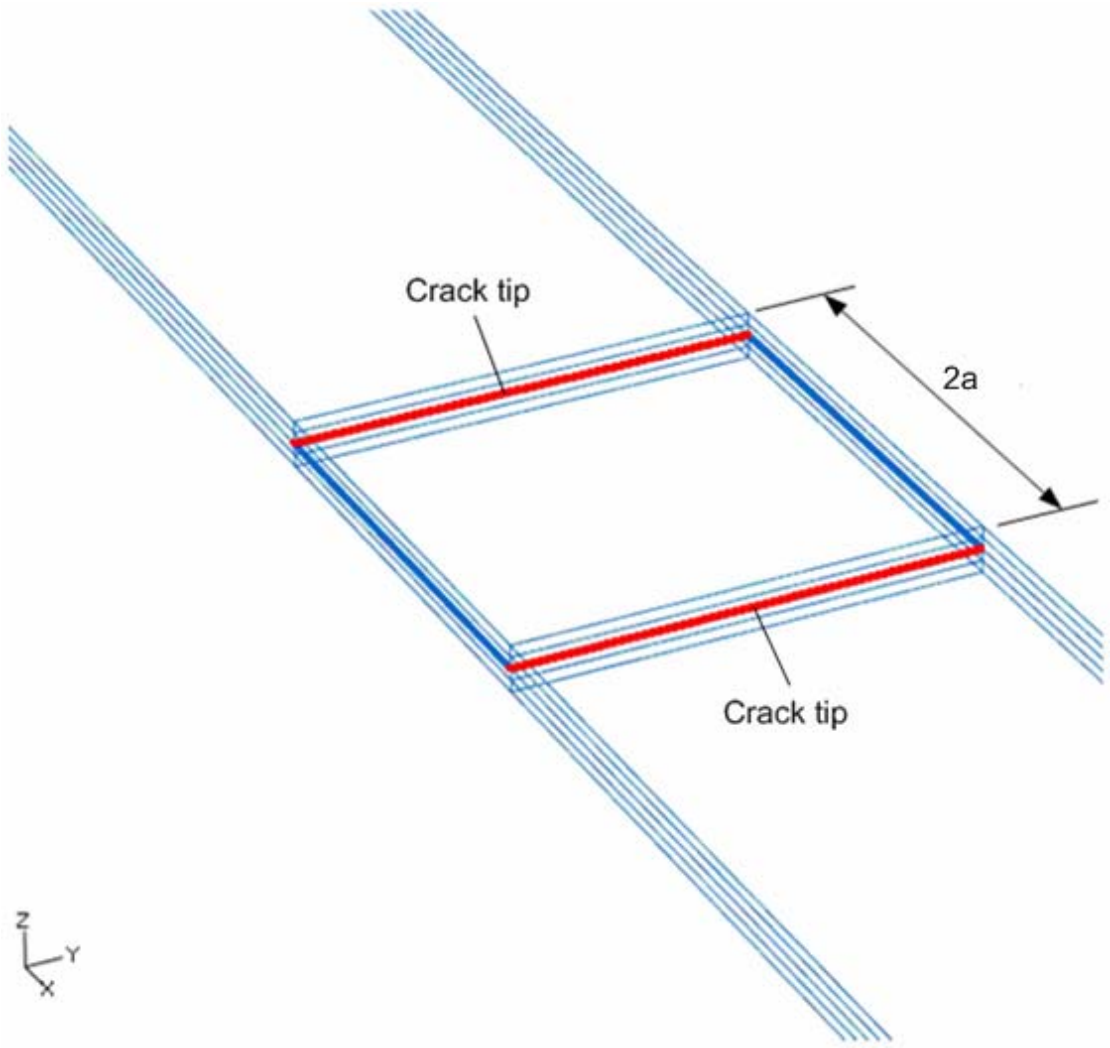

Figure 3. 4 : Seam at mid plane for full model.

3.2.3 Mesh refinement

In the crack problem, there will be stress singularities near the crack tip (marked by red lines in Figure 3.4). To catch these stress singularities, we need to use quadratic element and modify mesh in the vicinity of the crack tip. The mesh modification can be divided into two: mesh refinements and nodes modification. Both are needed to catch the singularity in the vicinity of the crack tip. Mesh refinements that is done to this model can be seen in Figure 3.5. Furthermore, nodes modification needs to be done for mid side node of elements in the vicinity of the crack tip. In this case, we will use mid side node parameter equal to 0.25. It means, mid side node for every elements in the vicinity of the crack tip will be grinded a quarter of the elements length to the crack tip. For clarity the result of node modification can be seen in Figure 3.6.

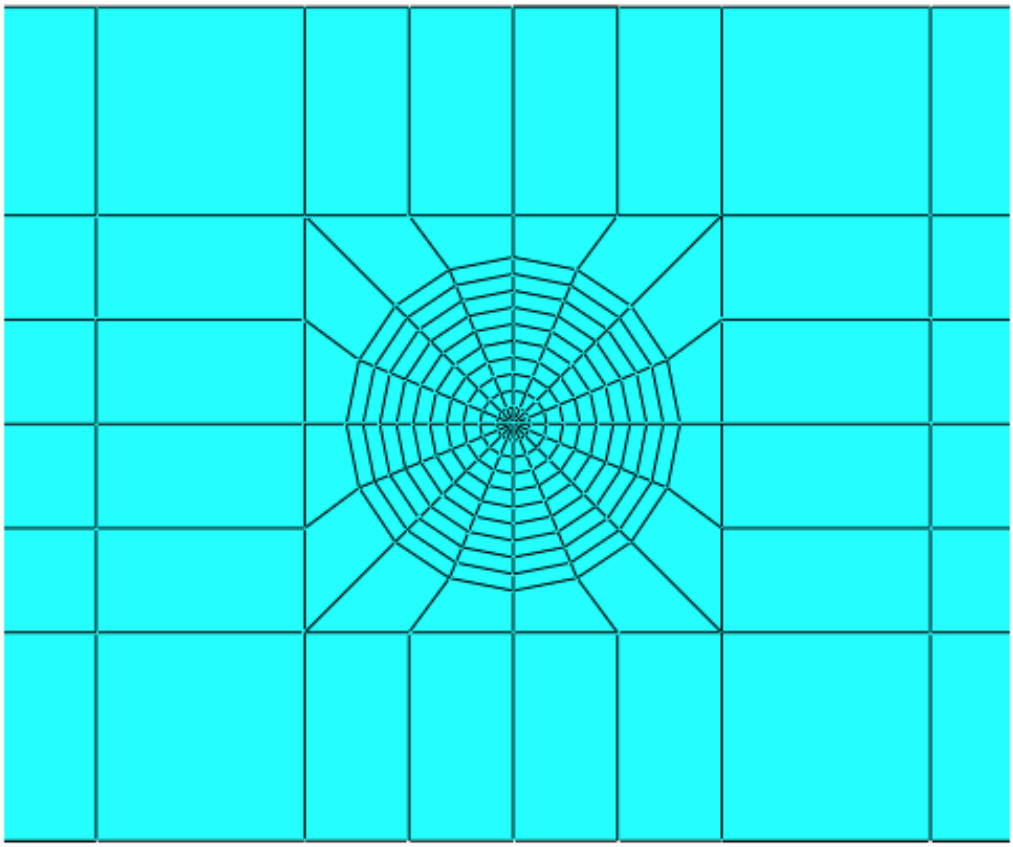

Figure 3. 5 : Mesh refinements in the vicinity of crack tip.

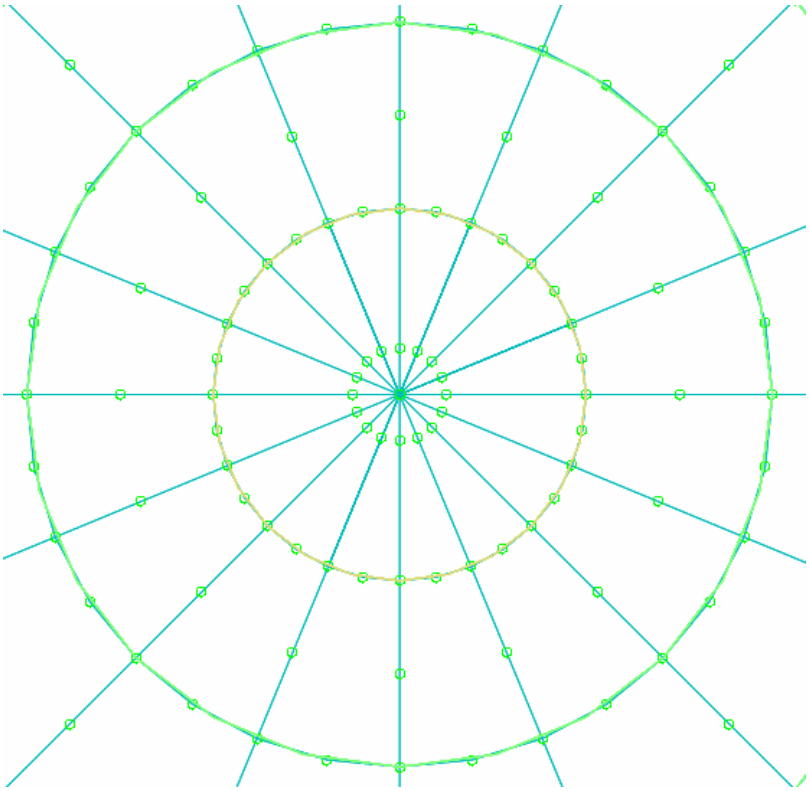

Figure 3. 6 : Nodes modification in the vicinity of crack tip.

Additionally, the crack propagation direction needs to be defined in order to measure the energy release rate. In reality, crack will propagate to the direction of the highest energy release rate. Figure 3.7 shows the model with 0° crack propagation direction.

Beside crack tip mesh refinement, side edge mesh refinement is also needed. It is needed to catch the side effect, which need very fine mesh at the edge. To make the model less expensive, very fine mesh only modeled at the edge and gradually modeled coarser along the width to the center part. The end result of the meshed model can be seen in Figure 3.8.

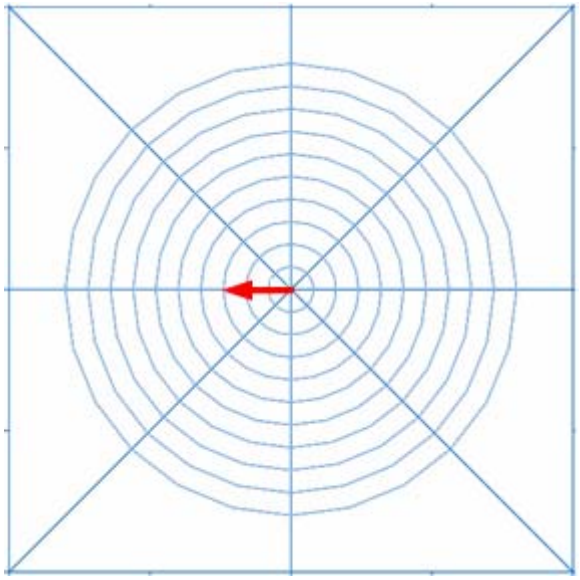

Figure 3. 7 : Model with 0° crack propagation direction.

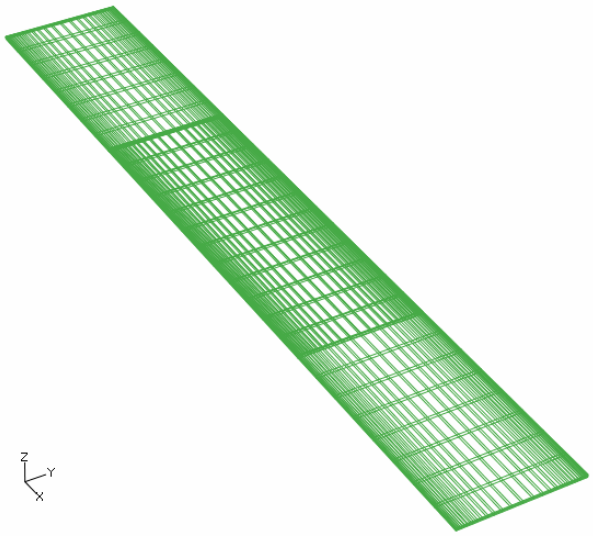

Figure 3. 8 : Meshed fracture mechanics model.

3.2.4 Constraining the model

How the model response to applied load or displacement depends very much on the constraints applied on the model. Furthermore, two constraints are needed in full model for measuring energy release rate, they are constraint at one end of the specimen which is clamped (U1=U2=U3=UR1=UR2=UR3=0) and constraint at another end of the specimen that represent the given load (U2=U3=UR1=UR2=UR3=0 and U1=0.3mm). Figure 3.9 shows the constraints that are applied on the model.

Additionally, as stated in chapter 2, after delamination emerges, it will cause coupling. As a result, bending or twisting may exist in the upper and lower part of

delamination. Thus, contact need to be modeled between the top delamination surface and bottom delamination surface to prevent overlapping between those areas.

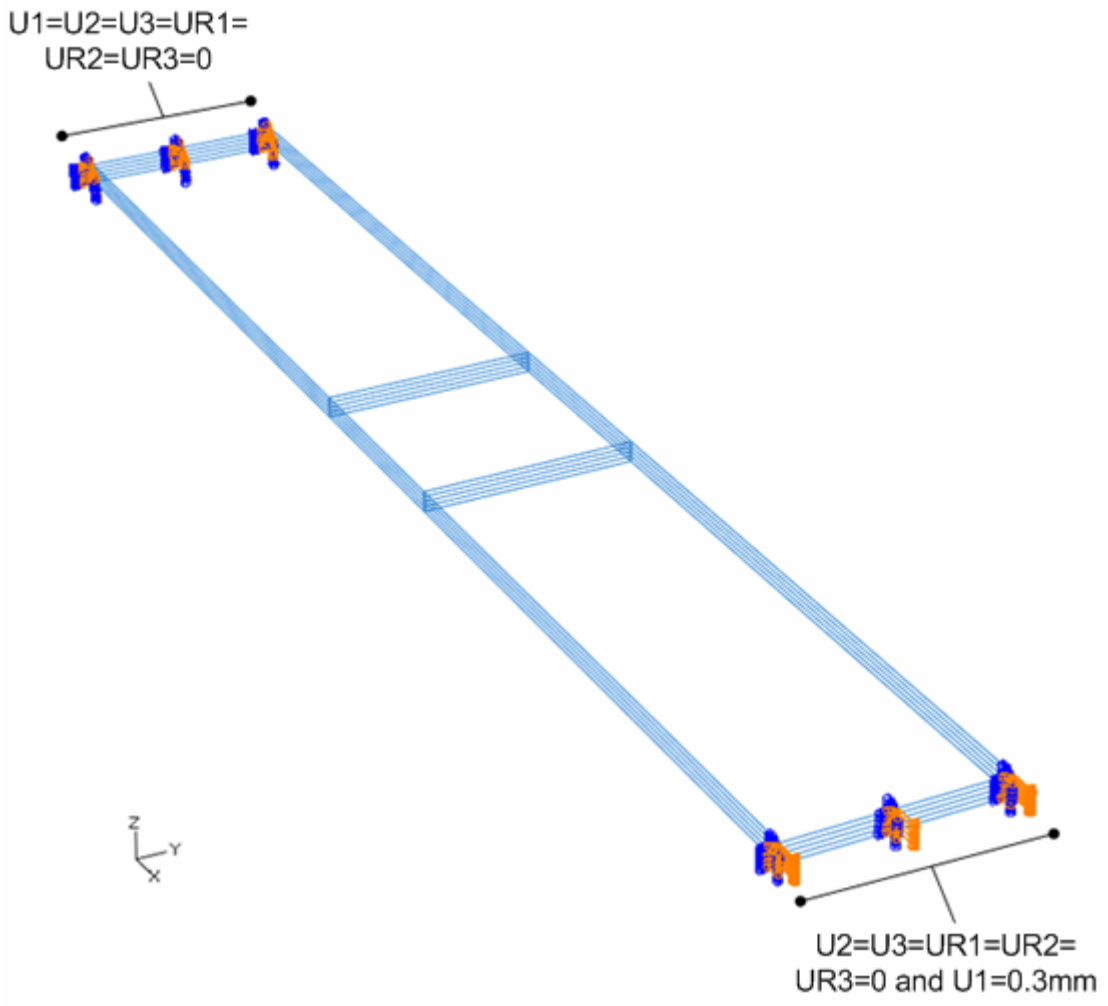

Figure 3. 9 : Constraints of fracture mechanics model.

3.3 Model Development for Measuring Failure Load

Next thing to do is to develop model to measure failure load. This is very important because we can see how critical the delamination is by comparing failure load of specimen with and without delamination. This model development will be divided into two parts, part modeling and constraint modeling.

3.3.1 Part modeling

All of the parts are modeled as continuum shell with Hashin failure theory. All properties are given in Table 3.1 and all the dimensions are the same as the dimensions of model to measure fracture mechanics parameters (given in Figure 3.3).

In order to make a better guess, elements at delamination area are made smaller than other areas. The end result of meshed part can be seen in Figure 3.10.

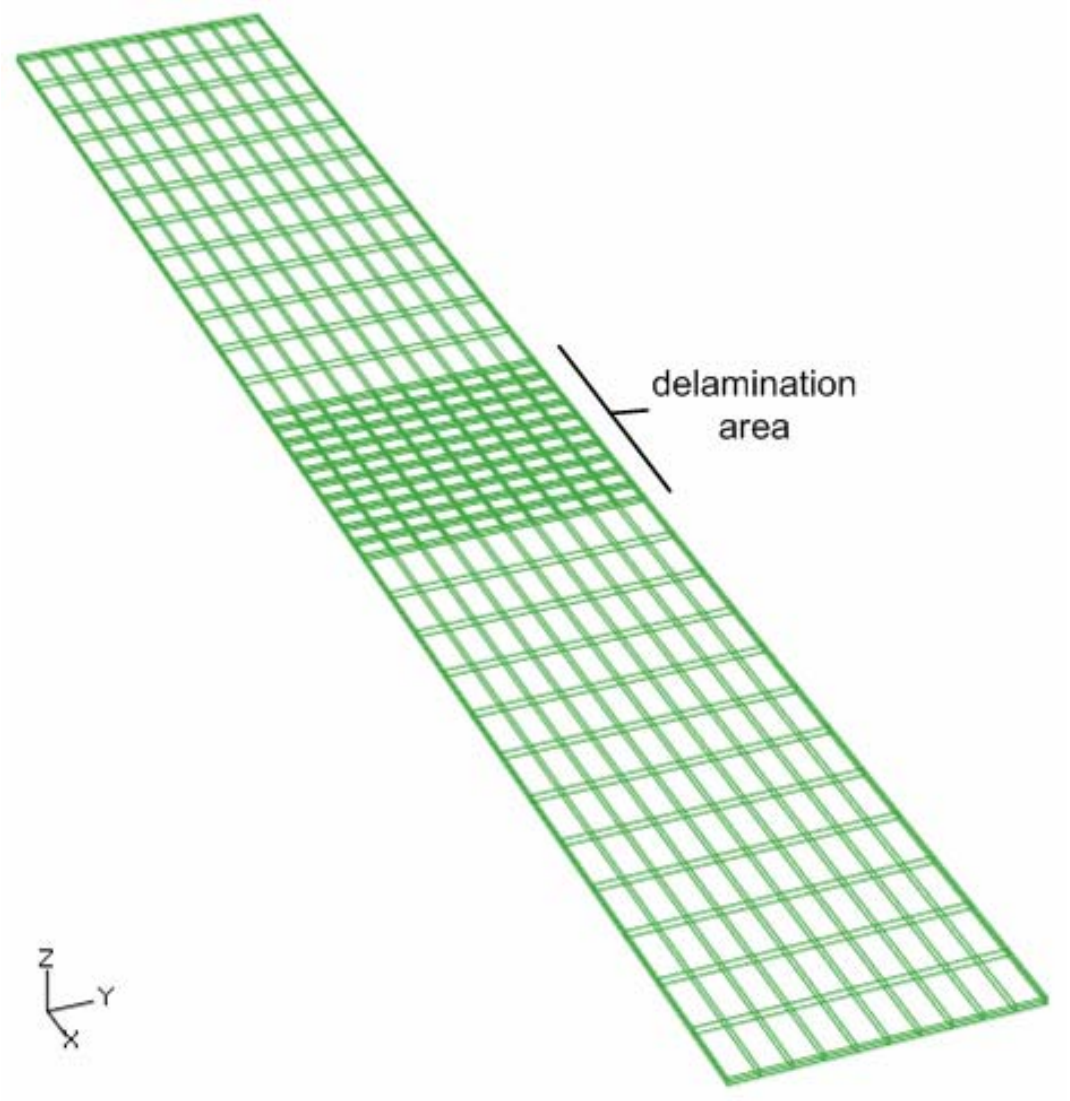

Figure 3. 10 : Meshed failure load model.

3.3.2 Constraint modeling

The model to measure failure load has the same constraints as those in section 3.2.4 except U1 (displacement in the x direction). In this model, displacement in the x direction is failure displacement of the specimen (D). Therefore U1 for one specimen and the other might be different. Figure 3.11 shows the constraints of model to measure failure load.

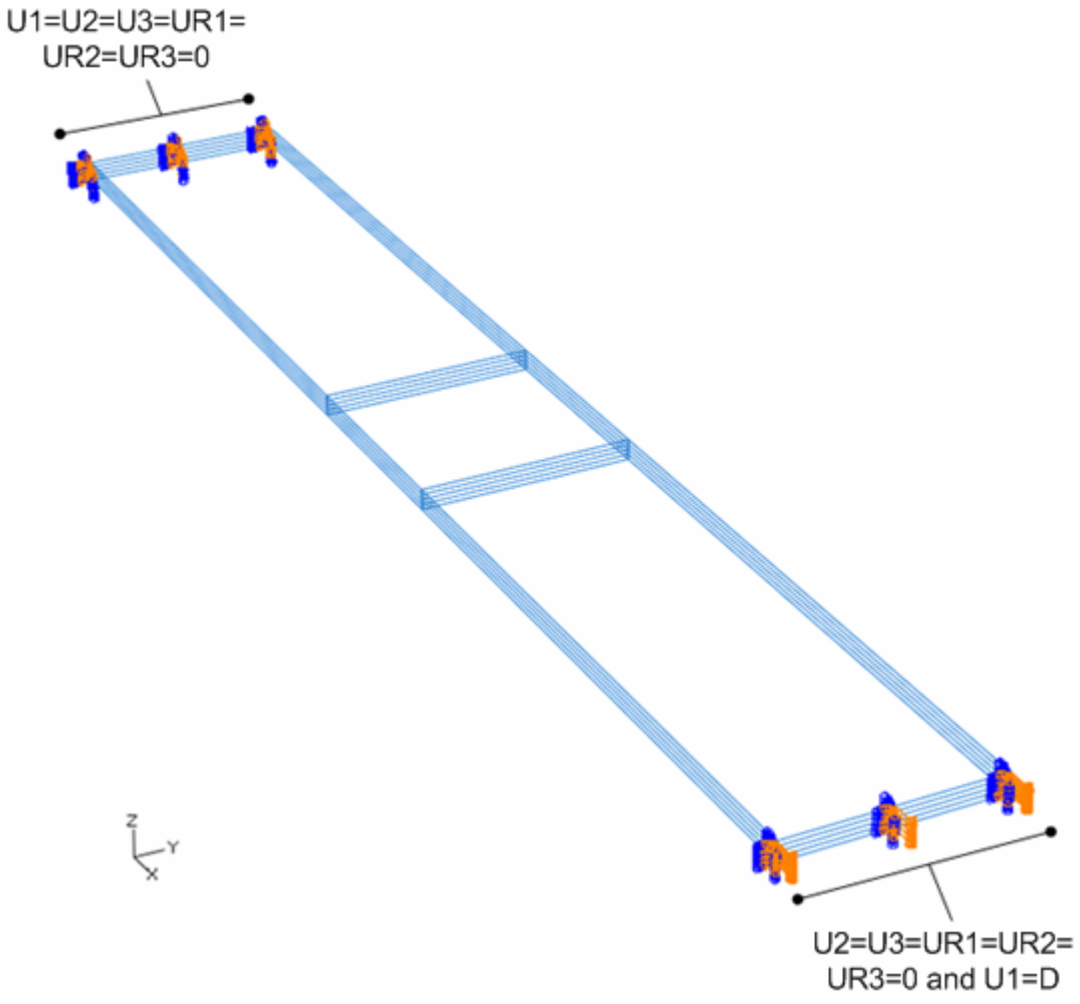

Figure 3. 11 : Constraints of failure load model.

Chapter Four

EXPERIMENTAL SET-UP

The result from finite element analysis needs to be compared with another result. In this case, it will be compared with the result from experimental observation. In this chapter, the preparation and set-up of the experiment are presented and discussed in details.

4.1 Specimen Preparation

Several step of preparation need to be done to make a complete specimen. They are: prepreg processing, curing, strain gauge mounting and end tab mounting. Those steps will be discussed individually here.

4.1.1 Prepreg processing

Prepreg continuous fiber composite is used here as the raw material to make composite specimen (Figure 4.1). Before curing process, prepreg need to be prepared by cutting and stacking it. As a result, the desirable prepreg arrangement has been made can be seen in Figure 4.2.

Figure 4. 1 : Prepreg continuous fiber composites before processing.

Figure 4. 2 : Prepreg continuous fiber composites after processing.

4.1.2 Curing process

After finishing the prepreg processing, the next step is curing process. Before curing, prepreg must be placed at aluminum plate that has been covered with non porous teflon, and several layers have to be added at the top of the prepreg. Figure 4.3 shows the arrangement for this problem, and Figure 4.4 shows the end result of the arrangement before curing process.

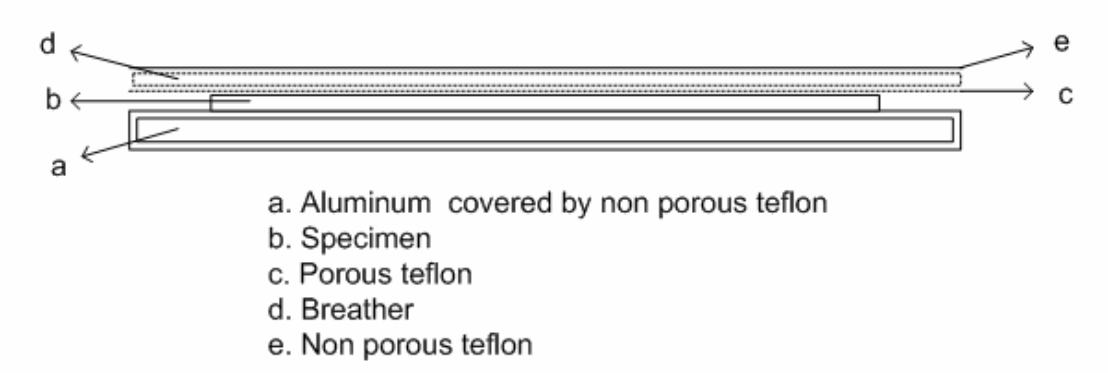

Figure 4. 3 : The arrangement of additional layers on prepreg before curing.

Figure 4. 4 : The end result of the arrangement before curing.

The following step is to place that prepreg arrangement to the curing table (Figure 4.5) and start the curing process. The curing process will need around three hours to finish. During this time, heat will be given to the prepreg, controlled by Heatcon 9200 (Figure 4.6). This three hours time can be divided into three major steps: temperature ramping, temperature dwelling, and cooling (Figure 4.7). At the first and second step, the curing table is covered with breather and the air conditioner is turned off. In contrast, at the third step, the breather cloth is detached from the curing table and the air conditioner and fan are turned on. After all of those steps, the prepreg set is left alone for 2 hours before the next step because the specimen will be still to hot. In the end, the composite specimen is completed as shown in Figure 4.8.

Figure 4. 5 : Curing table.

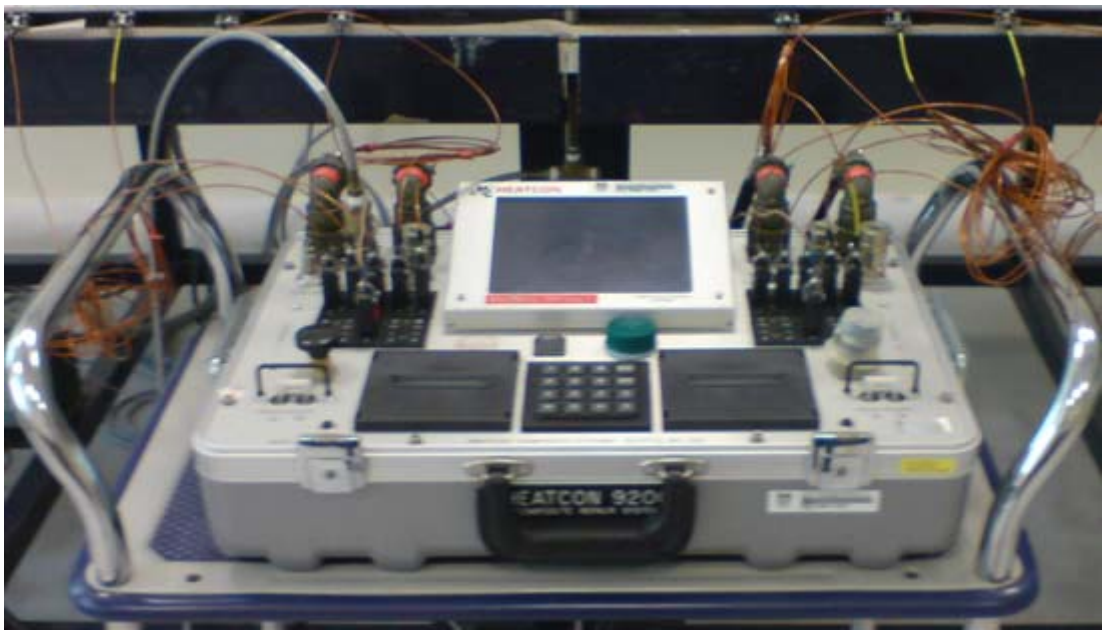

Figure 4. 6 : Heatcon 9200.

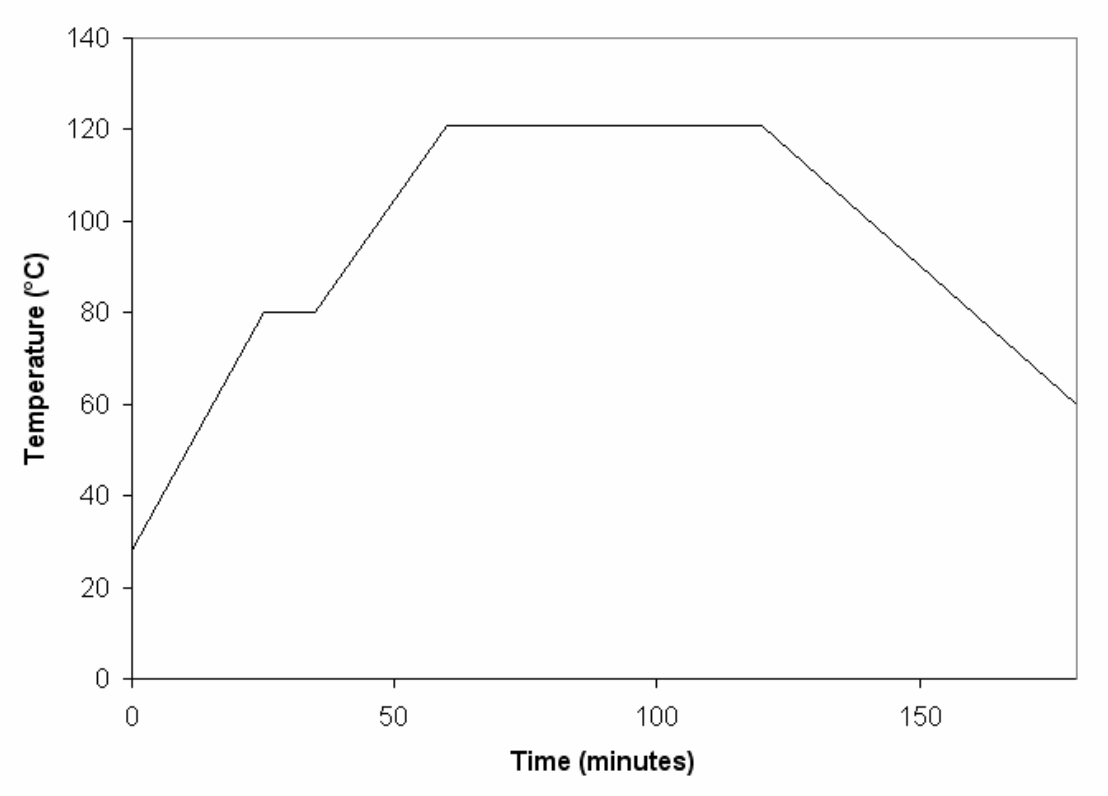

Figure 4. 7 : Curing process graph.

Figure 4. 8 : Composite specimen after curing.

4.1.3 Strain gauge and end tab mounting

Strain gauge is a very important device to measure strain. So, we need to attach it to the specimen. Beside strain gauge, end tabs are also important. End tab is used to prevent slip between specimen and the holder (part of tensile machine). The end result of the specimen after strain gauge and end tab are mounted on can be seen in Figure 4.9.

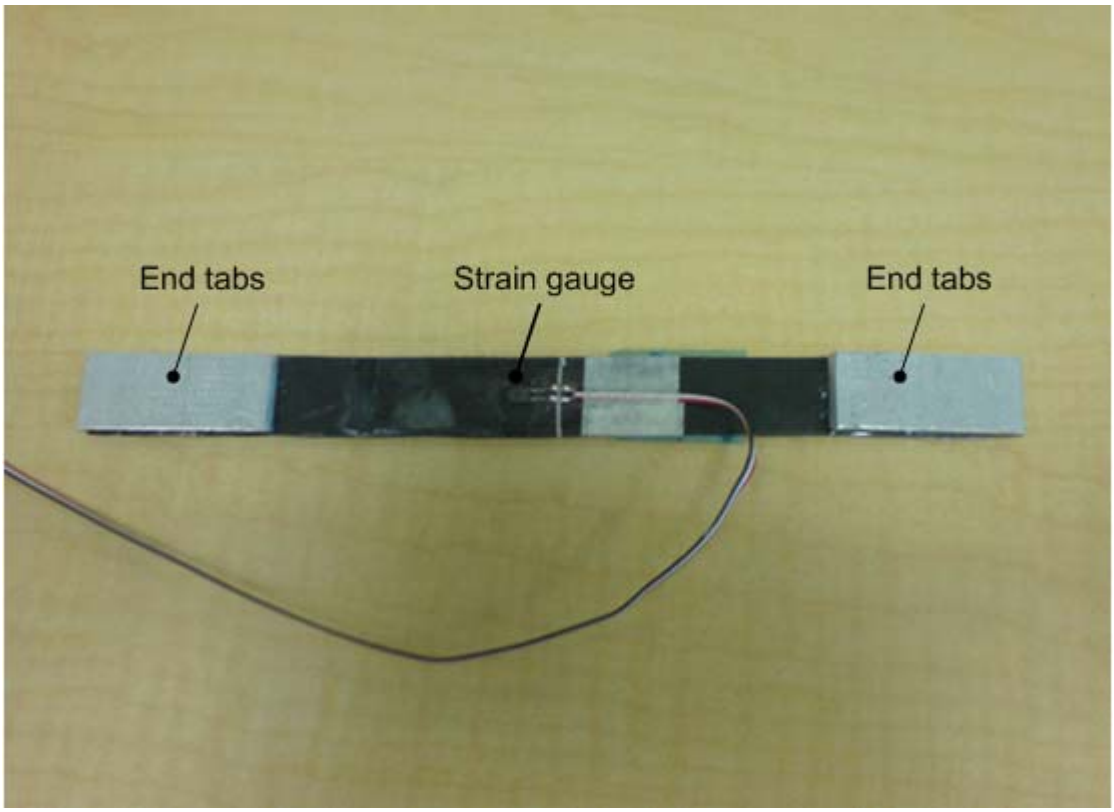

Figure 4. 9 : End result of the specimen after strain gauge and end tab are mounted on.

4.2 Specimen Testing

After specimen preparation finished, the next step is to test the specimen. The machine and equipment used are:

- Instron 5569 Universal Testing Machine

  Instron 5569 is a universal testing machine. It can be used for tensile and compression. Moreover, both tests in certain ambient temperature can be done too. Figure 4.10 shows the figure of this machine.

Figure 4. 10 : Instron 5569 Universal Testing Machine.

- Portable Data Logger TDS-303

  We will use strain gauge in the experiment. Thus, data logger to read the signal from strain gauge is needed. Data logger that will be used in this experiment is Portable Data Logger TDS-303 (Figure 4.11).

The next step is to arrange those devices for the experiment. The final arrangement for the experiment can be seen in Figure 4.12. In the end, the experiment can be started.

Figure 4. 11 : Portable Data Logger TDS-303.

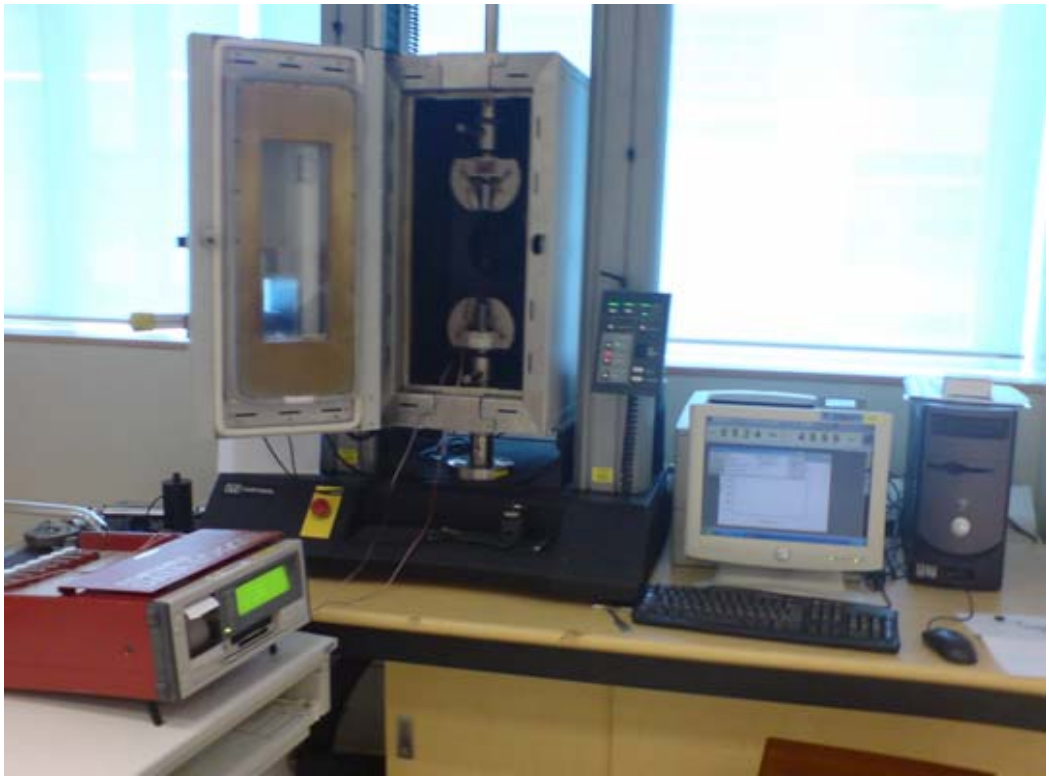

Figure 4. 12 : Final arrangement for the experiment.

Chapter Five

DELAMINATION PROPAGATION

A finite element model to measure energy release rates and stress intensity factors was proposed in Chapter 3 and the results obtained from it will be discussed in this chapter. Those results will be presented and discussed in three sections here: total energy release rate distribution, predominant failure load determination, and crack propagation determination.

5.1 Total Energy Release Rate Distribution

Only two kinds of laminates will be focused on here; symmetric cross ply laminates and symmetric angle ply laminates. Moreover, the effect of delamination position and laminate thickness are also analyzed. Based on that, this section is divided into 6 parts : total energy release rate distribution of $(90°/0°//0°/90°)_t$, $(0°/90°//90°/0°)_t$, $(\theta/-\theta//-\theta/\theta)_t$, $(90°//0°/0°/90°)_t$, $(0°//90°/90°/0°)_t$ and $(\theta//-\theta/-\theta\ /\theta)_t$.

5.1.1 $(90°/0°//0°/90°)_t$ total energy release rate distribution

For the $(90°/0°//0°/90°)_t$ laminate with delamination length equal to 60mm (Figure 5.1) the out of plane deflection results show an opening at the delamination part. Furthermore, Figure 5.2 shows the energy release rate distribution of $(90°/0°//0°/90°)_t$ laminate along the width. The opening that can be seen in Figure 5.1 makes the energy release rate at the mid span become nonzero. Moreover, at the edges the energy release rate results also gives nonzero value. It is mainly because of edge effect.

Practical composites can be of any shape and the thickness can vary from one layer to another. Therefore, study in the effect of thickness is also very important. Three different laminates with different thickness will be used here to study the effect of thickness on energy release rate in $(90°/0°//0°/90°)_t$ laminates. The stacking sequence of these laminates are in the form $((90°/0°)_n//(0°/90°)_n)_t$, where n is equal to 1 (0.5mm thickness), 2 (1mm thickness) and 4 (2mm thickness). The result shows that energy release rates tend to decrease as the thickness increases as shown in Figure 5.3. It is understandable because the magnitude of energy release rate depends on the

magnitude of coupling (in this case B_{11} and B_{22} terms in the classical lamination theory). Furthermore, the effect of coupling will diminish with increasing number of layers in laminate. As a result, the magnitude of energy release rate will be smaller for thicker laminate.

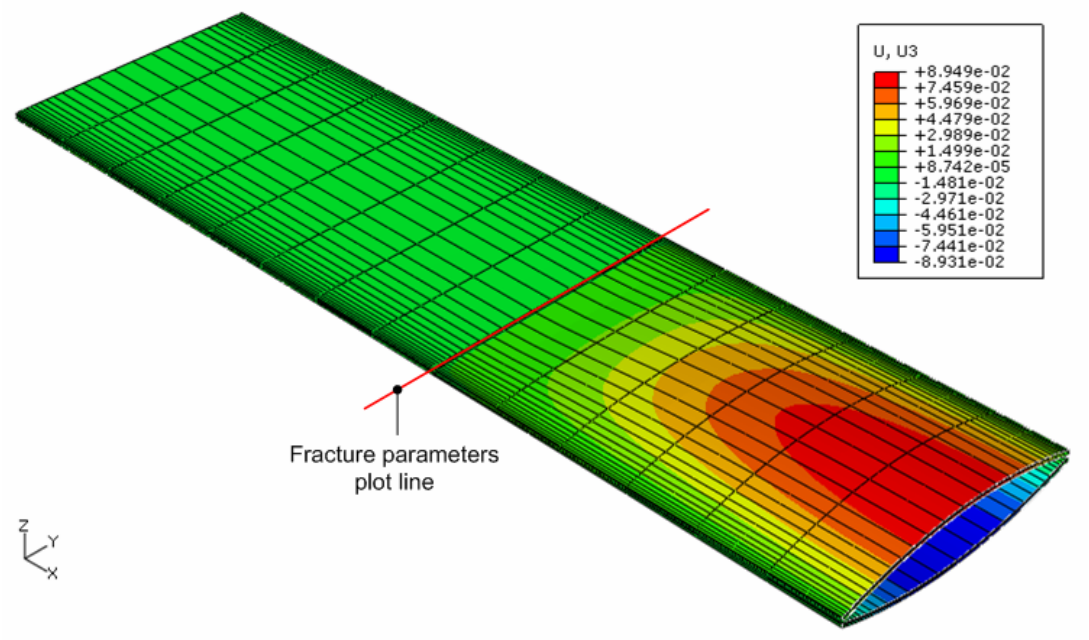

Figure 5. 1 : Finite element U3 deformation result of $(90°/0°//0°/90°)_t$ laminate.

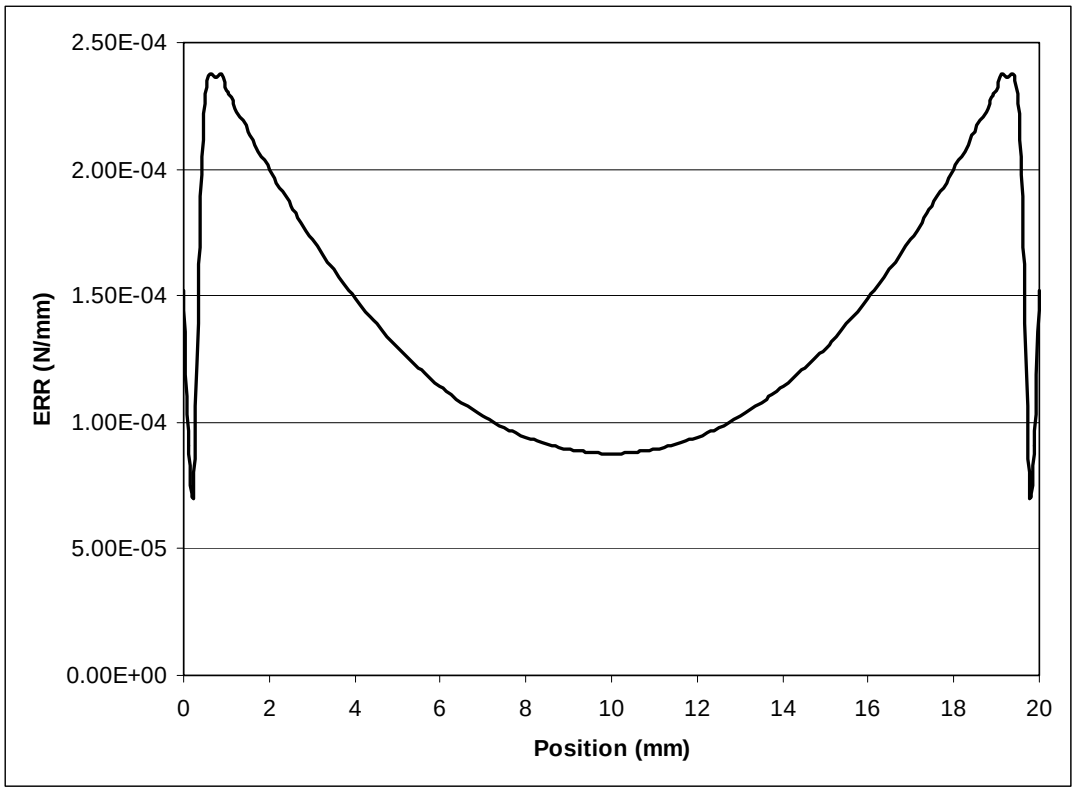

Figure 5. 2 : Energy release rate distribution of $(90°/0°//0°/90°)_t$ laminate.

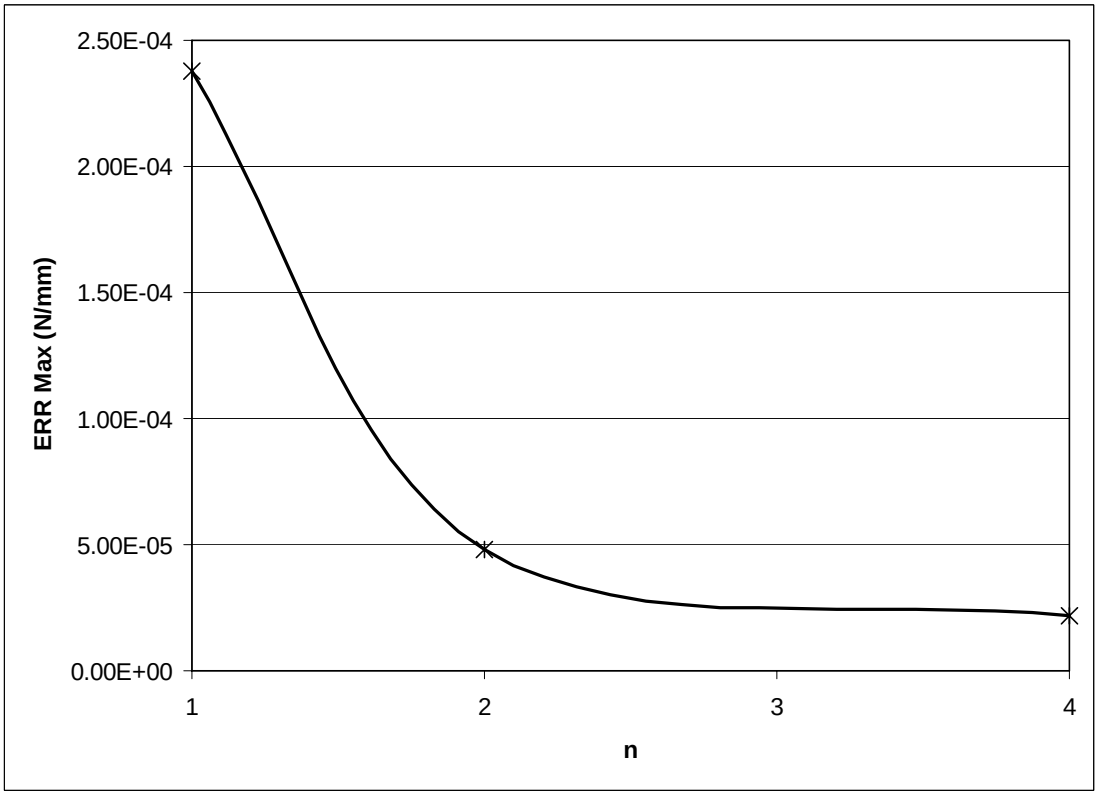

Figure 5. 3 : Maximum energy release rate of $((90°,0°)_n)_s$ laminates, for n equal to 1, 2 and 4.

5.1.2 $(0°/90°//90°/0°)_t$ total energy release rate distribution

The deformed shape of $(0°/90°//90°/0°)_t$ laminate can be seen in figure 5.4. The opening at the edge parts of the initial delamination is obvious and there is a contact in the center part of the delamination. The opening causes a significant increase in the energy release rates of $(0°/90°//90°/0°)_t$ laminate at the edges as shown in Figure 5.5. On the contrary, at the center part the energy release rate are almost zero. Furthermore, to study the thickness effect, we will use $((90°/0°)n//(0°/90°)n)_t$ laminates where n is equal to 1 (0.5mm thickness), 2 (1mm thickness) and 4 (2mm thickness). As shown in Figure 5.6, maximum energy release rate tends to decrease with increasing number of layers in laminate.

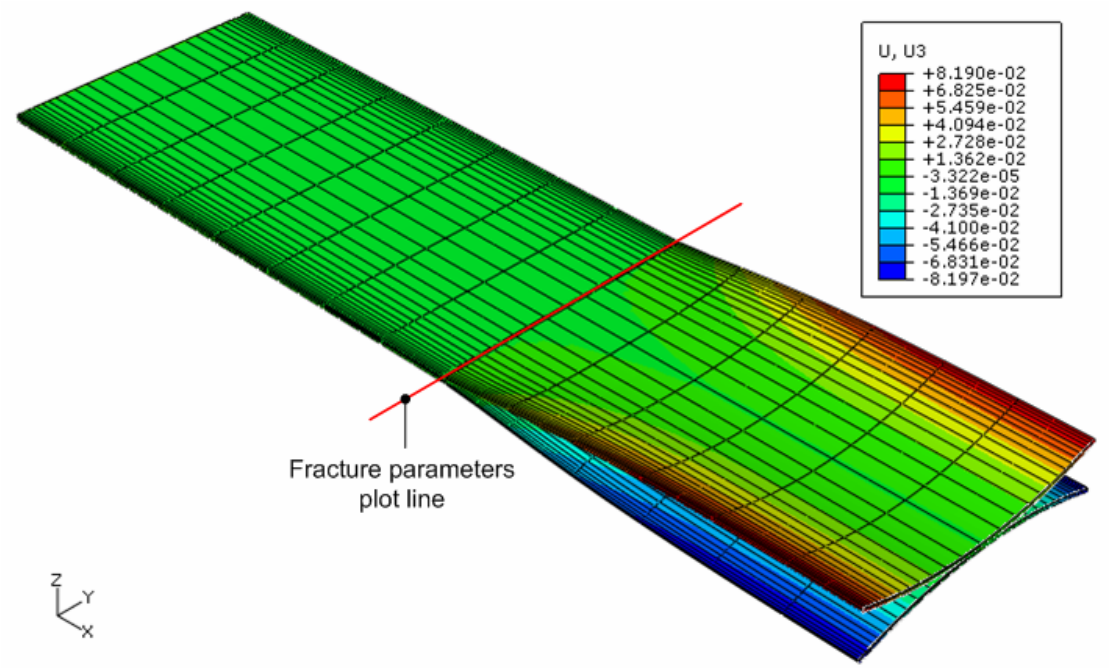

Figure 5. 4 : Finite element U3 deformation result of $(0°/90°//90°/0°)_t$ laminate.

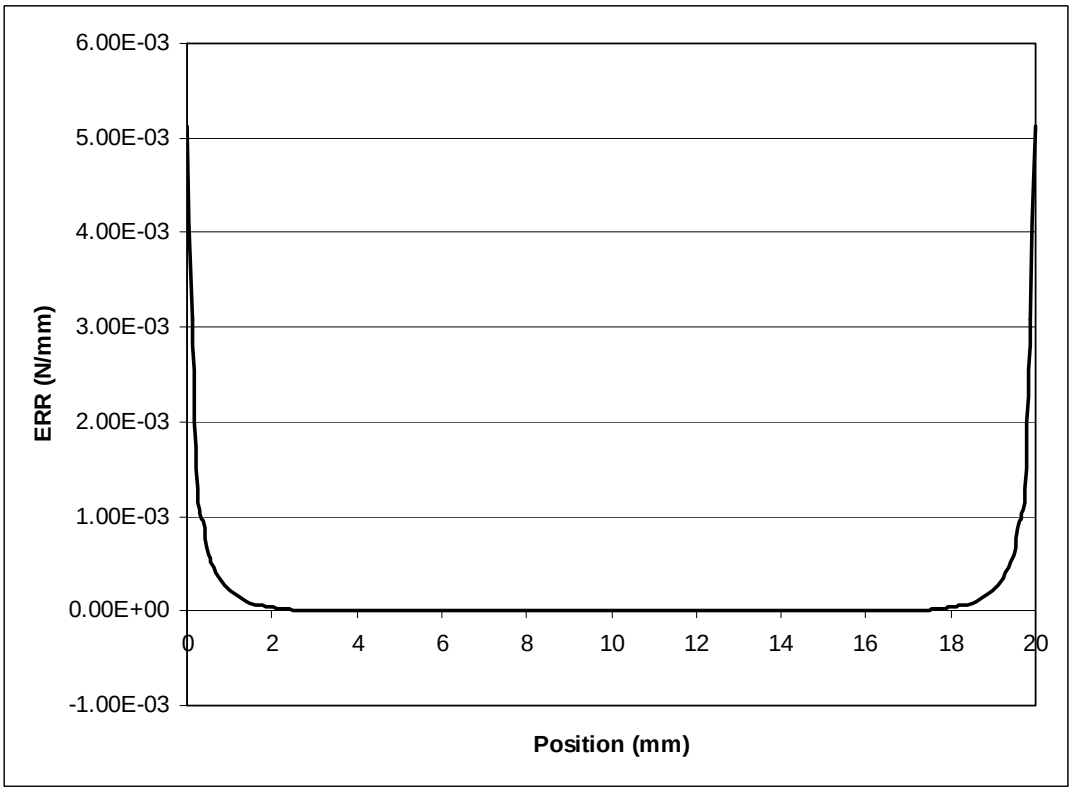

Figure 5. 5 : Energy release rate distribution of $(0°/90°//90°/0°)_t$ laminate for several crack angle.

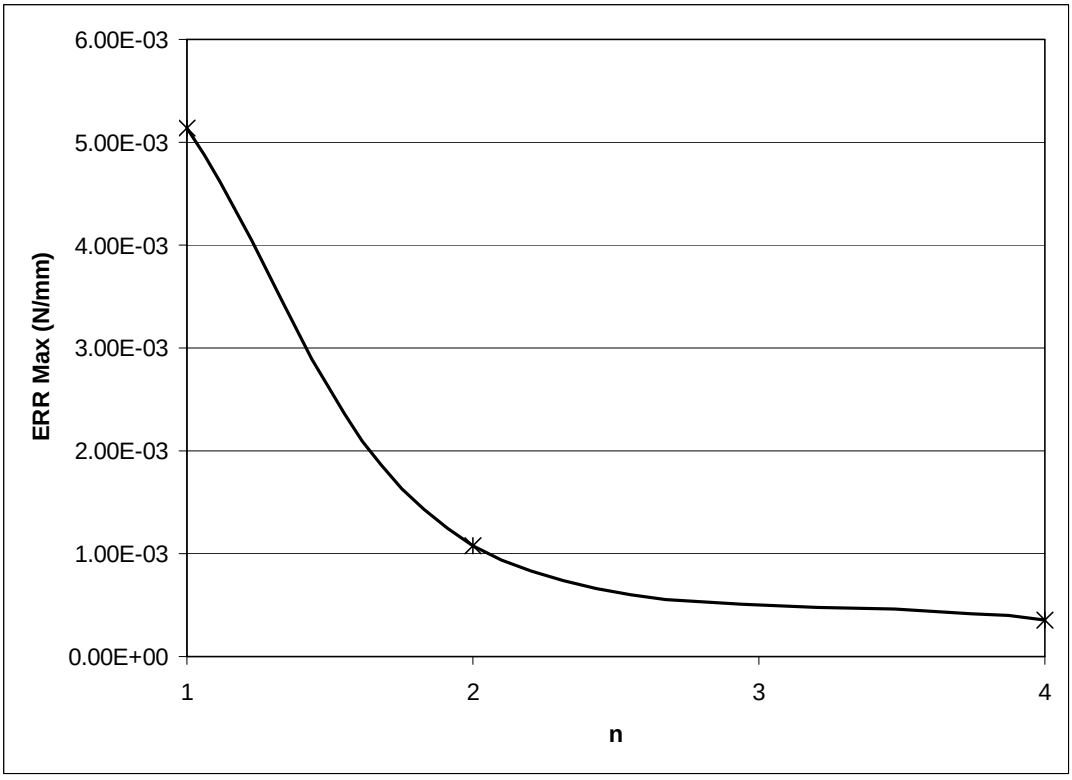

Figure 5. 6 : Maximum energy release rate of $((90°/0°)_n//(0°/90°)_n)_t$ laminates, for n equal to 1, 2 and 4.

5.1.3 $(\theta/-\theta//-\theta/\theta)_t$ total energy release rate distribution

There are three θ that will be used to represent $(\theta/-\theta//-\theta/\theta)_t$ laminate. They are 30°, 45° and 60°. Finite element U3 deformation results of $(30°/-30°//-30°/30°)_t$, $(45°/-45°//-45°/45°)_t$ and $(60°/-60°//-60°/60°)_t$ laminates are shown in Figures 5.7, 5.10 and 5.13 respectively. Unlike $(90°/0°//0°/90°)_t$ and $(0°/90°//90°/0°)_t$ laminates, $(\theta/-\theta//-\theta/\theta)_t$ laminates did not produce an obvious opening or twisting. As a result, compared to both laminates, $(\theta/-\theta//-\theta/\theta)_t$ laminates give less energy release rate (Figure 5.8, 5.11 and 5.14) except at the edge (in the order of 1.10^{-4} at the edge and in the order of 1.10^{-7} at the center part). It must be caused by the edge effect. Furthermore, Figures 5.9, 5.12 and 5.15 also show that the maximum energy release rates tend to decrease as the thickness increases.

The results on Figures 5.7, 5.10 and 5.13 show no twisting. Moreover, from the ABD matrices of upper part and lower part of the delamination in $(\theta/-\theta//-\theta/\theta)_t$ laminates, both B_{16} and B_{26} couplings are not zero. Which means twisting suppose to appear in $(\theta/-\theta//-\theta/\theta)_t$ laminates under tensile load. However, twisting that are produced by upper part and lower part of the delamination in $(\theta/-\theta//-\theta/\theta)_t$ laminates are in the opposite direction to each other. As a result, it makes no twisting appears in $(\theta/-\theta//-\theta/\theta)_t$ laminates.

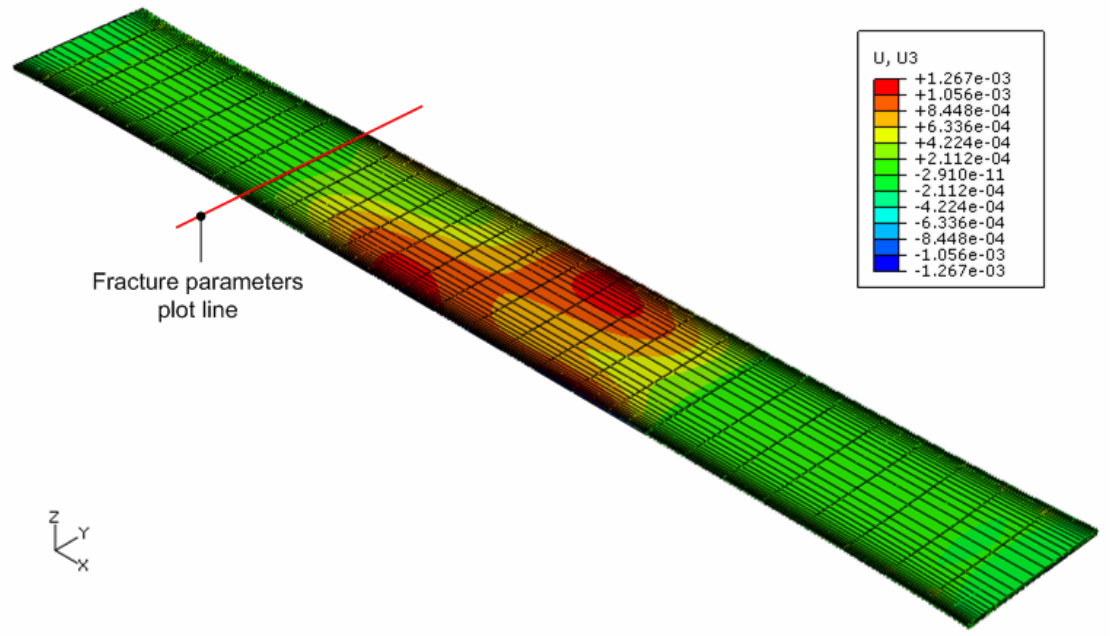

Figure 5. 7 : Finite element U3 deformation result of $(30°/-30°//-30°/30°)_t$ laminate.

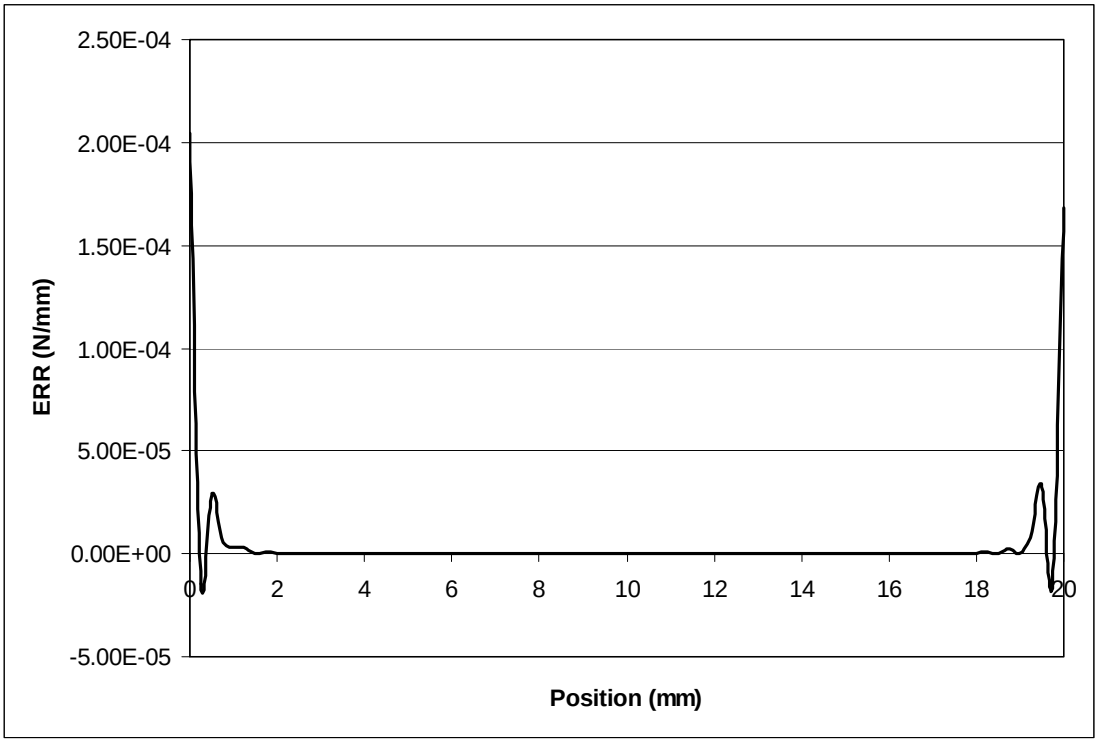

Figure 5. 8 : Energy release rate distribution of $(30°/-30°//-30°/30°)_t$ laminate.

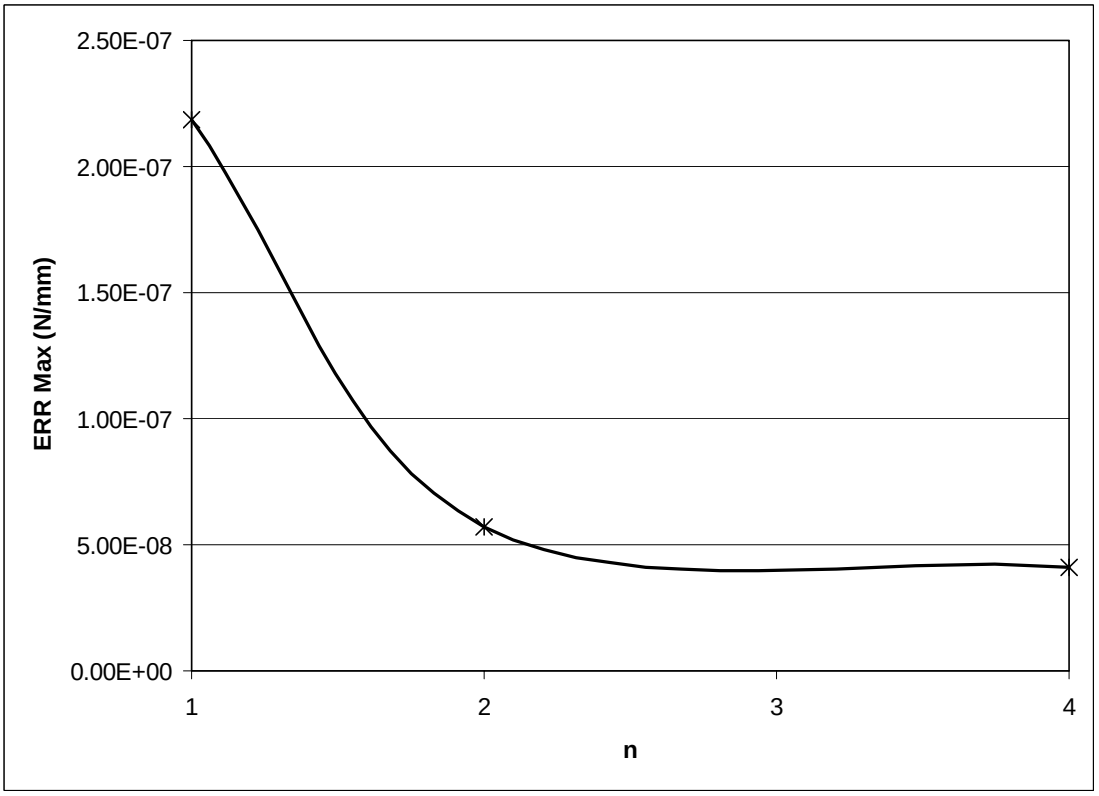

Figure 5. 9 : Maximum energy release rate of $((30°/-30°)_n//(-30°/30°)_n)_t$ laminates, for n equal to 1, 2 and 4.

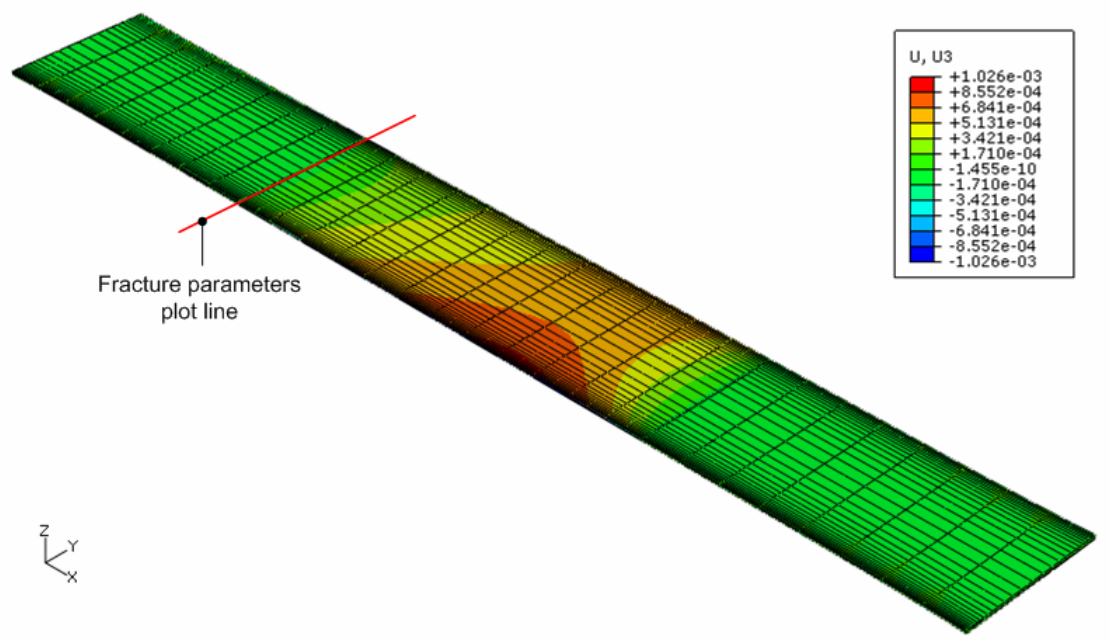

Figure 5. 10 : Finite element U3 deformation result of $(45°/-45°//-45°/45°)_t$ laminate.

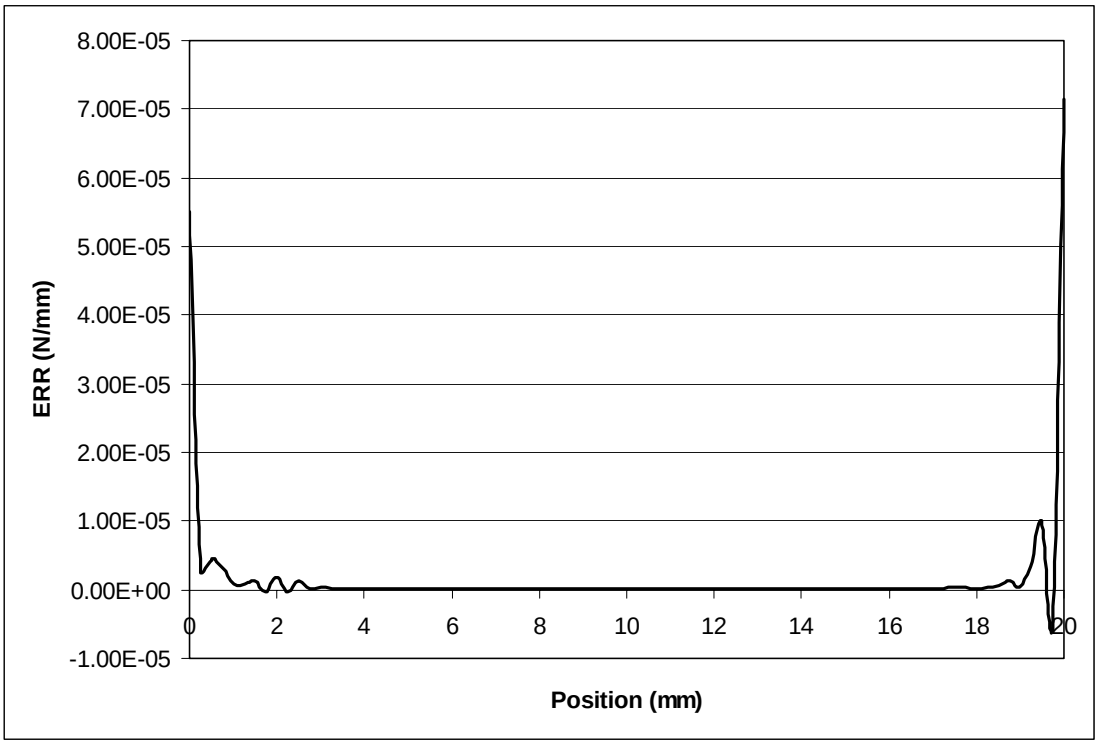

Figure 5. 11 : Energy release rate distribution of $(45°/-45°//-45°/45°)_t$ laminate.

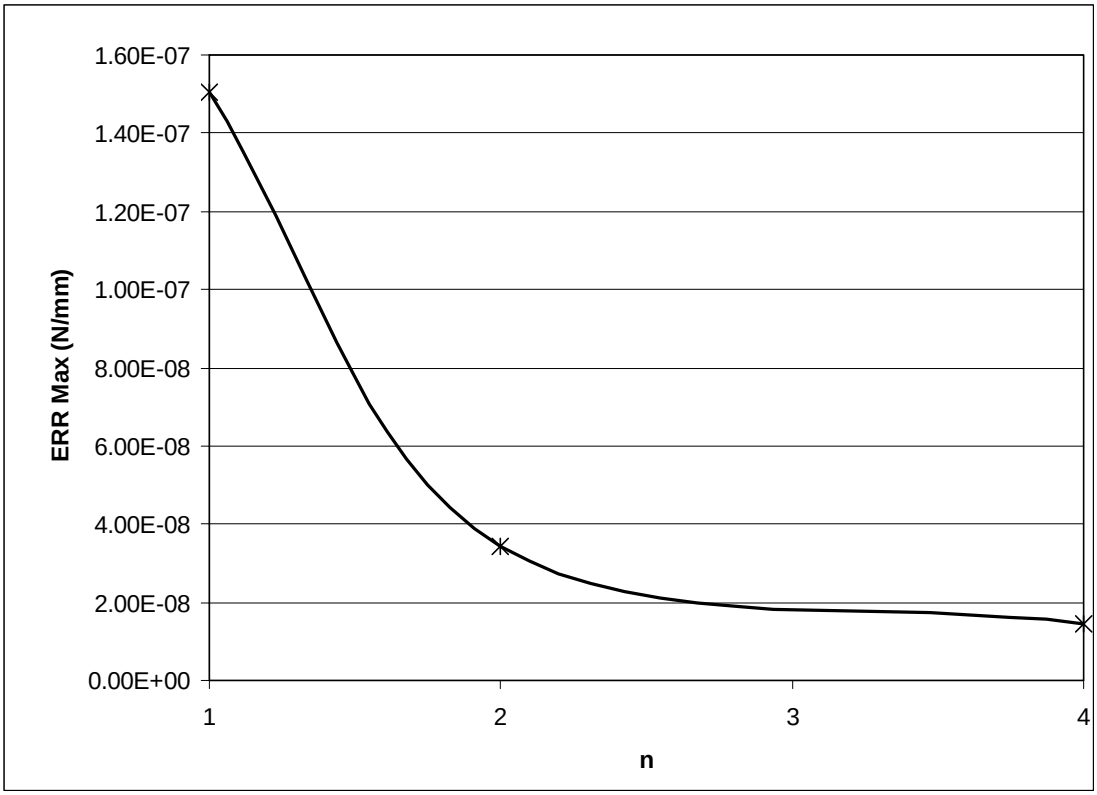

Figure 5. 12 : Maximum energy release rate of $((45°/-45°)_n//(-45°/45°)_n)_t$ laminates, for n equal to 1, 2 and 4.

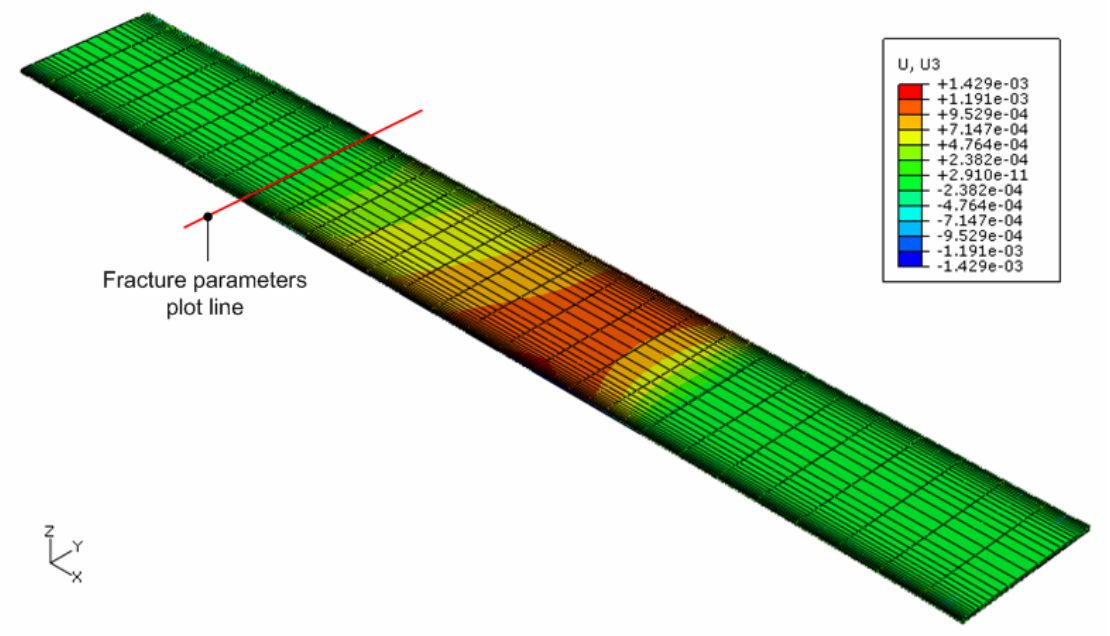

Figure 5. 13 : Finite element U3 deformation result of $(60°/-60°//-60°/60°)_t$ laminate.

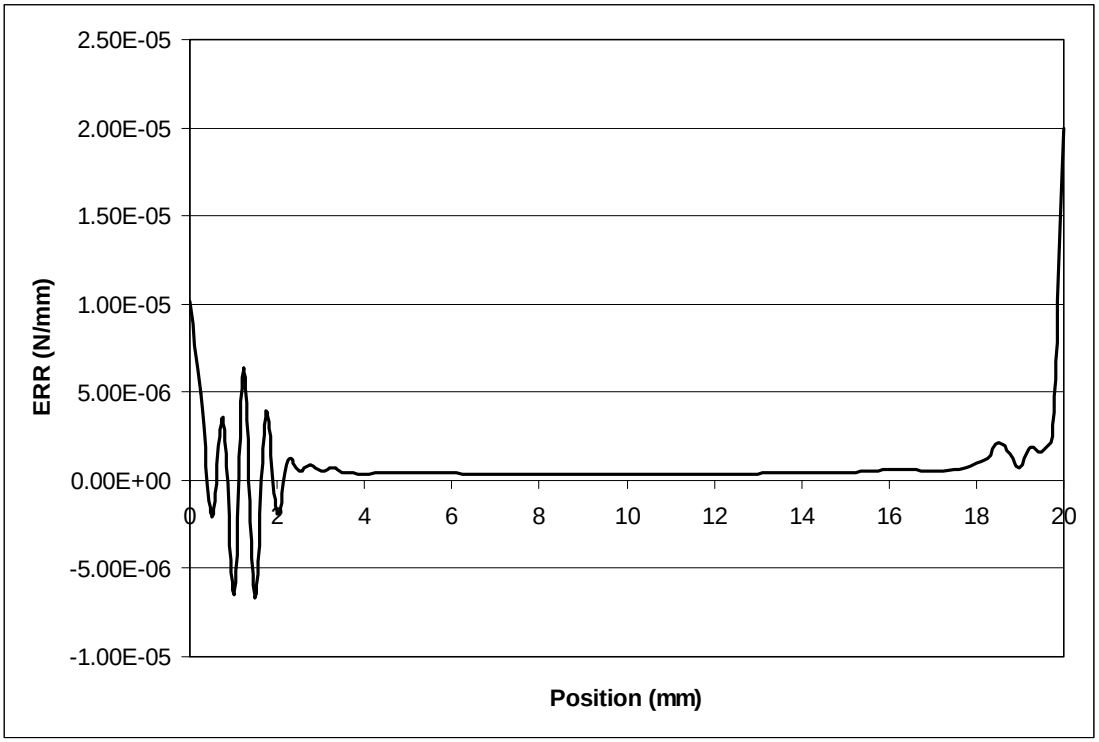

Figure 5. 14 : Energy release rate distribution of $(60°/-60°//-60°/60°)_t$ laminate.

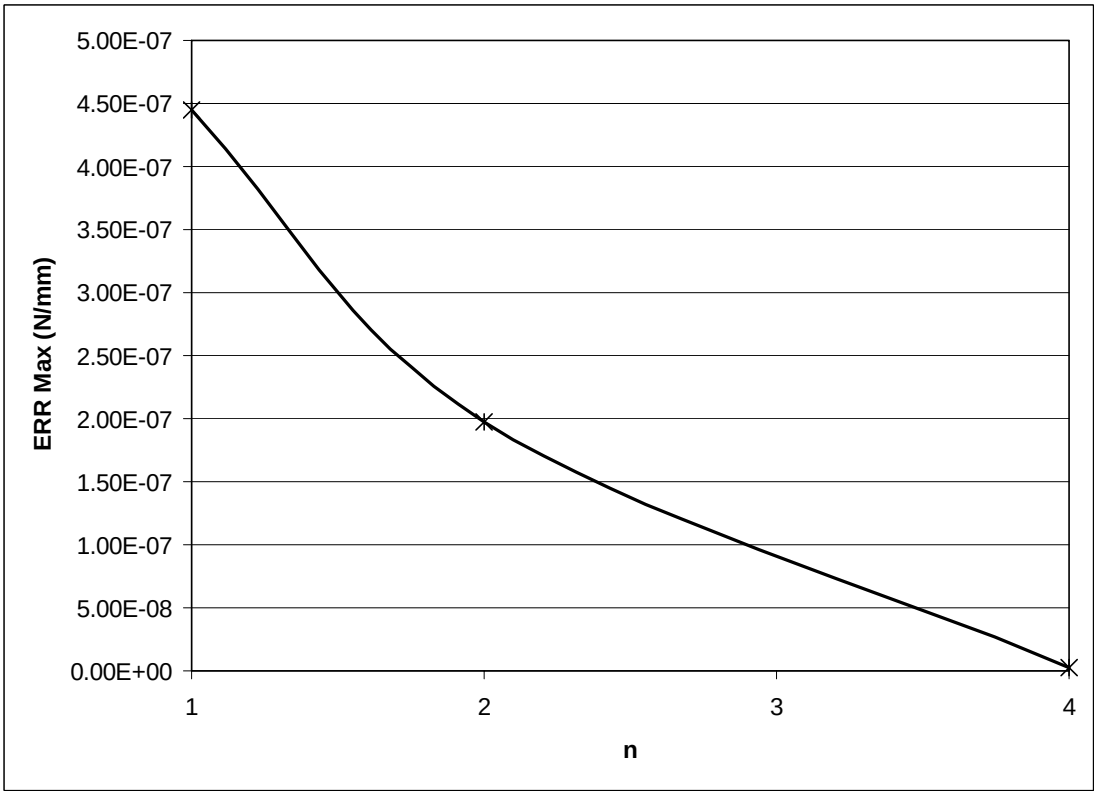

Figure 5. 15 : Maximum energy release rate of $((60°/-60°)_n//(-60°/60°)_n)_t$ laminates, for n equal to 1, 2 and 4.

5.1.4 $(90°//0°/0°/90°)_t$ total energy release rate distribution

Figure 5.16 shows the U3 deformation result of $(90°//0°/0°/90°)_t$ laminate (delamination length = 60mm). From that figure, an opening at the center part of delamination is observed. Compared to the opening that produced by $(90°/0°//0°/90°)_t$ laminate, the opening here is quite different. The opening that produced by $(90°/0°//0°/90°)_t$ laminate is symmetric towards delamination plane. On the other hand, the opening that produced here is not symmetric. It is reasonable because $(90°/0°)_t$ (part above the delamination plane in $(90°/0°//0°/90°)_t$ laminate) and $(0°/90°)_t$ (part under the delamination plane in $(90°/0°//0°/90°)_t$ laminate) give the same value of B_{11} and B_{22} couplings with the opposite sign. Conversely, in $(90°//0°/0°/90°)_t$ laminate, only $(0°/0°/90°)_t$ (part below the delamination plane in $(90°//0°/0°/90°)_t$ laminate) that have B_{11} and B_{22} couplings. As a result, the opening in $(90°//0°/0°/90°)_t$ laminate is not symmetric. Moreover, total energy release rate distribution of $(90°//0°/0°/90°)_t$ laminate can be seen in Figure 5.17. If we look back to Figure 5.16, we can see that the opening of $(90°//0°/0°/90°)_t$ laminate is mainly at the center part. Which means the total energy release rate distribution suppose to be higher at the center part too, unless it is mixed mode case. Later, it can be seen that this is actually mixed mode case and high value of total energy release rates at the edges mainly are caused by mode II and mode III.

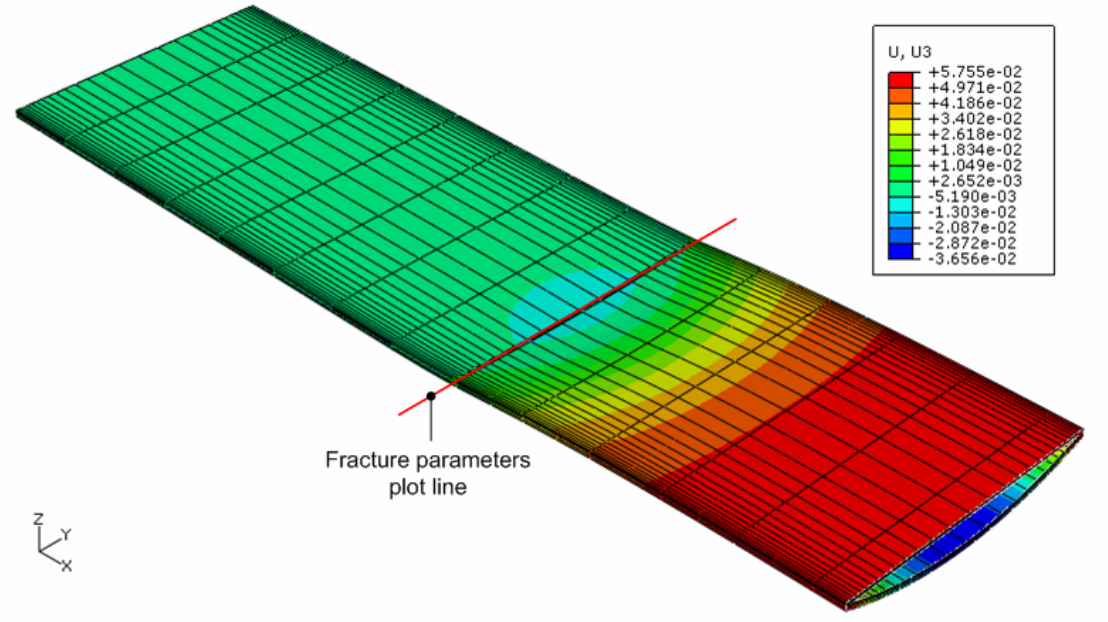

Figure 5. 16 : Finite element U3 deformation result of $(90°//0°/0°/90°)_t$ laminate.

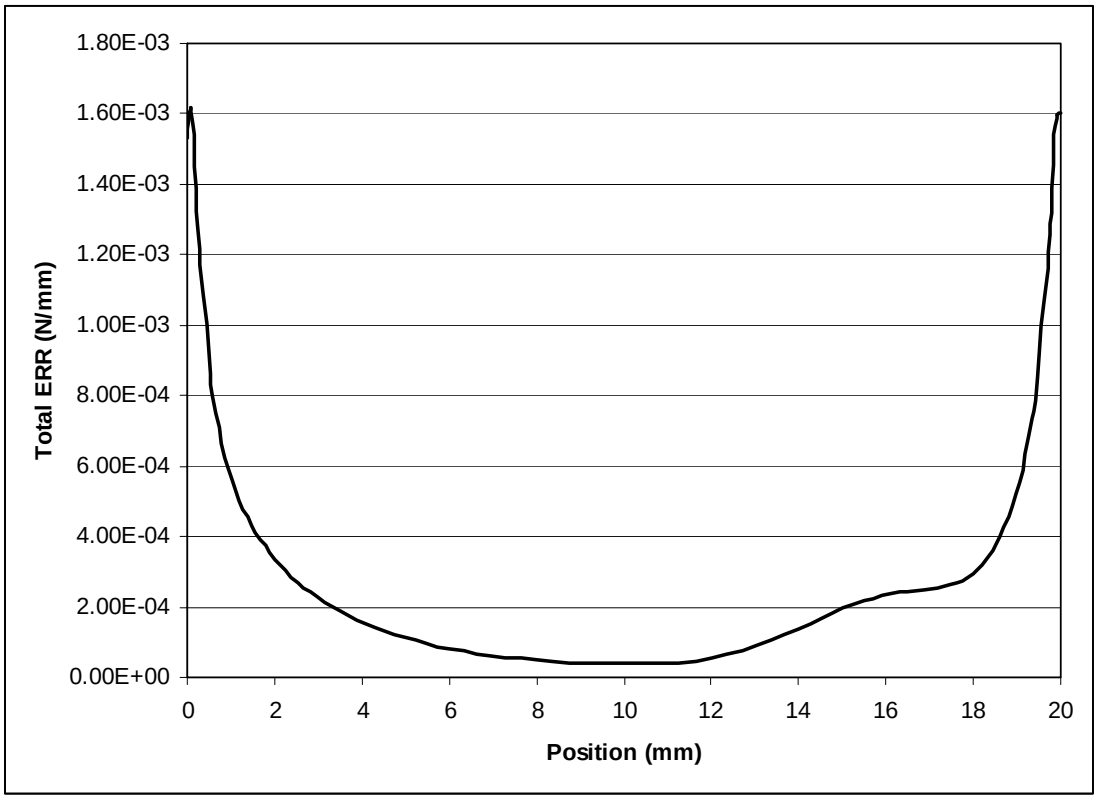

Figure 5. 17 : Energy release rate distribution of $(90°//0°/0°/90°)_t$ laminate.

5.1.5 $(0°//90°/90°/0°)_t$ total energy release rate distribution

Deformed $(0°/90°//90°/0°)_t$ laminate (delamination length = 60mm) shows the slight opening at the edges (Figure 5.18). The same as $(90°//0°/0°/90°)_t$ laminate, $(0°/90°//90°/0°)_t$ laminate also produced non symmetric opening towards the delamination plane. In addition, Figure 5.19 shows the total energy release rate distribution of $(0°/90°//90°/0°)_t$ laminate which gives the maximum value at the edges.

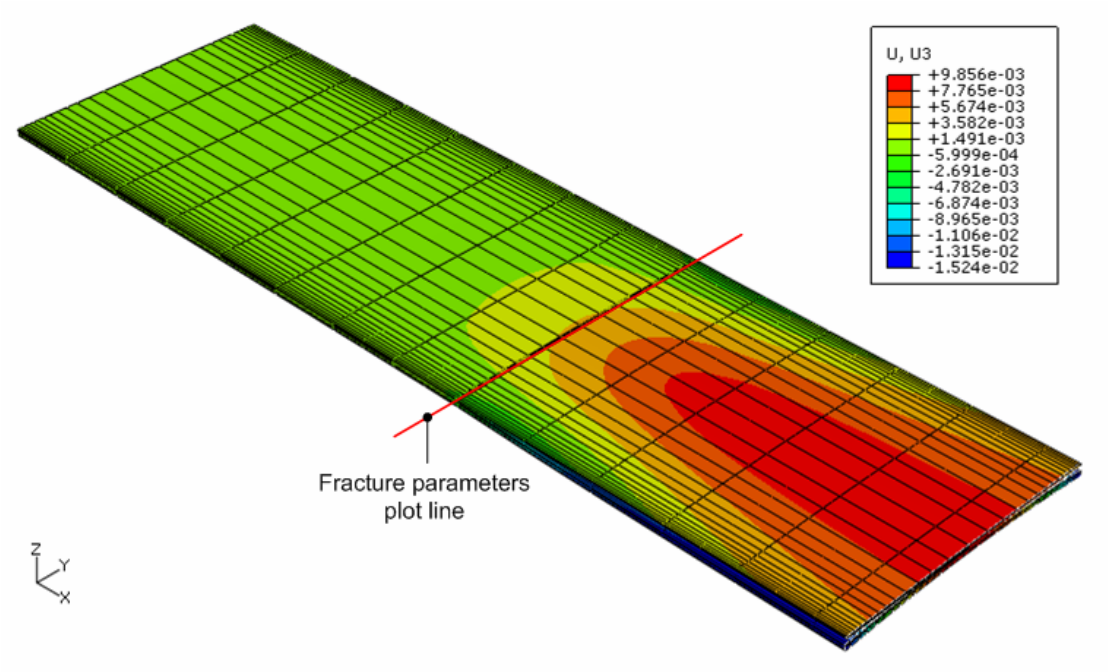

Figure 5. 18 : Finite element U3 deformation result of $(0°//90°/90°/0°)_t$ laminate.

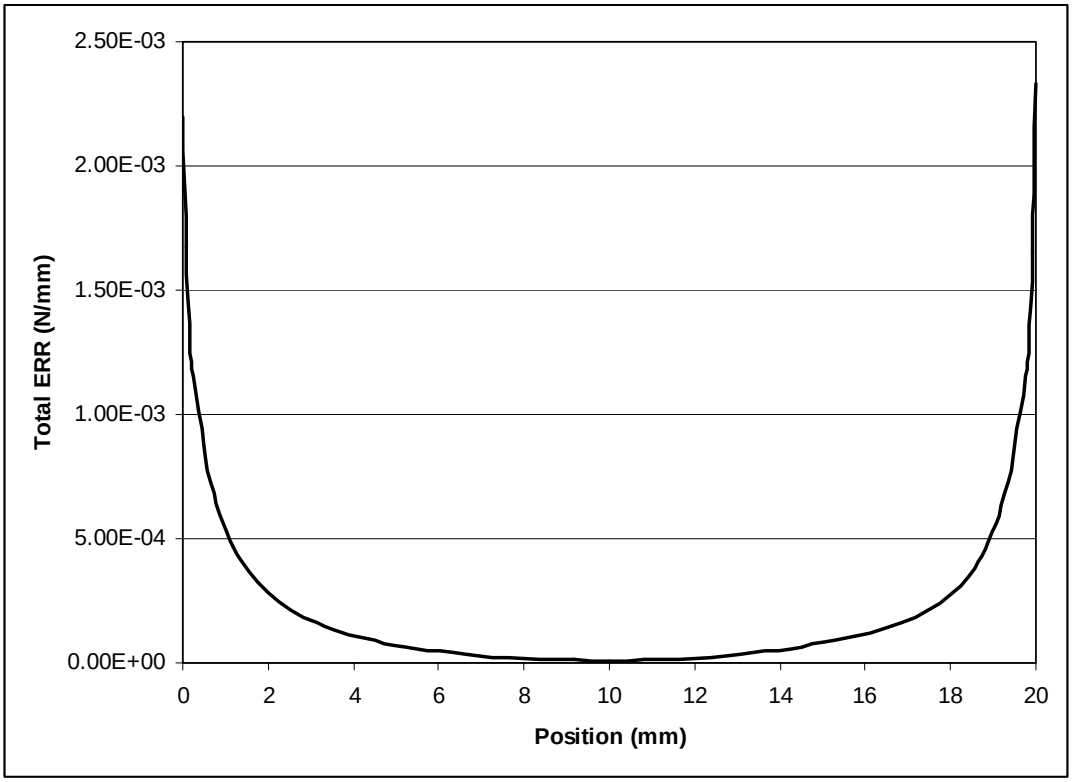

Figure 5. 19 : Total energy release rate distribution of $(0°//90°/90°/0°)_t$ laminate.

5.1.6 $(\theta//-\theta/-\theta/\theta)_t$ total energy release rate distribution

$(30°//-30°/-30°/30°)_t$, $(45°//-45°/-45°/45°)_t$ and $(60°//-60°/-60°/60°)_t$ laminates will be used to represent $(\theta//-\theta/-\theta/\theta)_t$ laminates. Furthermore, Figures 5.20, 5.22, 5.24 show the U3 deformation results of $(30°//-30°/-30°/30°)_t$, $(45°//-45°/-45°/45°)_t$ and $(60°//-60°/-60°/60°)_t$ laminates (delamination length = 60mm) respectively. We can see twisting from all of those figures. Unlike $(\theta/-\theta//-\theta/\theta)_t$ laminates, in $(\theta//-\theta/-\theta/\theta)_t$ laminates only the lower part of delamination ($(-\theta/-\theta/\theta)_t$) that produces B_{16} and B_{26} couplings. It makes twisting can appear in $(\theta/-\theta//-\theta/\theta)_t$ laminates. Additionally the distribution of total energy release rate in $(30°//-30°/-30°/30°)_t$, $(45°//-45°/-45°/45°)_t$ and $(60°//-60°/-60°/60°)_t$ laminates can be seen in Figures 5.21, 5.23 and 5.25 respectively. From the same figures we can see that compared to other laminates, $(\theta/-\theta//-\theta/\theta)_t$ laminates give much higher total energy release rates. It can be seen that $(30°//-30°/-30°/30°)_t$ gives total energy release rate in the order of 10^{-1} and the other laminates give the maximum total energy release rate in the order of 10^{-3}. Thus, it is important to study $(\theta/-\theta//-\theta/\theta)_t$ laminates thoroughly.

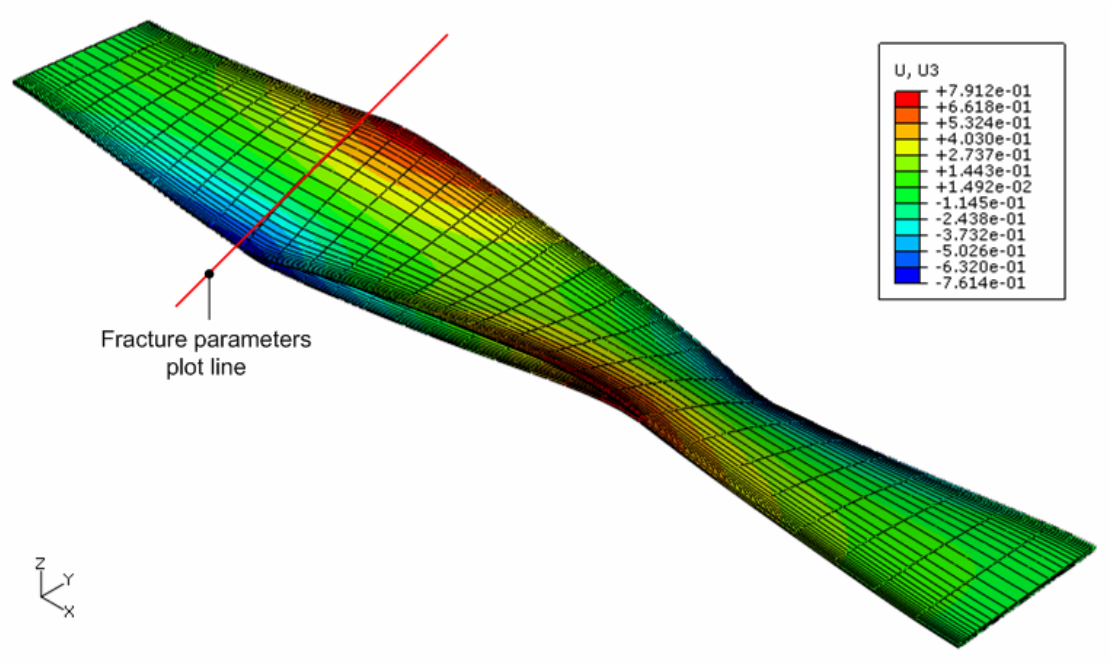

Figure 5. 20 : Finite element U3 deformation result of $(30°//-30°/-30°/30°)_t$ laminate.

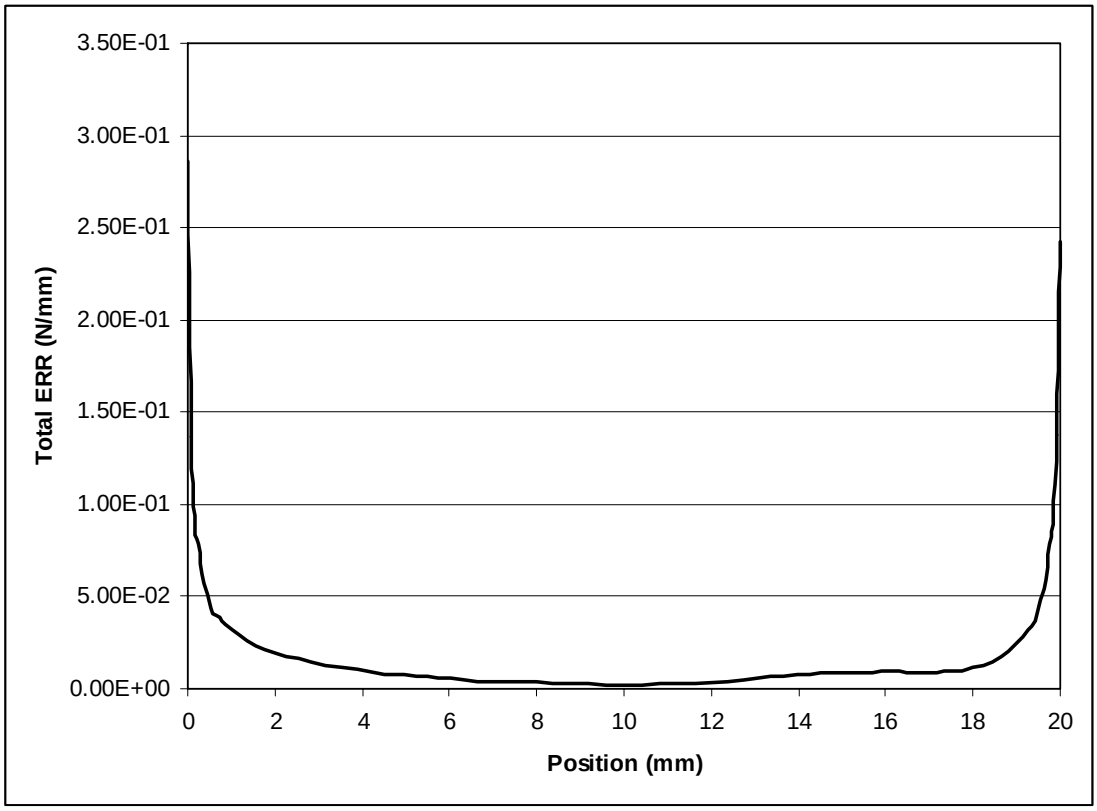

Figure 5. 21 : Total energy release rate distribution of $(30°//-30°/-30°/30°)_t$ laminate.

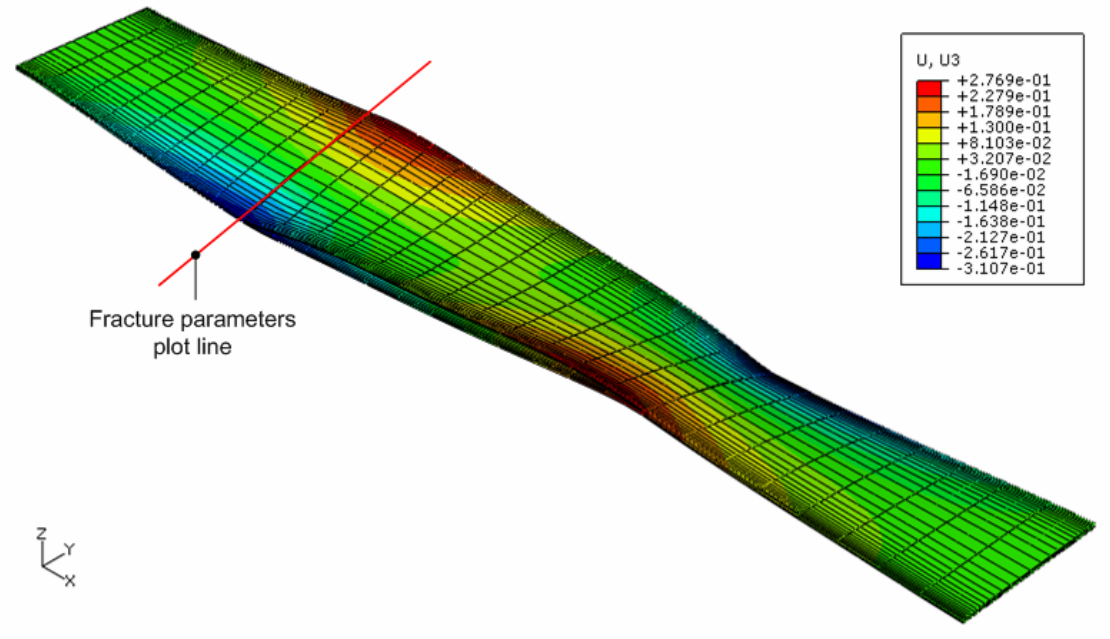

Figure 5. 22 : Finite element U3 deformation result of $(45°//-45°/-45°/45°)_t$ laminate.

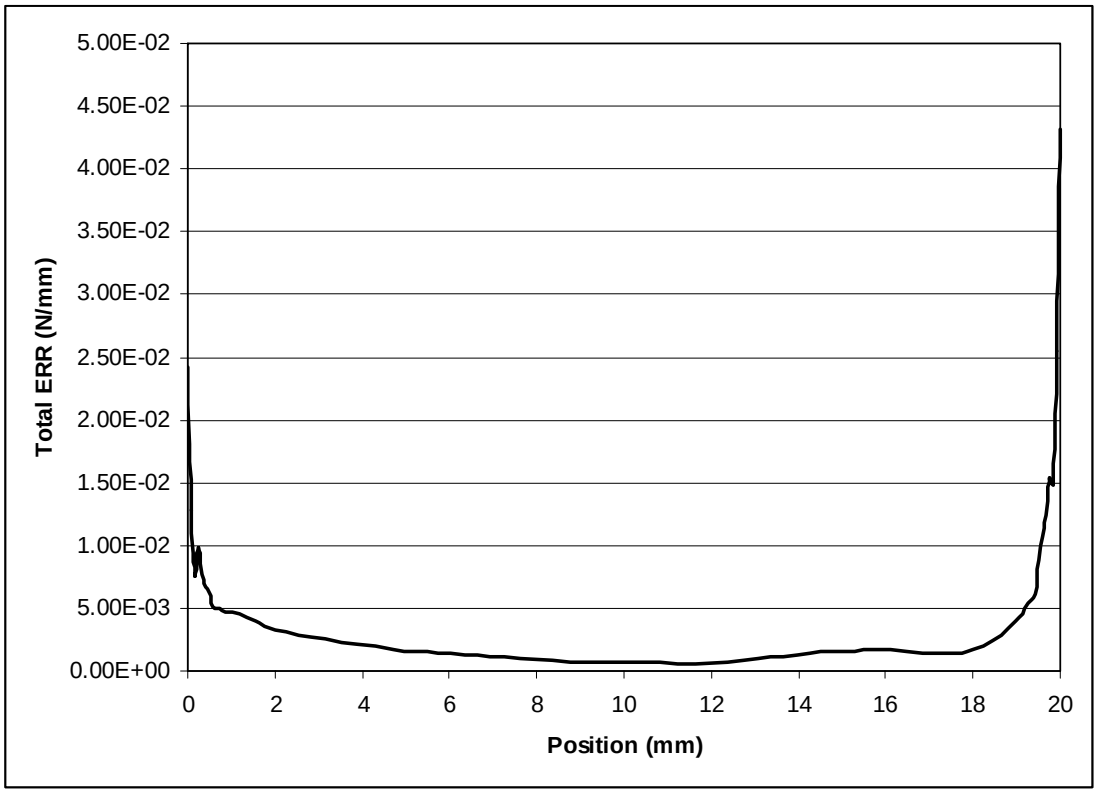

Figure 5. 23 : Total energy release rate distribution of $(45°//-45°/-45°/45°)_t$ laminate.

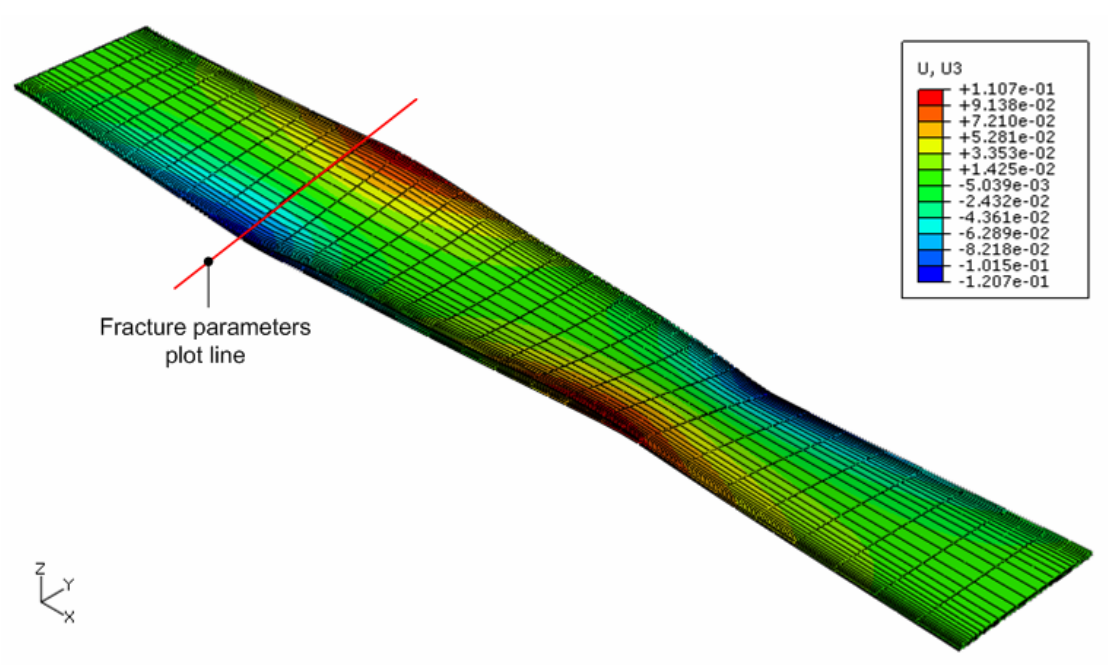

Figure 5. 24 : Finite element U3 deformation result of $(60°//-60°/-60°/60°)_t$ laminate.

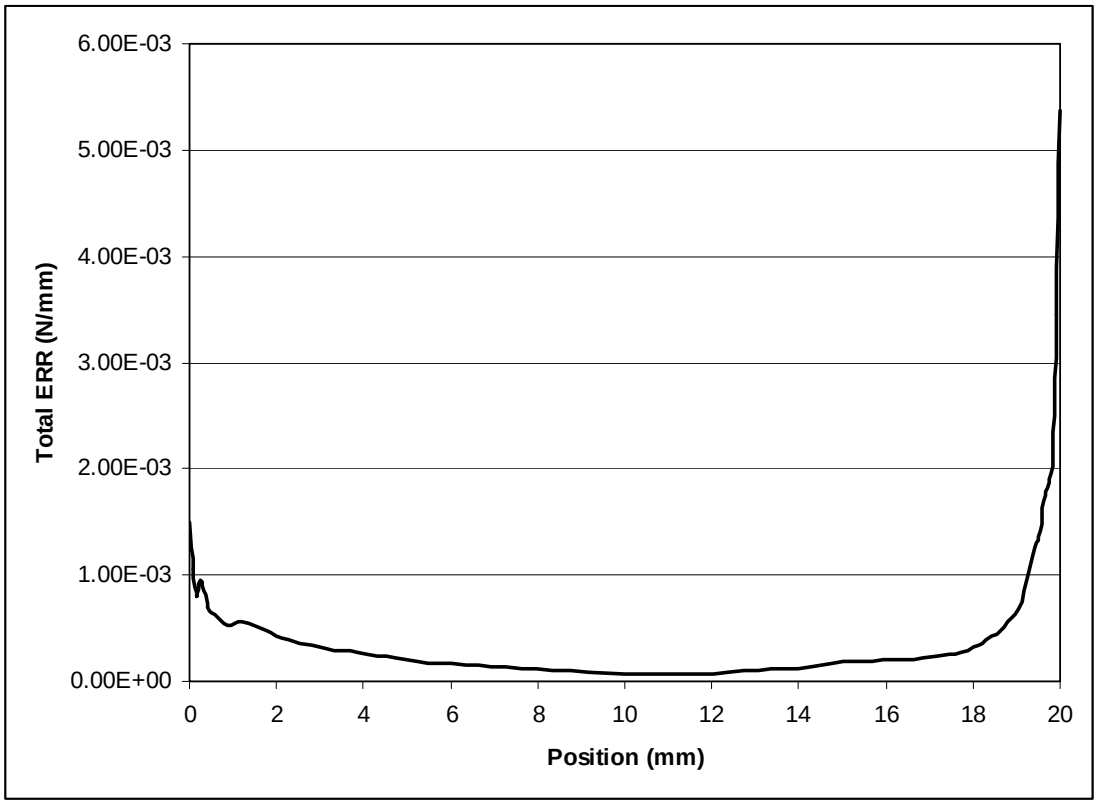

Figure 5. 25 : Total energy release rate distribution of $(60°//-60°/-60°/60°)_t$ laminate.

To study $(\theta/-\theta//-\theta/\theta)_t$ laminates thoroughly, the delamination length as well as the lamination angle (θ) are varied. The delamination length will be used here are 10mm, 20mm, 40mm, 60mm, and 100mm. Furthermore, beside 30°, 45° and 60° lamination angles, we also studied 10°, 20° and 80° lamination angles. The maximum total energy release rates with variation in delamination length and lamination angle can be seen in Figures 5.26 and 5.27 respectively. From Figure 5.26, it is obvious that the highest maximum total energy release rates emerge when delamination length reach 40mm to 60mm. Moreover, Figure 5.27 shows that $(20°//-20°/-20°/20°)_t$ laminate is the most critical one in almost every delamination length (except delamination length = 100mm).

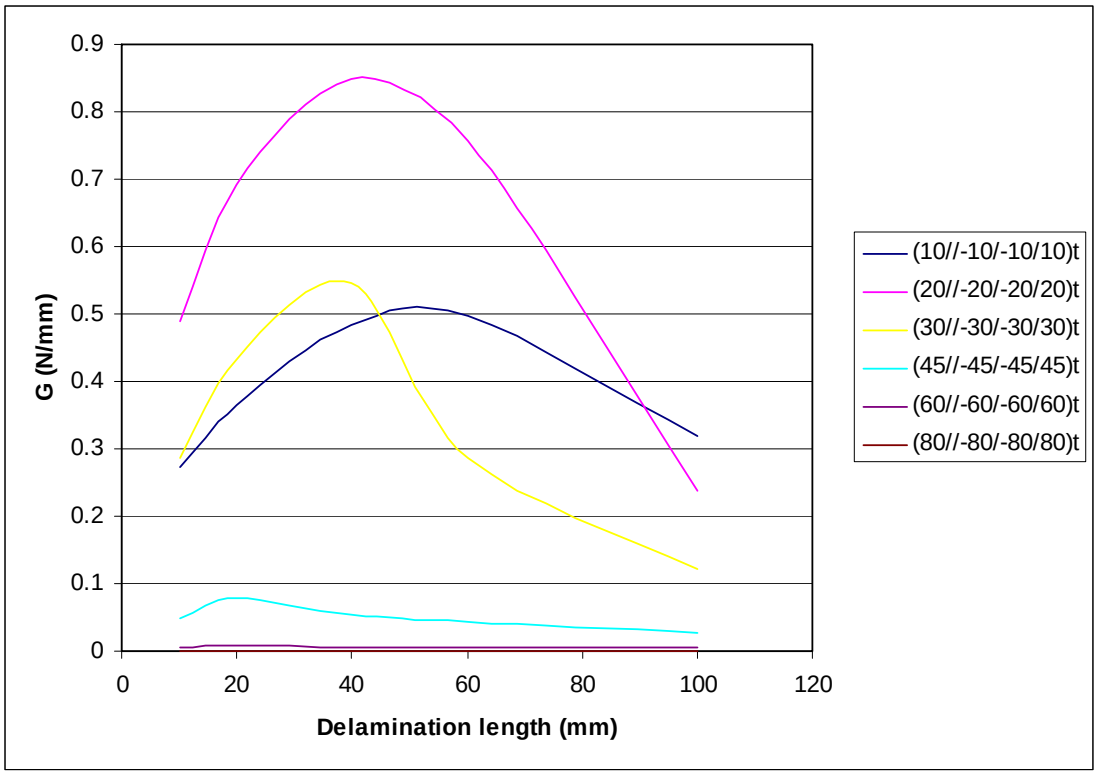

Figure 5. 26 : Maximum total energy release rates comparison with variation in delamination length.

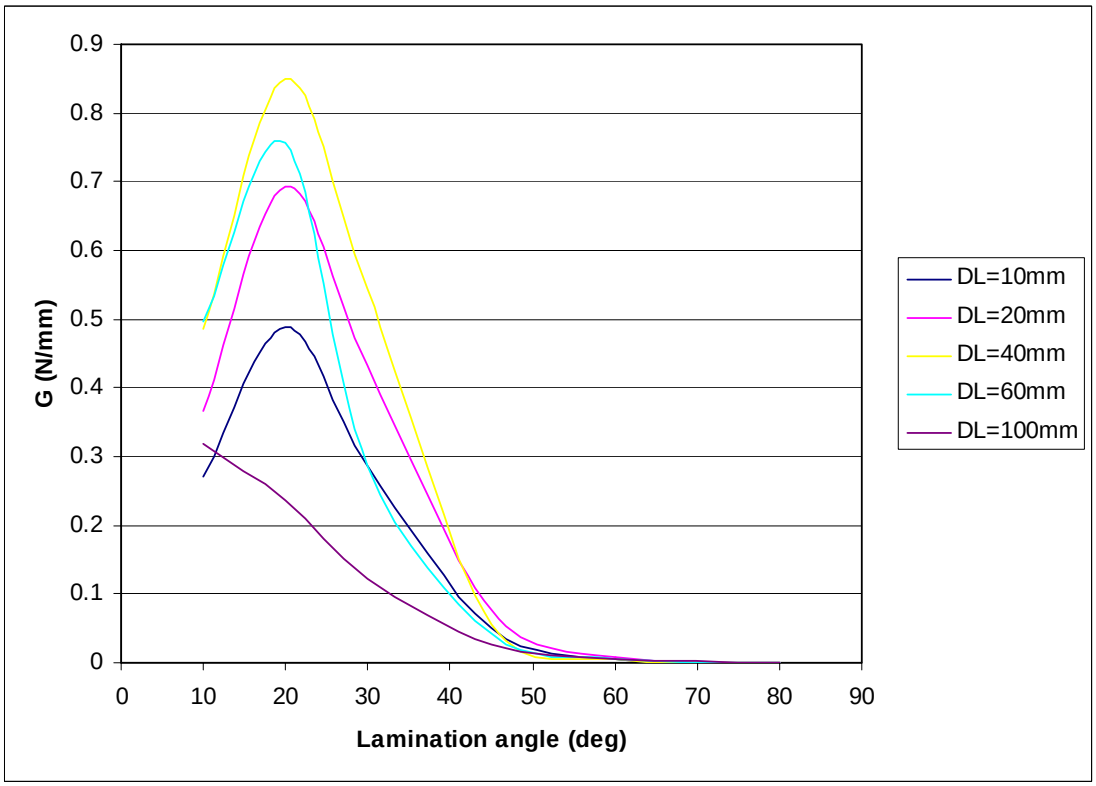

Figure 5. 27 : Maximum total energy release rates comparison with variation in lamination angle.

5.2 Predominant Failure Mode Determination

In chapter 2, 3 possible modes of failure were discussed: opening (mode I), shearing (mode II) and tearing (mode III). The purpose of this subchapter is to find out the predominant failure mode so the way crack will propagate can be predicted. Therefore, each mode of fracture toughness parameter will be compared with each other. In this subchapter, fracture toughness parameter that will be used is stress intensity factor.

5.2.1 $(90°/0°//0°/90°)_t$ laminates predominant failure mode determination

In Figure 5.1, the predominant failure mode for $(90°/0°//0°/90°)_t$ laminate appears to be the mode I. This deduction is further confirmed with the results of K_I, K_{II} and K_{III} distribution of $(90°/0°//0°/90°)_t$ laminate (Figure 5.28). Thus, can be concluded that the predominant mode for $(90°/0°//0°/90°)_t$ laminate is the opening mode (mode I).

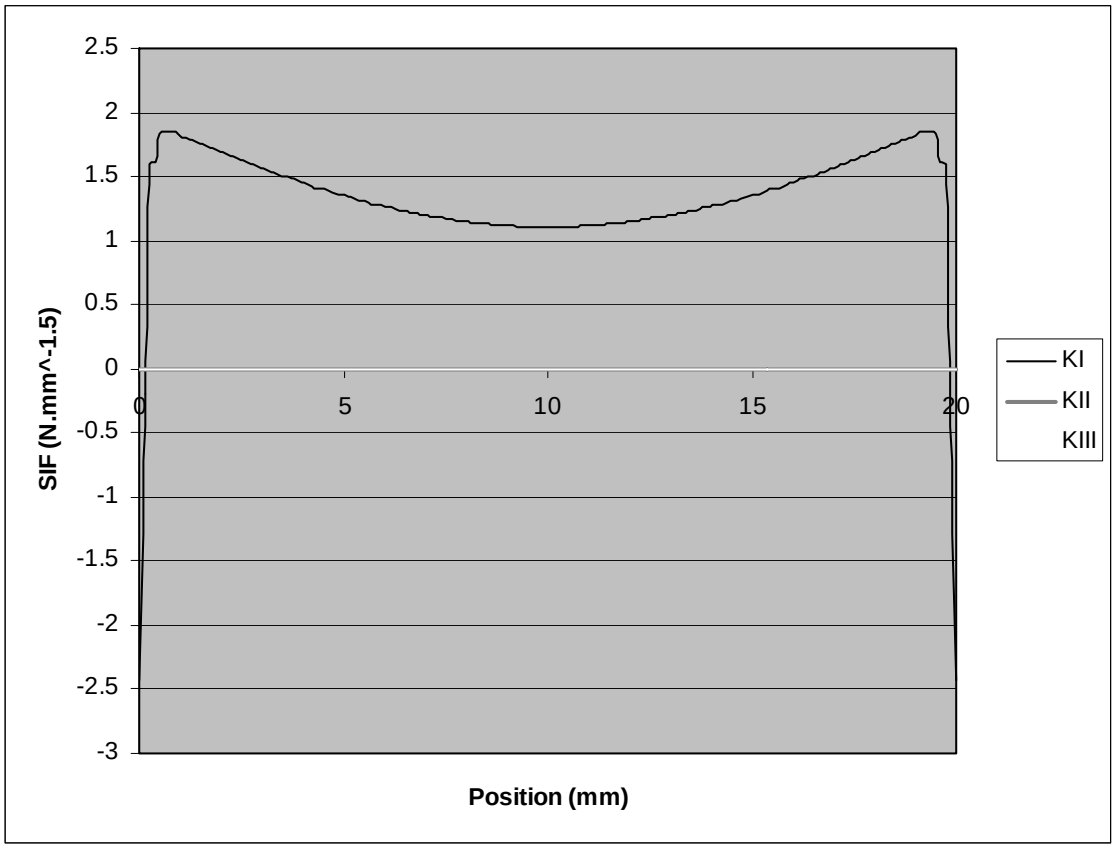

Figure 5. 28 : K_I, K_{II} and K_{III} distribution of $(90°/0°//0°/90°)_t$ laminate.

5.2.2 $(0°/90°//90°/0°)_t$ laminates predominant failure mode determination

Figure 5.29 shows the distribution of K_I, K_{II} and K_{III} for the $(0°/90°//90°/0°)_t$ laminate. From this figure, we can see that the value of K_I is much higher than K_{II} and K_{III}. Referring back to Figure 5.4, the $(0°/90°//90°/0°)_t$ laminate specimen opens up indicating a probable mode I type of fracture. As a result, it can be concluded that the predominant failure mode in $(0°/90°//90°/0°)_t$ laminate is the opening mode (mode I).

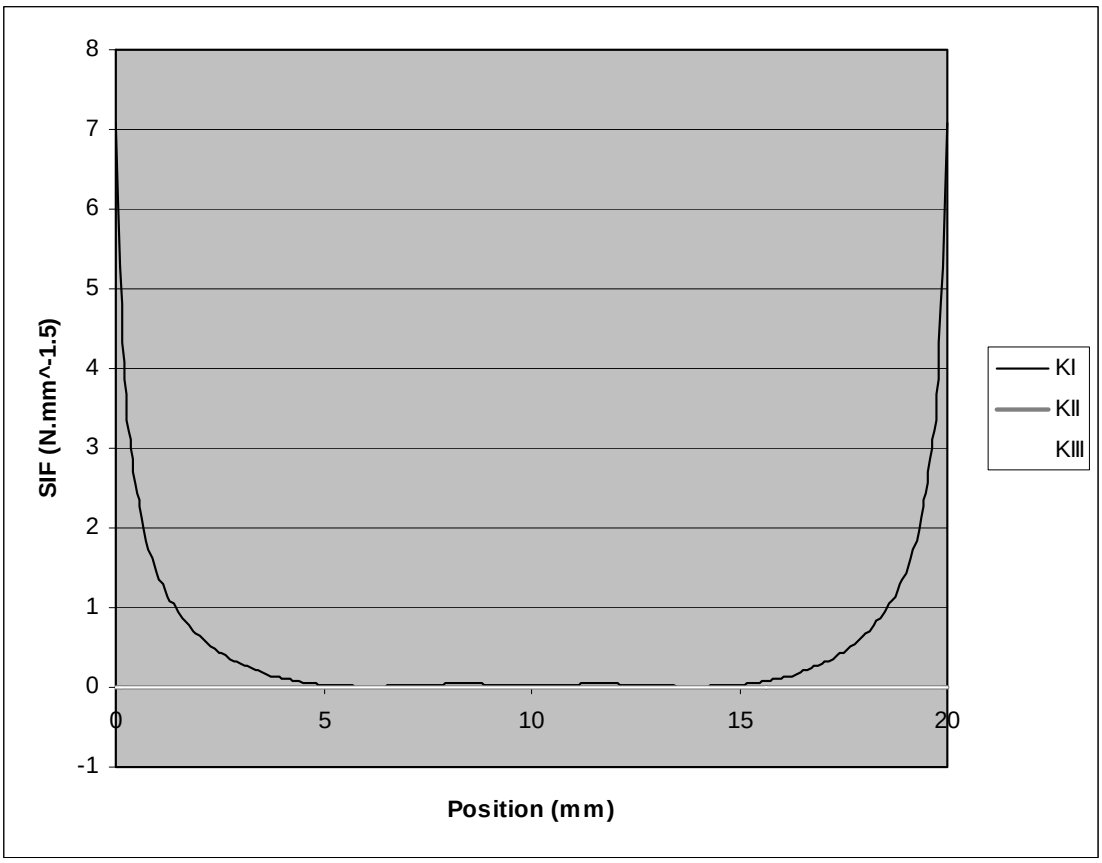

Figure 5. 29 : K_I, K_{II} and K_{III} distribution of $(0°/90°//90°/0°)_t$ laminate.

5.2.3 $(\theta/-\theta//-\theta/\theta)_t$ laminates predominant failure mode determination

Referring back to Figures 5.7, 5.10 and 5.13, $(\theta/-\theta//-\theta/\theta)_t$ laminates did not give an opening or twisting. Despite that fact, Figures 5.30, 5.31 and 5.32 show the distribution of K_I, K_{II} and K_{III} for $(30°/-30°//-30°/30°)_t$, $(45°/-45°//-45°/45°)_t$ and $(60°/-60°//-60°/60°)_t$ laminates, which show that K_I is much higher than K_{II} and K_{III}. Consequently, it can be concluded the predominant mode of failure of $(\theta/-\theta//-\theta/\theta)_t$ laminates are the opening mode (mode I).

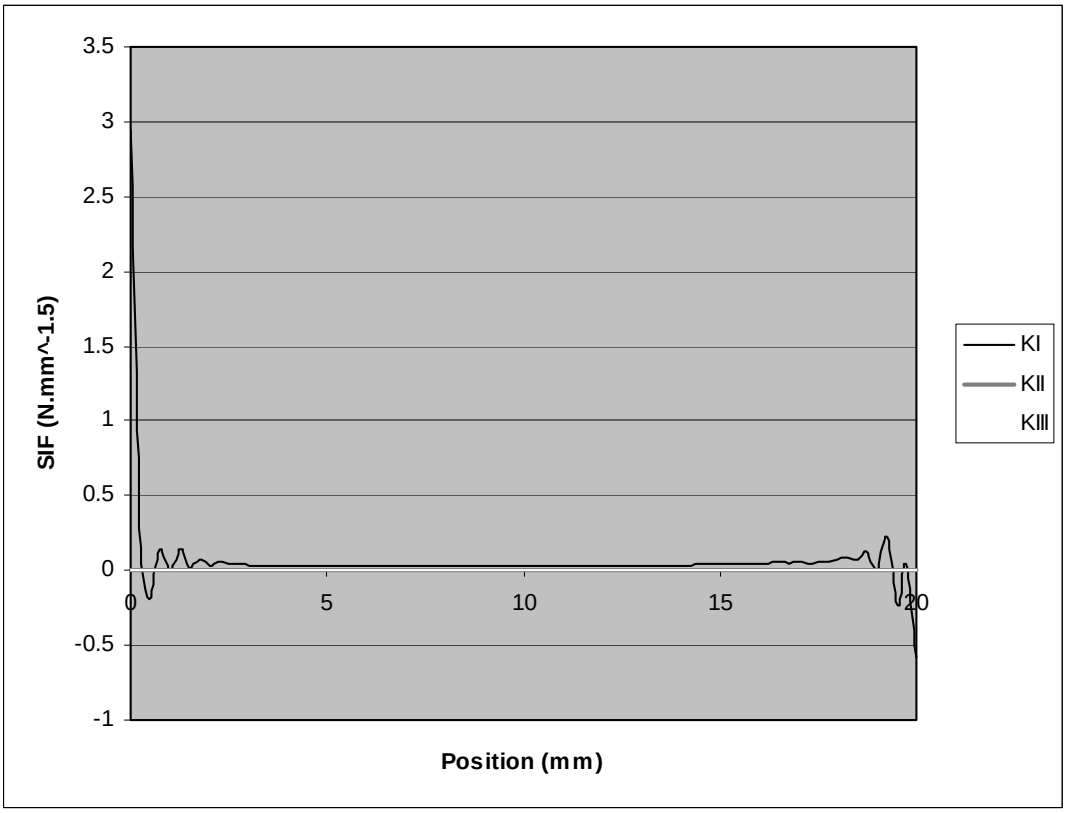

Figure 5. 30 : K_I, K_{II} and K_{III} distribution of $(30°/-30°//-30°/30°)_t$ laminate.

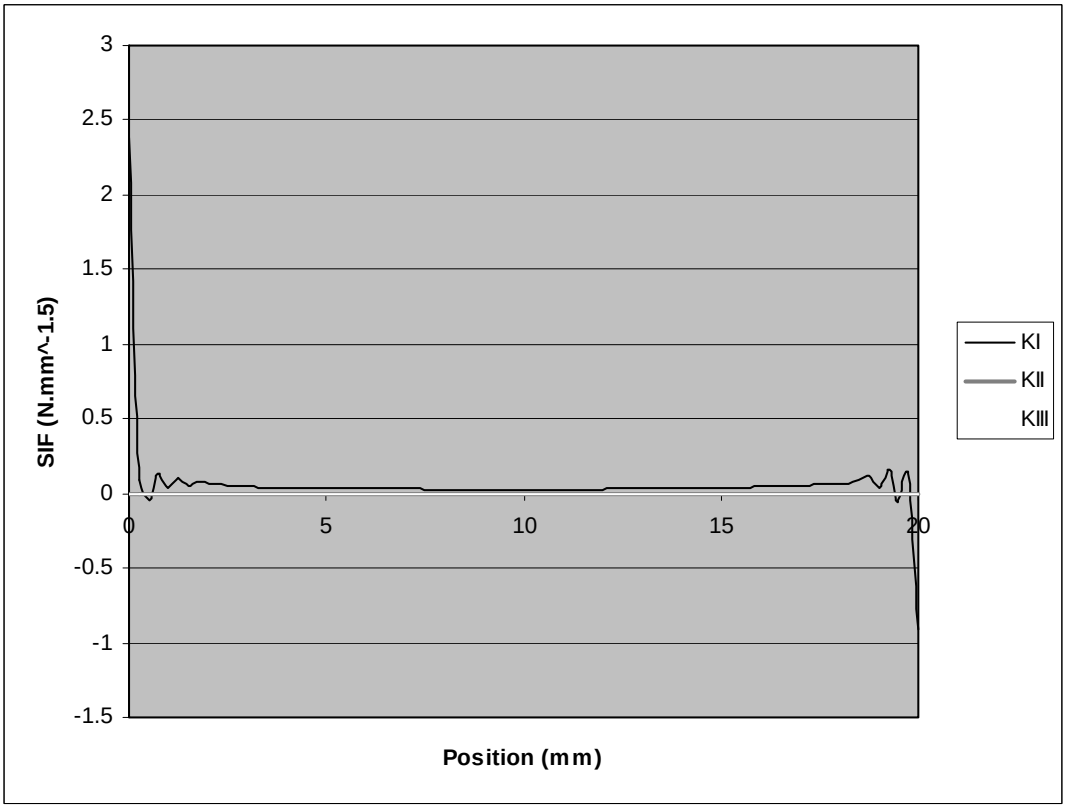

Figure 5. 31 : K_I, K_{II} and K_{III} distribution of $(45°/-45°//-45°/45°)_t$ laminate.

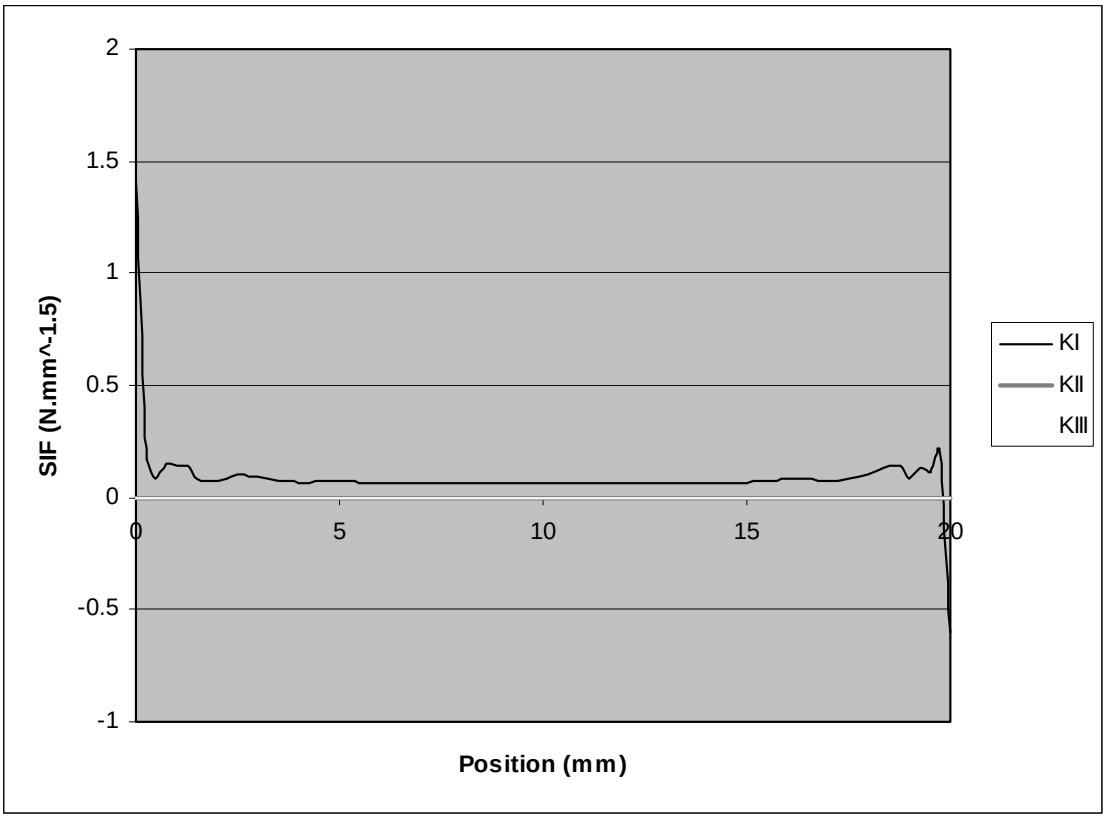

Figure 5. 32 : K_I, K_{II} and K_{III} distribution of $(60°/-60°//-60°/60°)_t$ laminate.

5.2.4 $(90°//0°/0°/90°)_t$ laminates predominant failure mode determination

Figure 5.16 shows the opening of $(90°//0°/0°/90°)_t$ laminate at the center part. It confirmed by the distribution of K_I in Figure 5.33 that gives highest value at the center line. In addition, K_{II} and K_{III} give the result that can not be neglected, which cause the total energy release rate distribution at the edges become higher that at the center part (Figure 5.17). As a result, It can be concluded that the crack propagation in $(90°//0°/0°/90°)_t$ laminate is mixed mode crack propagation.

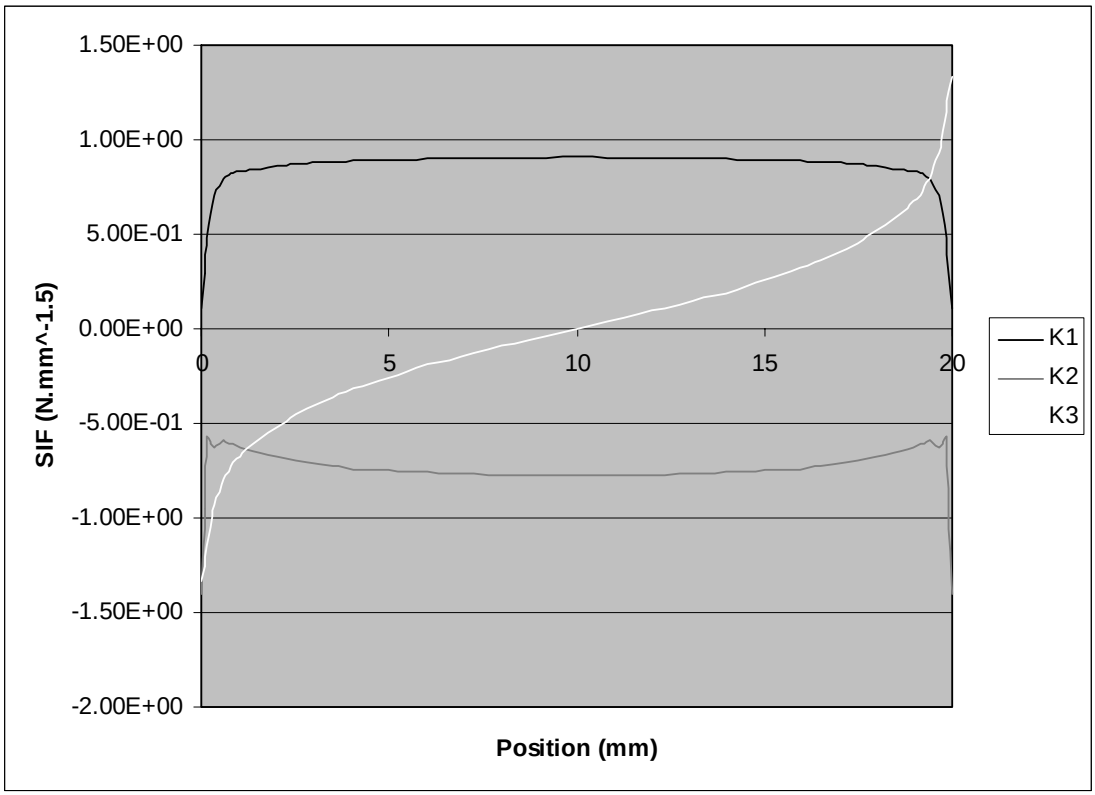

Figure 5. 33 : K_I, K_{II} and K_{III} distribution of $(90°/0°//0°/90°)_t$ laminate.

5.2.5 $(0°//90°/90°/0°)_t$ laminates predominant failure mode determination

Figure 5.34 shows the distribution of K_I, K_{II} and K_{III} of $(0°//90°/90°/0°)_t$ laminate. From the same figure, we can see distribution of K_I which gives highest value at the edges and lower at the center part, as predicted from Figure 5.18 which gives slight opening at the edges. Furthermore, the crack propagation in $(0°//90°/90°/0°)_t$ laminate is also mixed mode crack propagation because the value of K_{II} and K_{III} as can be seen in Figure 5.34 can not be neglected.

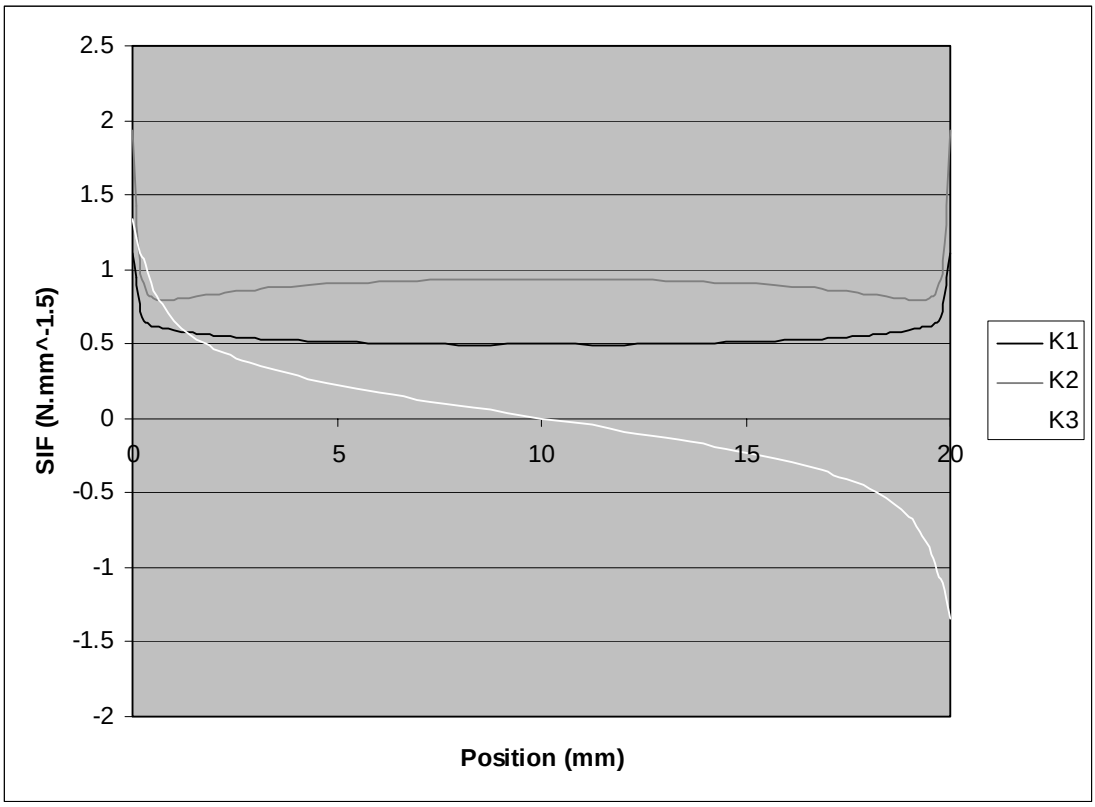

Figure 5. 34 : K_I, K_{II} and K_{III} distribution of $(0°/90°//90°/0°)_t$ laminate.

5.2.6 $(\theta//-\theta/-\theta/\theta)_t$ laminates predominant failure mode determination

As can be seen in Figures 5.20, 5.22 and 5.24, $(\theta//-\theta/-\theta/\theta)_t$ laminates give obvious twisting, which can cause mixed mode crack propagation. It is confirmed in Figures 5.35, 5.36 and 5.37, which show K_I, K_{II} and K_{III} distribution of $(30°//-30°/-30°/30°)_t$, $(45°//-45°/-45°/45°)_t$ and $(60°//-60°/-60°/60°)_t$ laminates respectively. Those figures show that none of K_I, K_{II} and K_{III} that can be neglected.

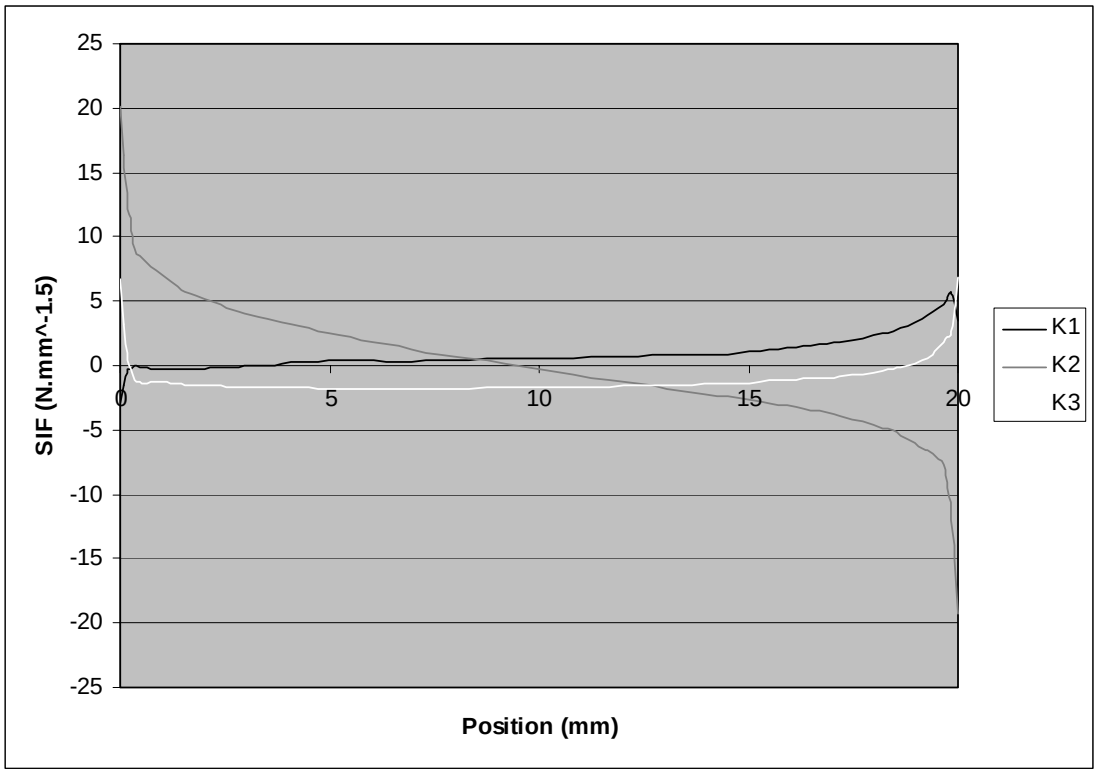

Figure 5. 35 : K_I, K_{II} and K_{III} distribution of $(30°/-30°//-30°/30°)_t$ laminate.

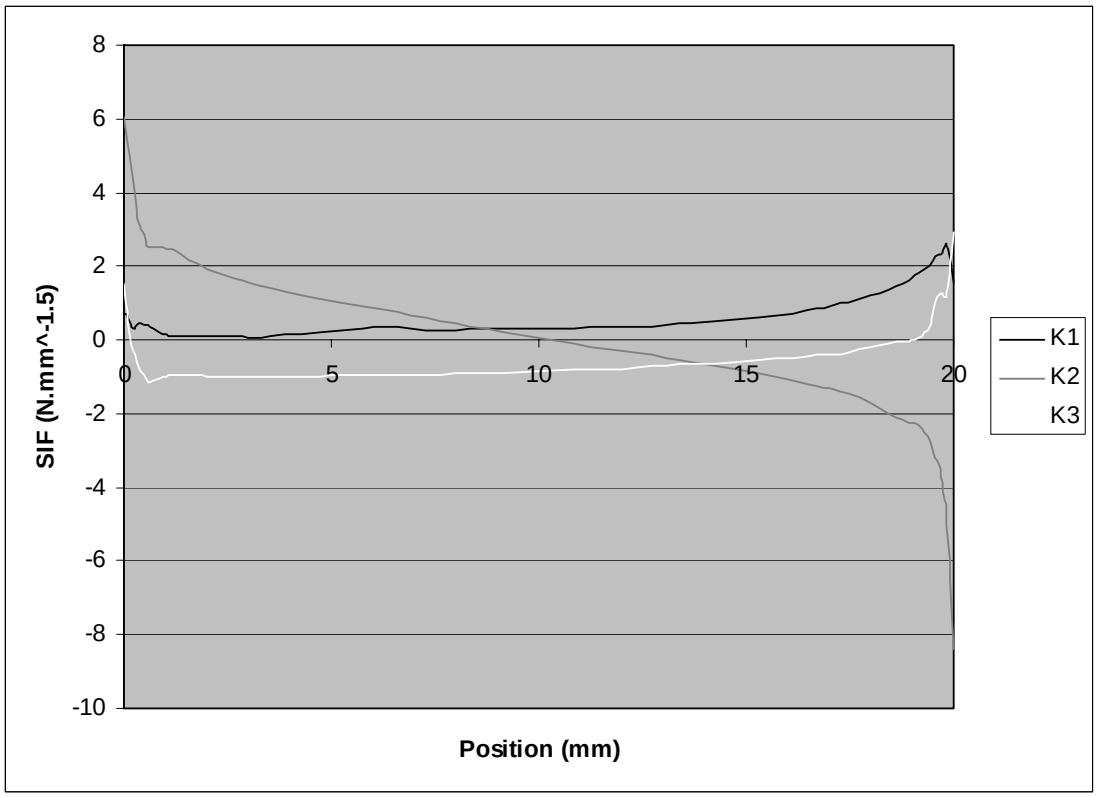

Figure 5. 36 : K_I, K_{II} and K_{III} distribution of $(45°/-45°//-45°/45°)_t$ laminate.

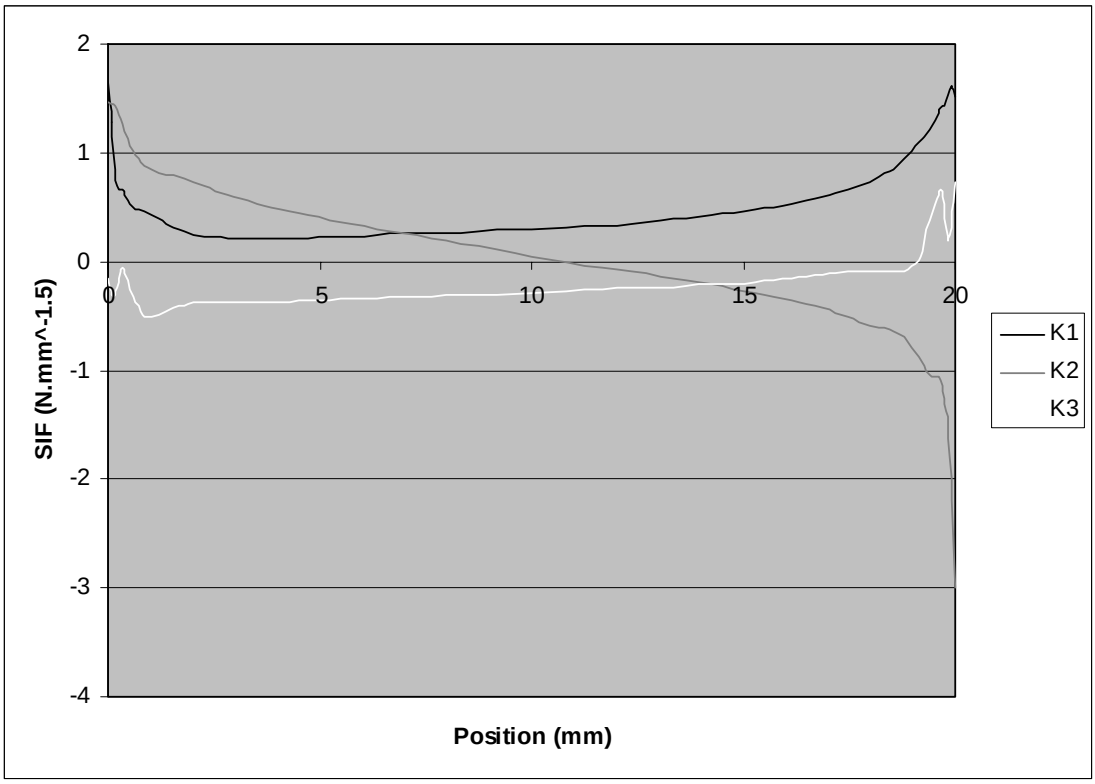

Figure 5. 37 : K_I, K_{II} and K_{III} distribution of $(60°/-60°//-60°/60°)_t$ laminate.

5.3 Delamination Propagation Determination

After studying about the total energy release rate distribution and the predominant failure mode, the next thing to do is to determine whether the delamination will propagate or not. This subchapter will be divided into two parts: mid plane delamination and delamination between 1st and 2nd layers.

5.3.1 Mid plane delamination

There are three laminates that have mid plane delamination, they are $(90°/0°//0°/90°)_t$, $(0°/90°//90°/0°)_t$ and $(\theta/-\theta//-\theta/\theta)_t$ laminates. From section 5.2 it can be seen that mode I is the predominant failure mode for all of those laminates and effect of the other mode can be neglected. Thus, to know whether the delamination will propagate or not, the maximum energy release rate of those laminates are compared with G_{IC} (critical energy release rate for opening mode) value. As discussed in chapter 2, delamination fracture toughness depends on several things one of those is adjacent plies direction. G_{IC} value for delamination between 0° laminae (0°//0°) is equal to 0.2077 N/mm [83]. On the other hand, the value of G_{IC} for 90° laminae (90°//90°) is equal to 0.25 N/mm [84]. Furthermore, G_{IC} value for delamination

between θ laminae (θ// θ) must be in between those values. The maximum energy release rates of $(90°/0°//0°/90°)_t$, $(0°/90°//90°/0°)_t$ and $(\theta/-\theta//-\theta/\theta)_t$ laminates are much smaller than those values. Thus, it can be concluded that the delamination in $(90°/0°//0°/90°)_t$, $(0°/90°//90°/0°)_t$ and $(\theta/-\theta//-\theta/\theta)_t$ laminates will not propagate.

5.3.2 Delamination between 1st and 2nd layers

The delamination of $(90°//0°/0°/90°)_t$, $(0°//90°/90°/0°)_t$ and $(\theta//-\theta/-\theta/\theta)_t$ laminates are placed in between 1st and 2nd layers. Unlike $(90°/0°//0°/90°)_t$, $(0°/90°//90°/0°)_t$ and $(\theta/-\theta//-\theta/\theta)_t$ laminates, $(90°//0°/0°/90°)_t$, $(0°//90°/90°/0°)_t$ and $(\theta//-\theta/-\theta/\theta)_t$ laminates tend to have mixed mode delamination propagation. It can be seen clearly in section 5.2. Beside the adjacent plies direction, the value of G_C (critical energy release rate) in the case of mixed mode delamination propagation is also affected by the proportion of each failure mode. It makes this problem become very complicated. At first, the G_C with certain mode proportion of certain spot must be determined. Then, Gt of that spot is compared with G_C value that was obtained earlier. Furthermore, this needs to be done for all points along the width. Beside that, no one has plotted the value of G_C for every proportion of each failure mode for this material. It makes, this delamination propagation prediction become very hard, thus the results obtained are only very academic until proven otherwise.

At first, the values of G_{IC}, G_{IIC} and G_{IIIC} must be known. The values of G_{IC}, G_{IIC} and G_{IIIC} respectively for delamination between 90° laminae (90°//90°) are 0.25 N/mm, 0.8 N/mm and 0.9 N/mm [84]. Furthermore, the values of G_{IC} and G_{IIC} respectively for delamination between 0° laminae (0°//0°) are 0.207 N/mm and 0.758 N/mm. For mixed mode crack propagation, G_C suppose to be in between those values [85]. The maximum energy release rate values of $(90°//0°/0°/90°)_t$ and $(0°//90°/90°/0°)_t$ laminates are very small compared to those values. We can conclude that the delamination in $(90°//0°/0°/90°)_t$ and $(0°//90°/90°/0°)_t$ laminates will not propagate.

In chapter 2, it was discussed that in delamination at ±θ interface G_C tends to increases when θ increases. Thus, because the value of maximum total energy release rates of $(45°//-45°/-45°/45°)_t$, $(60°//-60°/-60°/60°)_t$ and $(80°//-80°/-80°/80°)_t$ laminates (Figure 5.26) are smaller than 0.207 N/mm (G_{IC} value of delamination between 0° laminae), we conclude that the delamination in those laminates most likely will not propagate (the Gt values are smaller than the smallest value between G_{IC} and $G_{IIC)}$. On

the other hand, the maximum values of total energy release rates of $(10°//-10°/-10°/10°)_t$, $(20°//-20°/-20°/20°)_t$ and $(30°//-30°/-30°/30°)_t$ laminates are bigger than 0.207 N/mm. As a result it can be concluded that delamination in $(10°//-10°/-10°/10°)_t$, $(20°//-20°/-20°/20°)_t$ and $(30°//-30°/-30°/30°)_t$ laminates have probability to propagate.

Chapter Six

TWISTING EFFECT IN $(\theta//-\theta/-\theta/\theta)_t$ LAMINATES

As discussed earlier, twisting emerges in $(\theta//-\theta/-\theta/\theta)_t$ laminates under tensile load. In this chapter, twisting angle in $(\theta//-\theta/-\theta/\theta)_t$ laminates will be studied thoroughly and the effect of twisting in failure load also will be studied.

6.1 Twisting Angle Comparison in $(\theta//-\theta/-\theta/\theta)_t$ Laminates

To study twisting in $(\theta//-\theta/-\theta/\theta)_t$ laminates, both the lamination angle and delamination length must be varied. There are six lamination angle that are studied, they are 10°, 20°, 30°, 45°, 60° and 80°. Furthermore, we also will vary the delamination length starting from 10mm to 120mm. Figure 6.1 shows the twisting angle of $(\theta//-\theta/-\theta/\theta)_t$ laminates with variation in delamination length. Moreover, Figure 6.2 shows the twisting angle of $(\theta//-\theta/-\theta/\theta)_t$ laminates with variation in lamination angle. From Figure 6.1, it can be seen that almost in all of lamination angles, DL (delamination length) = 60mm produces the maximum twisting angle. On the other hand, Figure 6.2 shows that $(10°//-10°/-10°/10°)_t$ and $(20°//-20°/-20°/20°)_t$ laminates produce the maximum twisting angle. In addition, from all of those lamination angle and delamination length variations, the maximum twisting angle is 6.28° which is produced by $(20°//-20°/-20°/20°)_t$ laminate with DL=60mm.

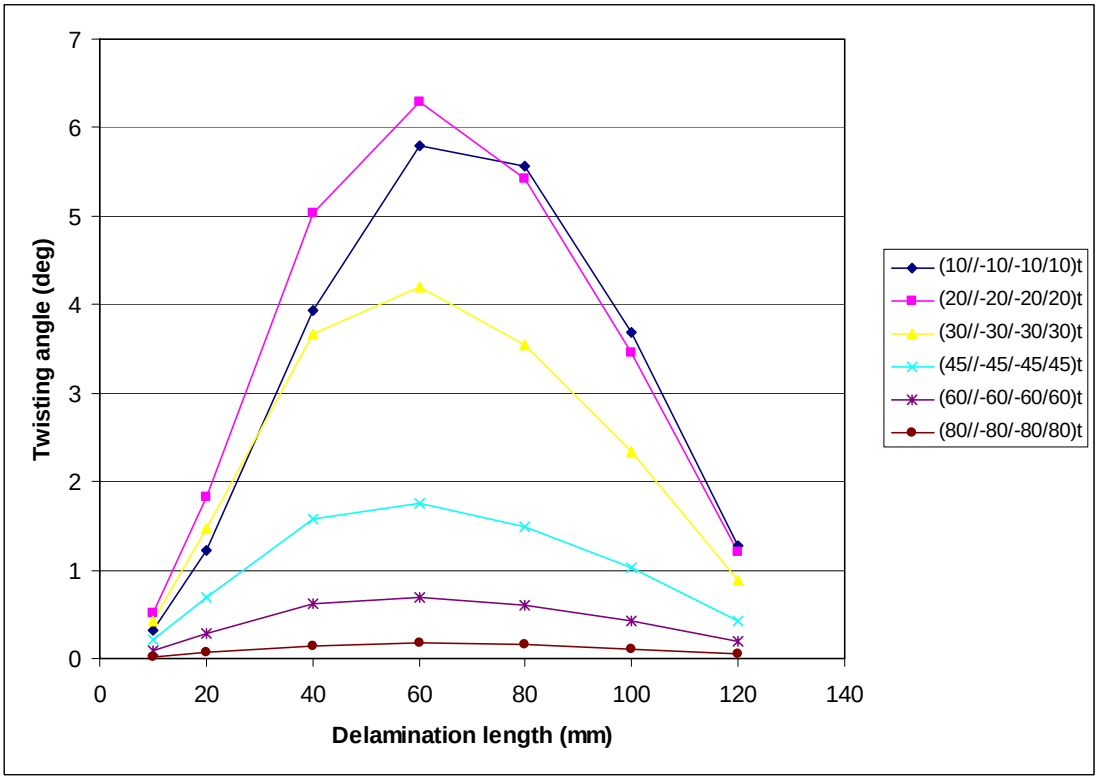

Figure 6. 1: Twisting angle of $(\theta//-\theta/-\theta/\theta)_t$ laminates with variation in delamination length.

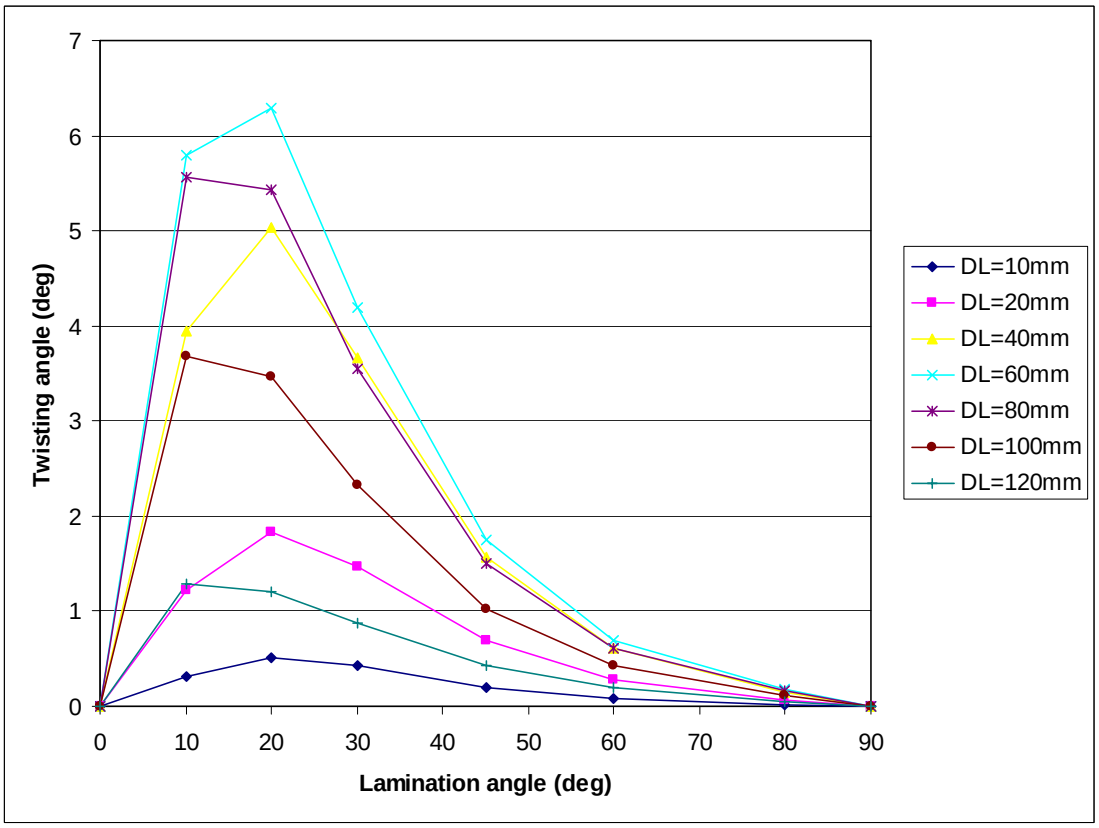

Figure 6. 2: Twisting angle of $(\theta//-\theta/-\theta/\theta)_t$ laminates with variation in lamination angle.

To verify this result, several tests have been done in $(10°//-10°/-10°/10°)_t$, $(20°//-20°/-20°/20°)_t$ and $(45°//-45°/-45°/45°)_t$ laminates with DL=60mm. Unfortunately, the twisting that happened can not be seen clearly during the tests. Thus, other way is used to confirm the result. Several strain gauges are glued at the specimens at certain spot as can be seen in Figure 6.3. Furthermore, the strain results from the experiment are compared to strain results from finite element to confirm the result. The comparison of strain result from experimental and finite element for $(10°//-10°/-10°/10°)_t$, $(20°//-20°/-20°/20°)_t$ and $(45°//-45°/-45°/45°)_t$ laminates with DL=60mm can be seen in Figures 6.4, 6.5 and 6.6 respectively. Although results from finite element are little bit different from experiment, the error that is produced still acceptable.

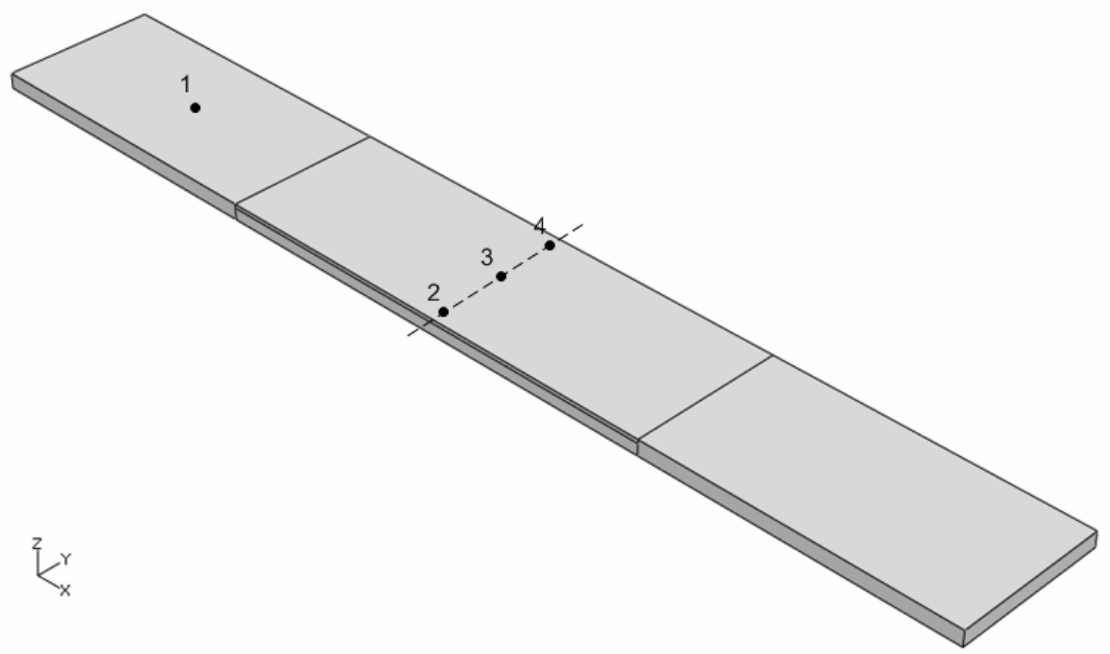

Figure 6. 3: Strain gauge position numbering.

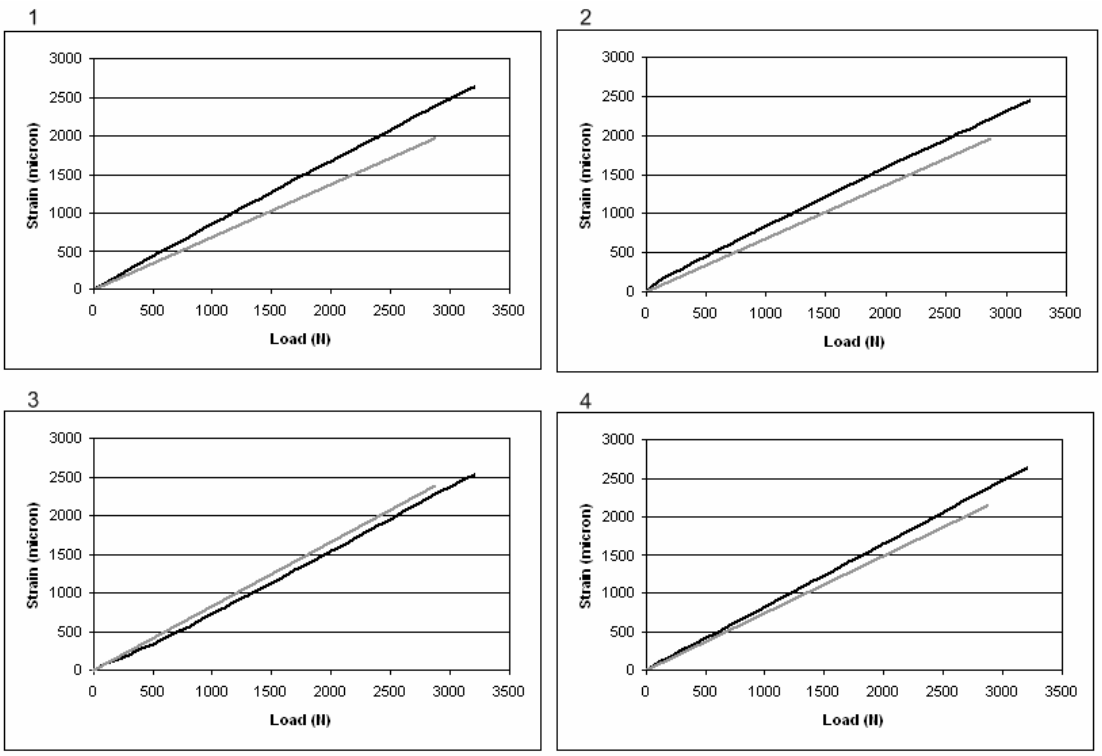

Figure 6. 4: Strain comparison of $(10°//-10°/-10°/10°)_t$ DL=60mm for every strain gauge position (black= experiment, gray=Abaqus).

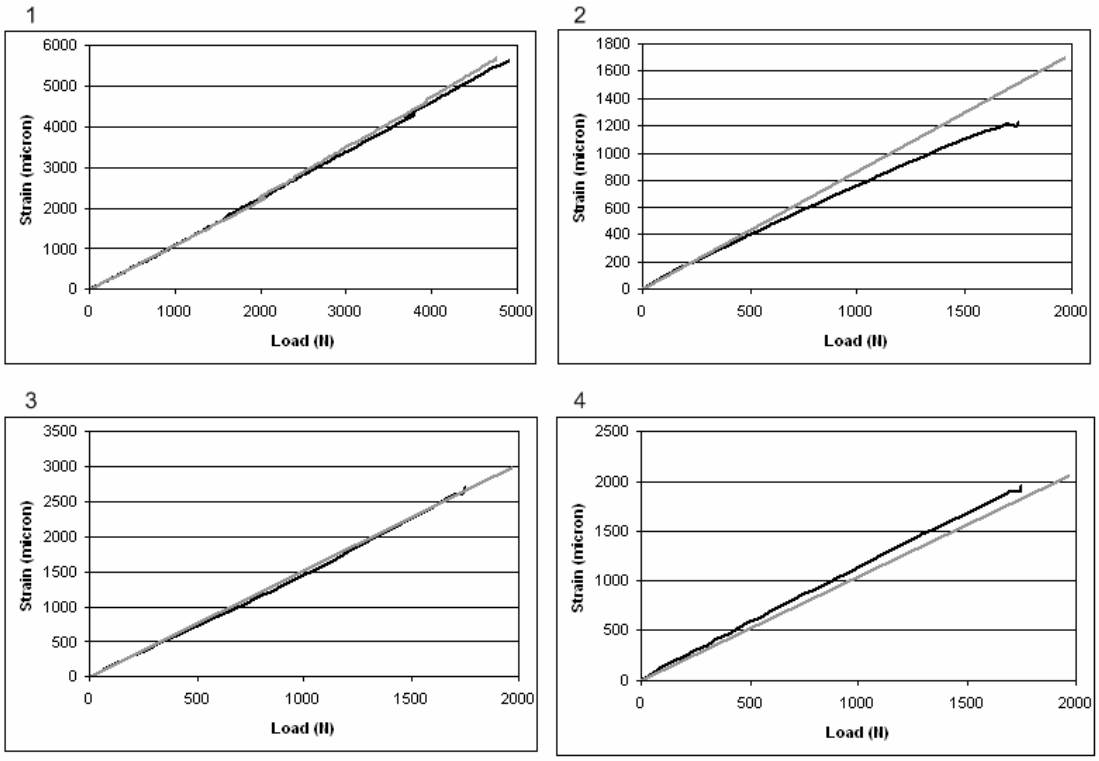

Figure 6. 5: Strain comparison of $(20°//-20°/-20°/20°)_t$ DL=60mm for every strain gauge position (black= experiment, gray=Abaqus).

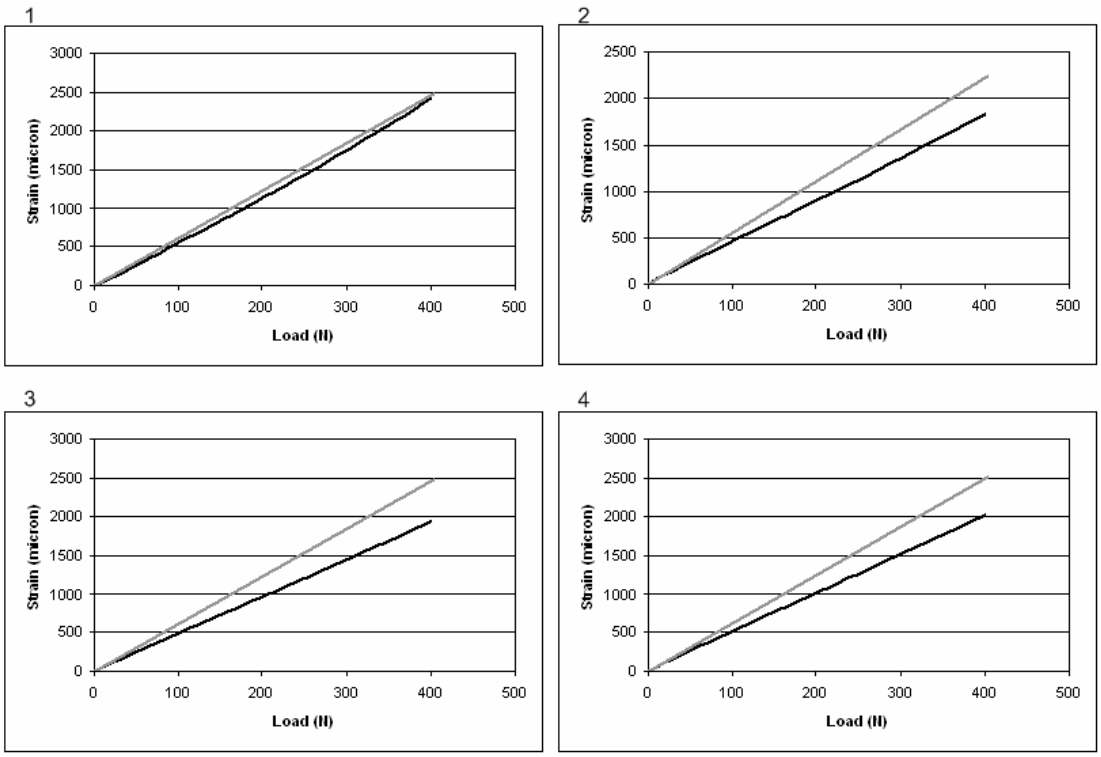

Figure 6. 6: Strain comparison of (45°//-45°/-45°/45°)$_t$ DL=60mm for every strain gauge position (black= experiment, gray=Abaqus).

6.2 Failure Load Comparison

The next thing to do is to check the effect of twisting that happen in (θ//-θ/-θ/θ)$_t$ laminates to the whole structure. The easiest way is by checking the failure load of those structures. Therefore, we studied the failure load of (θ//-θ/-θ/θ)$_t$ laminates with variation in lamination angle and delamination length. One phenomenon that happens is there will always a first failure before a complete failure for lamination angle lower than 60° with 10mm delamination length or more. One example will be given for (30°//-30°/-30°/30°)$_t$ laminates. Figure 6.7 shows the load vs displacement of (30°/-30)s without delamination. It can be observed that the first failure is the same as the final failure. On the other hand, (30°//-30°/-30°/30°)$_t$ laminates DL=60mm gives quite different result (Figure 6.8). It shows 1st failure at the load approximately half of the final failure. By analyzing the specimen thoroughly, it can seen that the 1st failure was happened at the 1st ply with the position as can be seen in Figure 6.9 (the part with red color) and the failure mode is tensile matrix (TM). From the same figure, it can be seen that the 1st failure was happened at corner of the delamination area where twisting angle shows the maximum result, then it propagates and causes 1st

ply failure (Figure 6.10). In the end, as the load keep increasing, last failure happen (Figure 6.11). Furthermore, the 1st failure mode and final failure mode of $(\theta//-\theta/-\theta/\theta)_t$ laminates for every θ and delamination are given in Table 6.1. In addition, Figures 6.12 to 6.22 show the 1st failure and the final failure load graph of $(\theta//-\theta/-\theta/\theta)_t$ laminates. Experimental result of 1st failure and final failure load for $(10°//-10°/-10°/10°)_t$, $(20°//-20°/-20°/20°)_t$ and $(45°//-45°/-45°/45°)_t$ laminates with DL=60mm are also plotted in Figures 6.13, 6.14 and 6.17. From those figures, it can be seen that the finite element result give quite good prediction for both 1st failure and final failure load of course with certain error.

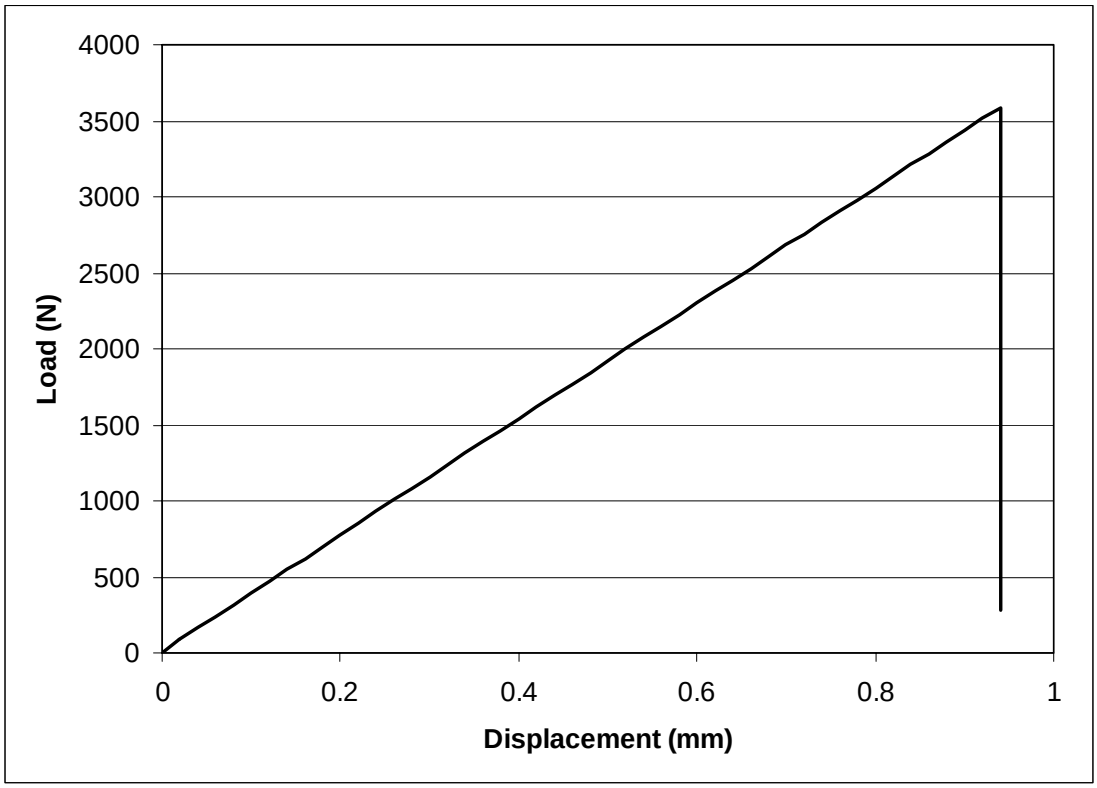

Figure 6. 7: Load vs displacement graph of $(30°/-30°)_s$.

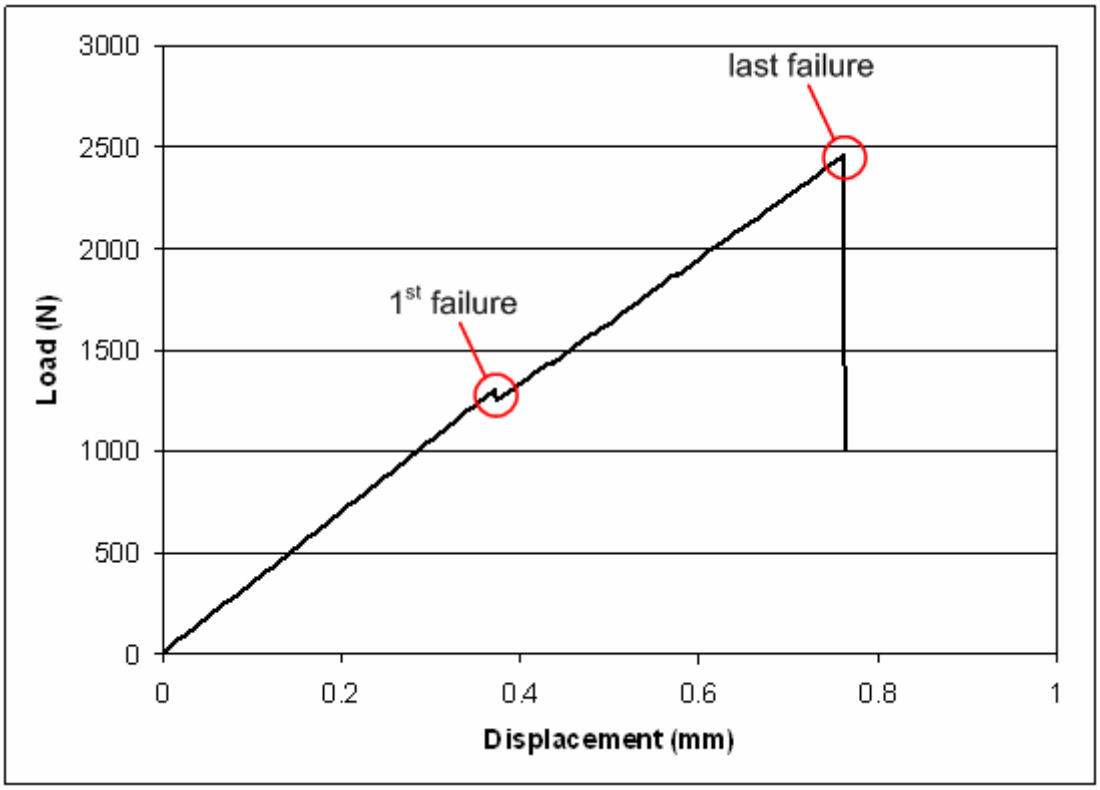

Figure 6. 8: Load vs displacement graph of $(30°//-30°/-30°/30°)_t$ DL=60mm.

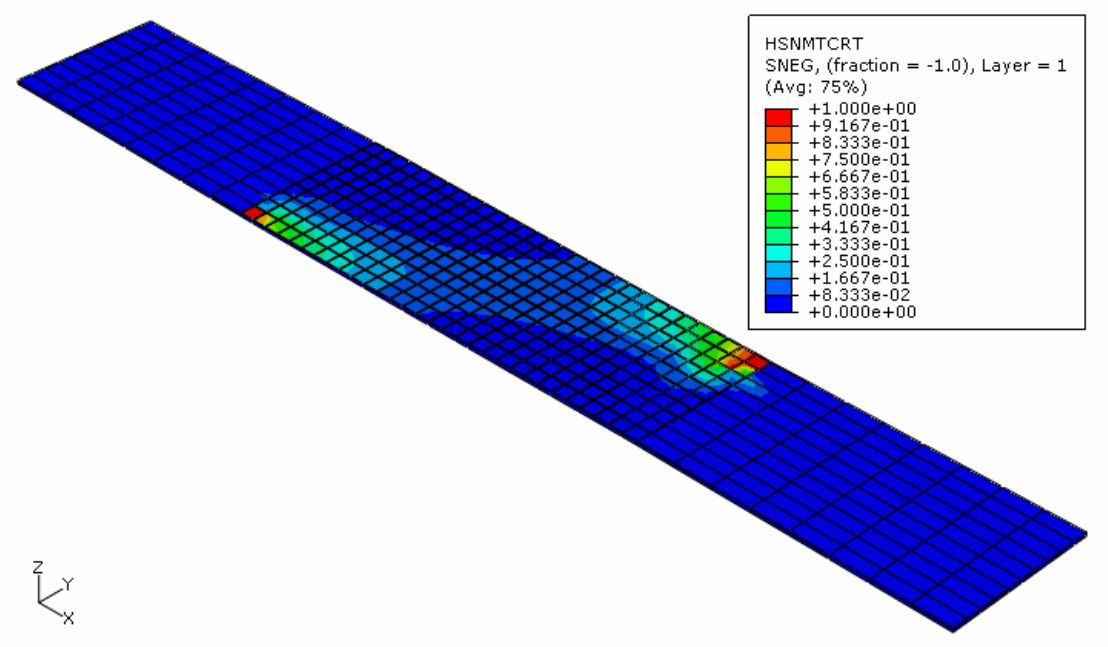

Figure 6. 9: 1st failure position of $(30°//-30°/-30°/30°)_t$ DL=60mm.

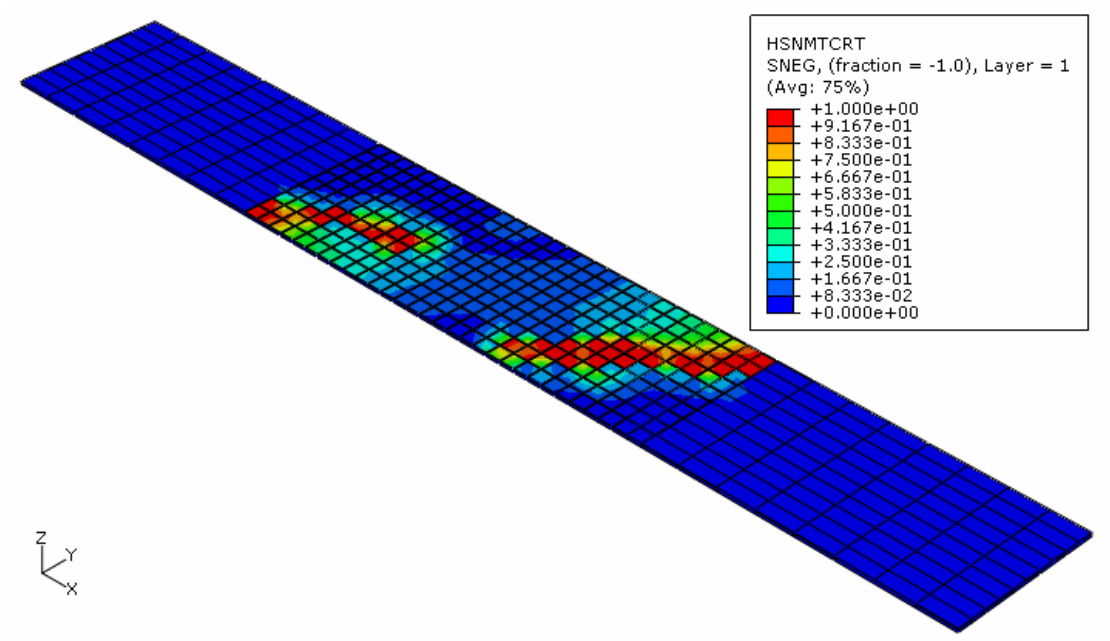

Figure 6. 10: 1st ply failure plot of $(30°//-30°/-30°/30°)_t$ DL=60mm.

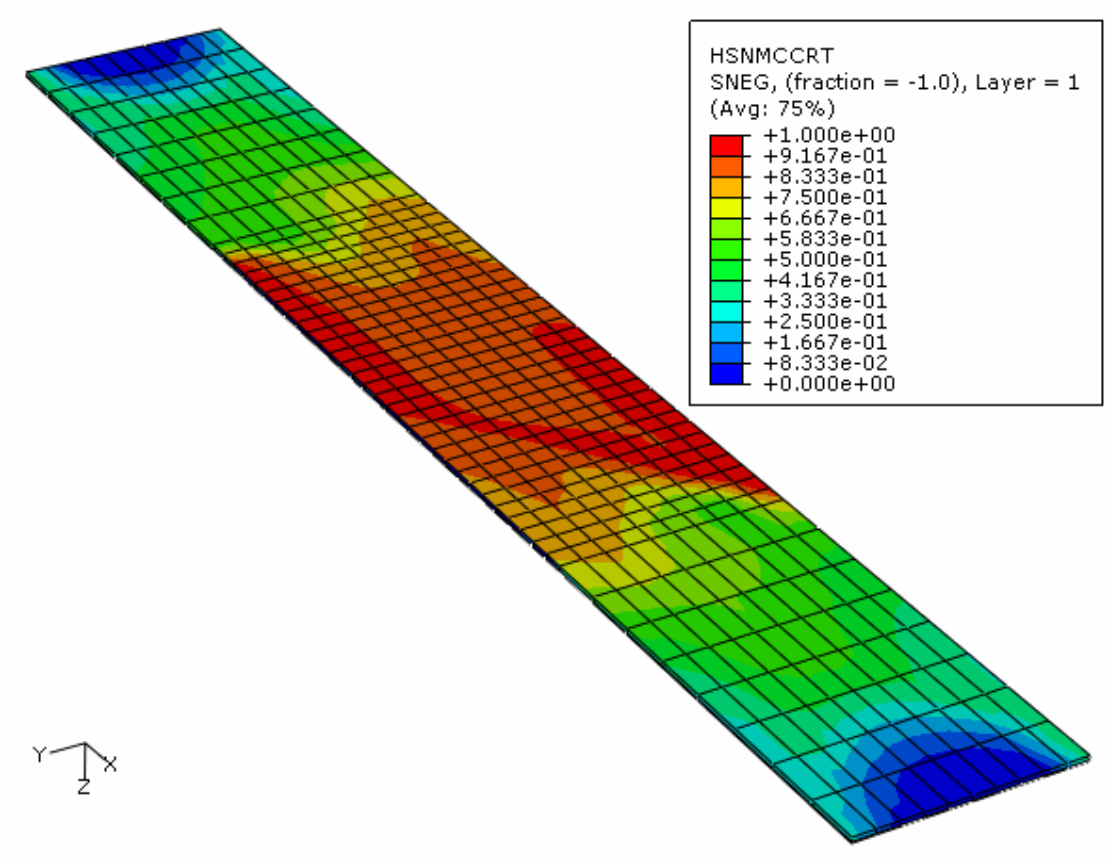

Figure 6. 11: Total failure plot of $(30°//-30°/-30°/30°)_t$ DL=60mm.

Table 6.1 Failure mode list of $(\theta//-\theta/-\theta/\theta)_t$ laminates

DL	θ																					
	0°		10°		20°		30°		40°		45°		50°		60°		70°		80°		90°	
	1st	last	1st	last	1st	last	1st	last	1st	last	1st	last	1st	last	1st	last	1st	last	1st	last	1st	last
0	TF	TF	TF	TF	CM	CM	CM	CM	CM	CM	TM+CM	TM+CM	TM	TM	TM	TM	TM	TM	TM	TM	TM	TM
10	TF	TF	TM	TF	TM	CM	TM	CM	TM	CM	TM	TM+CM	TM	TM	TM	TM	TM	TM	TM	TM	TM	TM
20	TF	TF	TM	TF	TM	CM	TM	CM	TM	CM	TM	TM+CM	TM	TM	TM	TM	TM	TM	TM	TM	TM	TM
40	TF	TF	TM	TF	TM	CM	TM	CM	TM	CM	TM	TM+CM	TM	TM	TM	TM	TM	TM	TM	TM	TM	TM
60	TF	TF	TM	TF	TM	CM	TM	CM	TM	CM	TM	TM+CM	TM	TM	TM	TM	TM	TM	TM	TM	TM	TM
80	TF	TF	TM	TF	TM	CM	TM	CM	TM	CM	TM	TM+CM	TM	TM	TM	TM	TM	TM	TM	TM	TM	TM
100	TF	TF	TM	TF	TM	CM	TM	CM	TM	CM	TM	TM+CM	TM	TM	TM	TM	TM	TM	TM	TM	TM	TM
120	TF	TF	TM	TF	TM	CM	TM	CM	TM	CM	TM	TM+CM	TM	TM	TM	TM	TM	TM	TM	TM	TM	TM

Note:

TF : Tensile fiber failure mode

CF : Compression fiber failure mode

TM : Tensile matrix failure mode

CM : Compression matrix failure mode

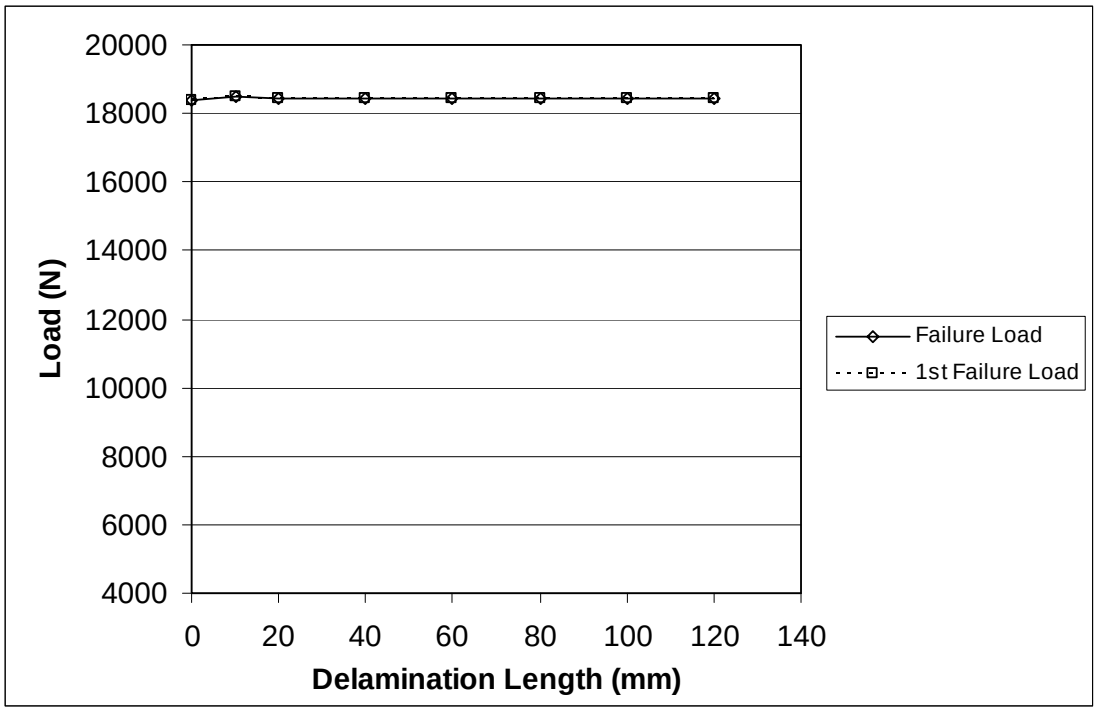

Figure 6. 12: Failure load of $(0°//0°/0°/0°)_t$ with several delamination length.

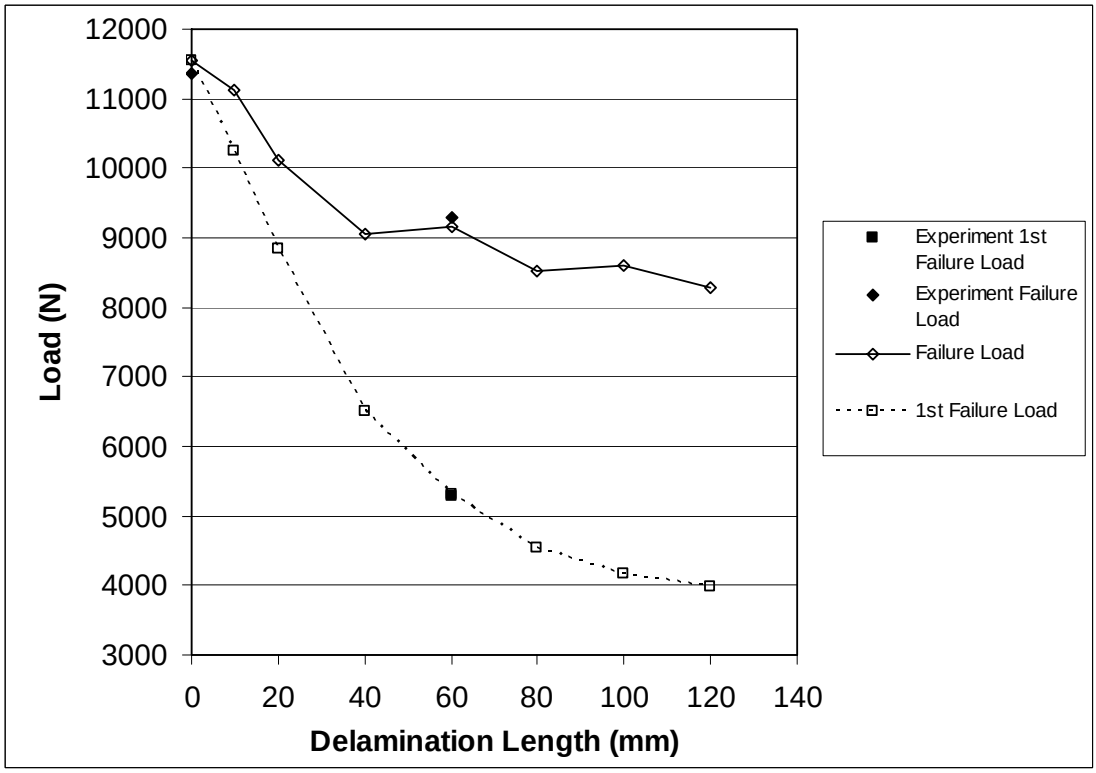

Figure 6. 13: Failure load of $(10°//-10°/-10°/10°)_t$ with several delamination length.

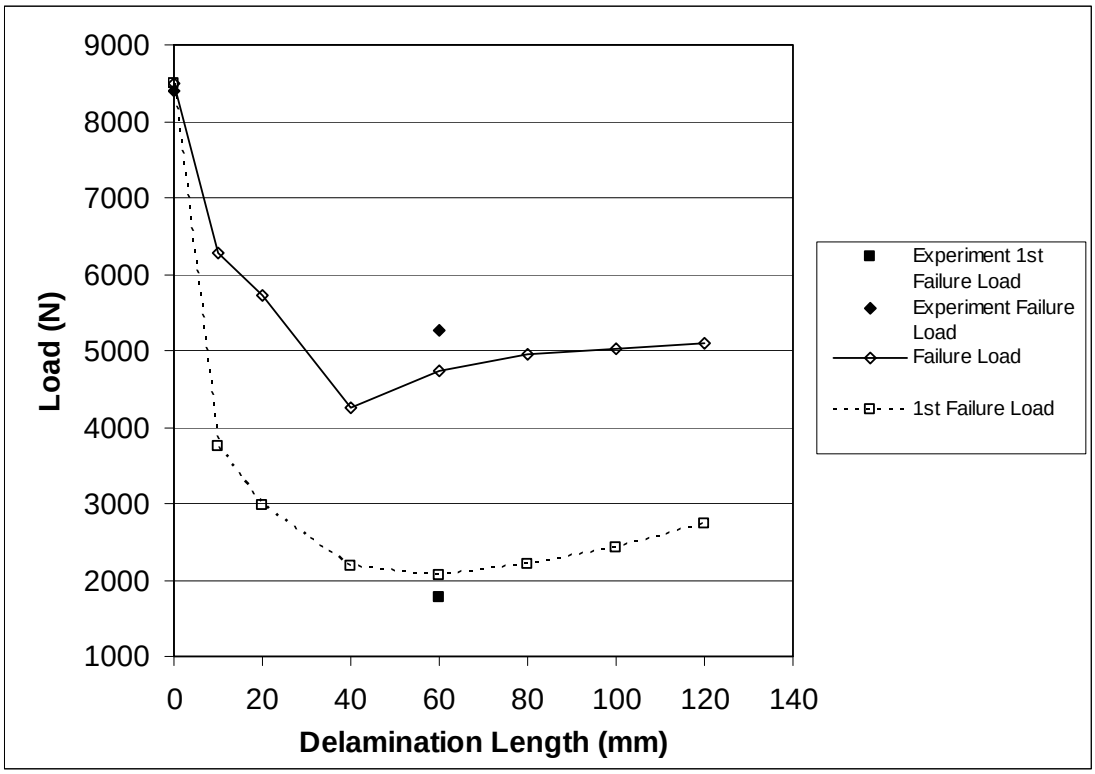

Figure 6. 14: Failure load of $(20°//-20°/-20°/20°)_t$ with several delamination length.

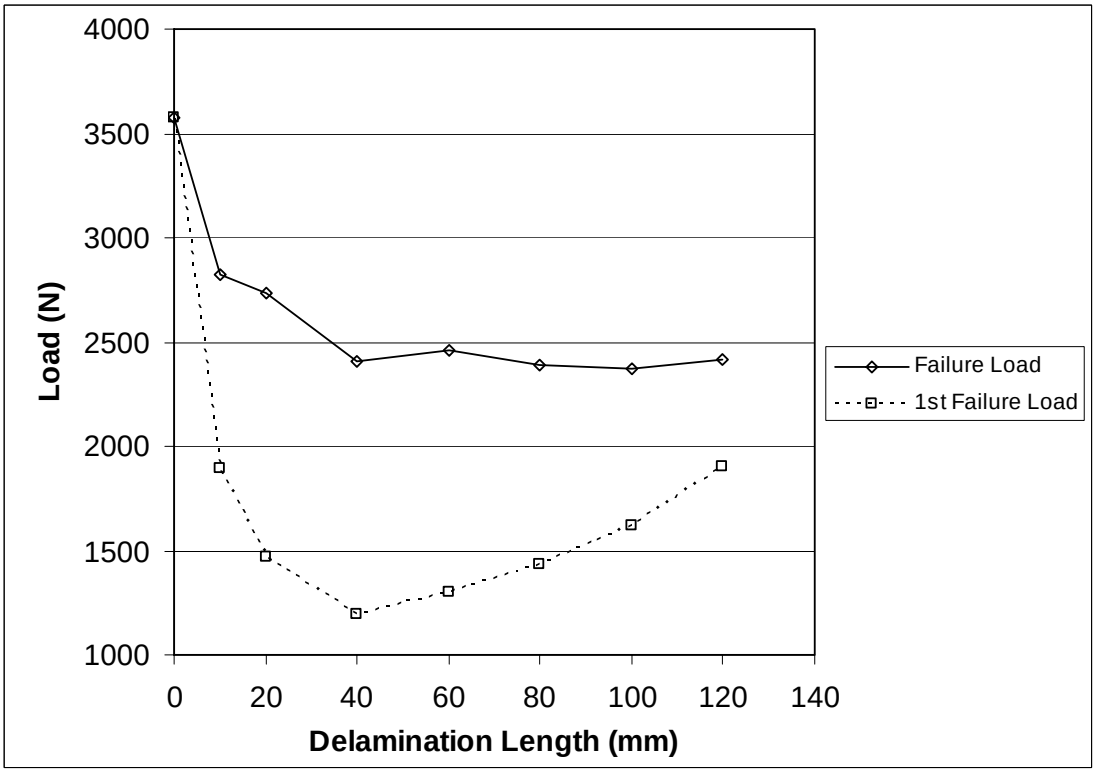

Figure 6. 15: Failure load of $(30°//-30°/-30°/30°)_t$ with several delamination length.

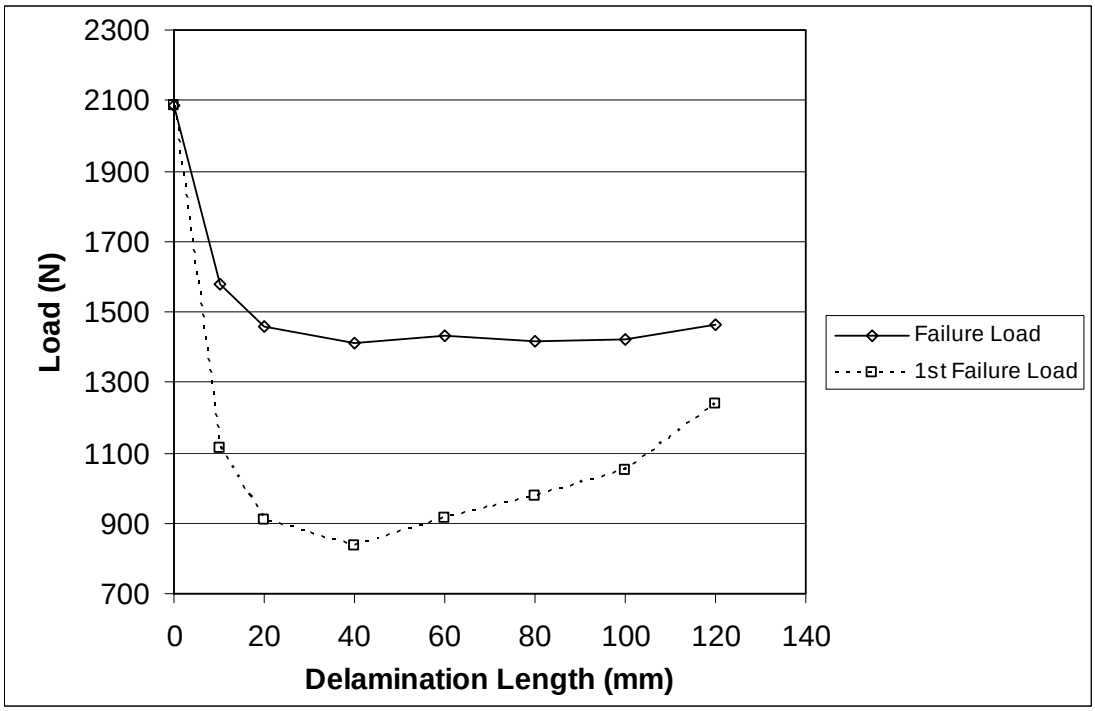

Figure 6. 16: Failure load of $(40°//-40°/-40°/40°)_t$ with several delamination length.

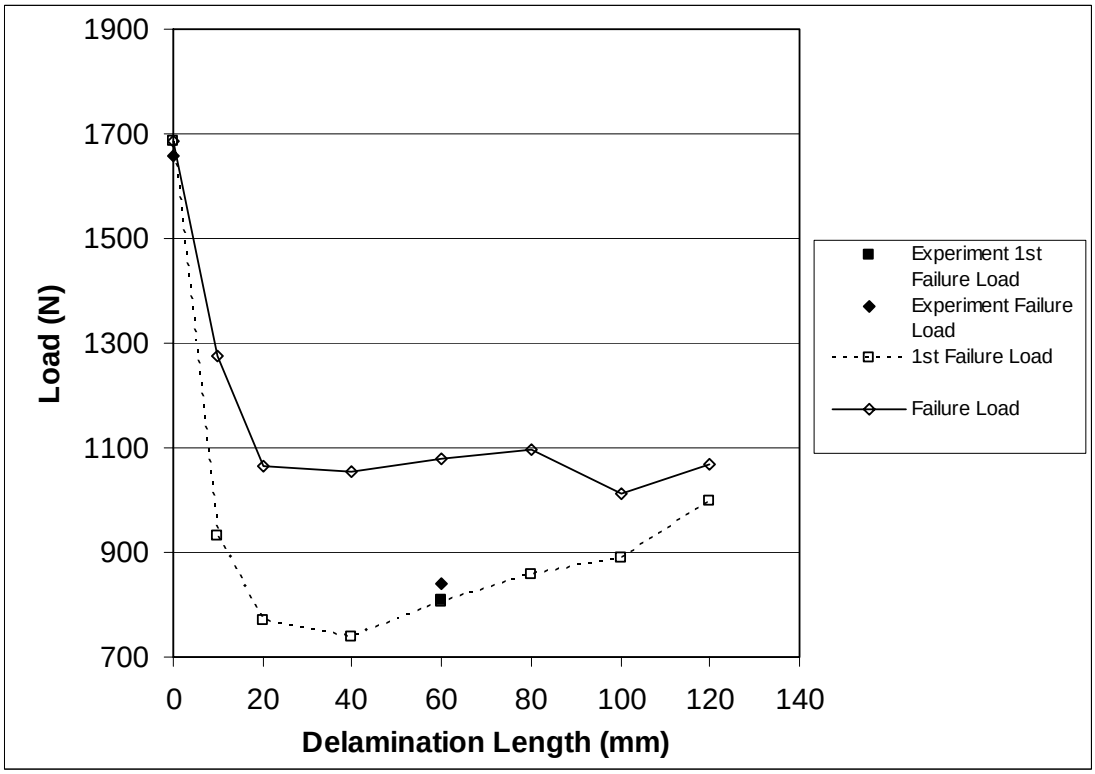

Figure 6. 17: Failure load of $(45°//-45°/-45°/45°)_t$ with several delamination length.

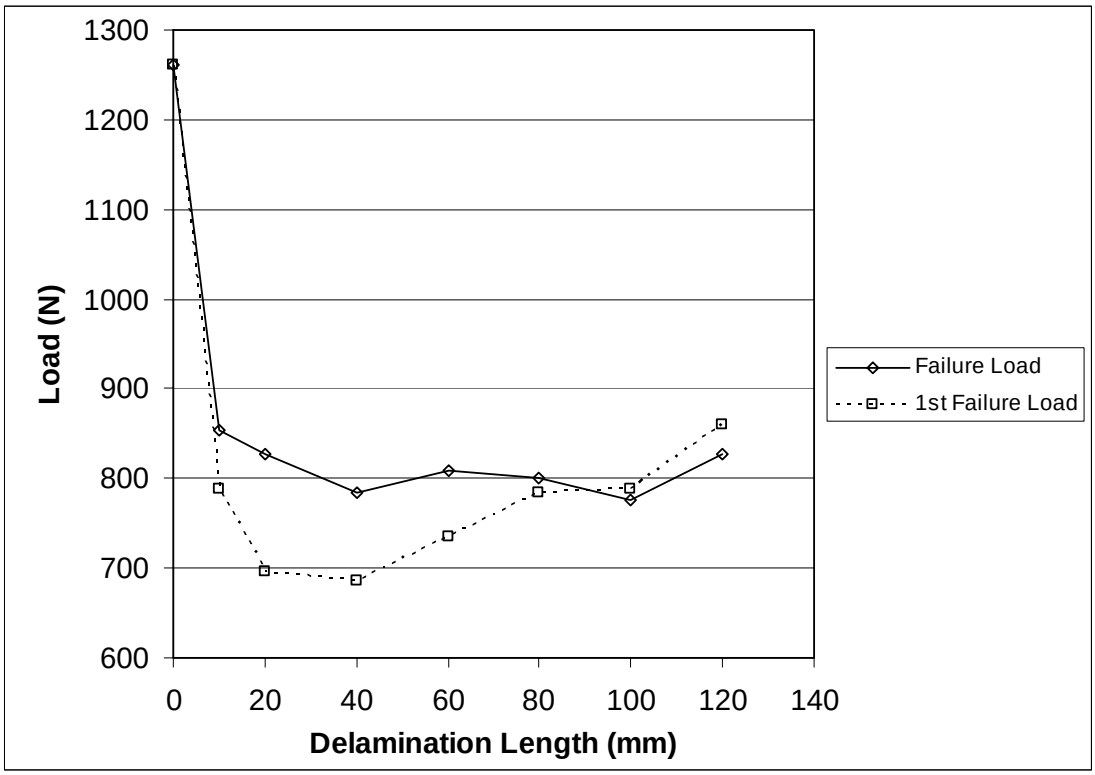

Figure 6. 18: Failure load of $(50°//-50°/-50°/50°)_t$ with several delamination length.

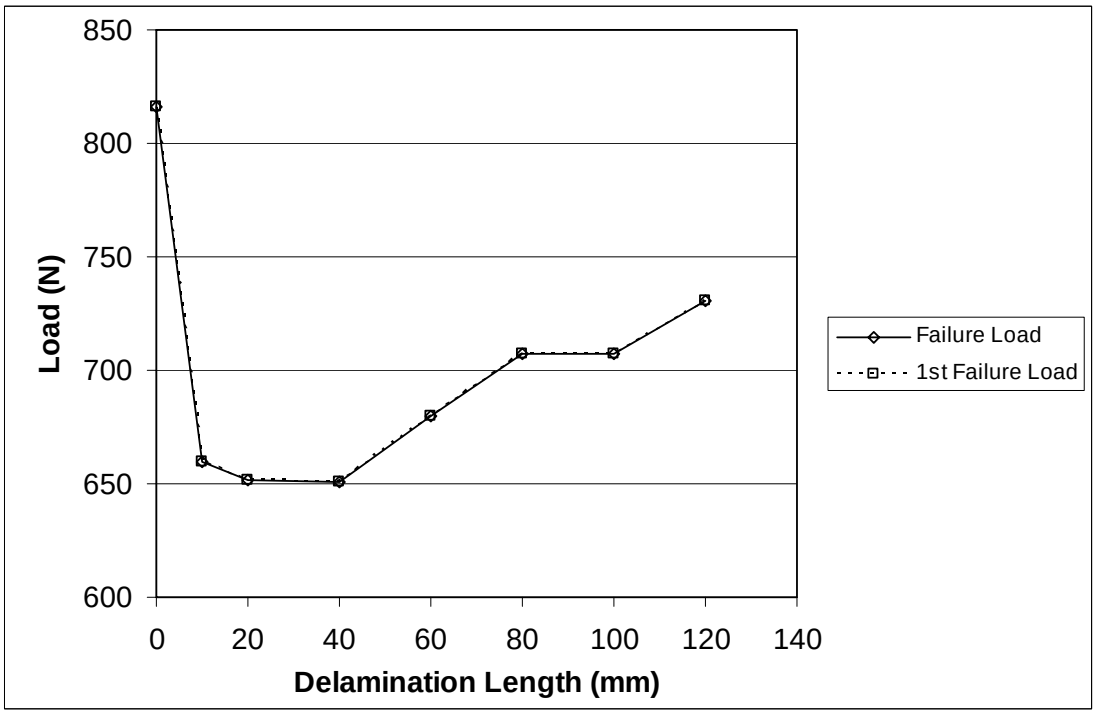

Figure 6. 19: Failure load of $(60°//-60°/-60°/60°)_t$ with several delamination length.

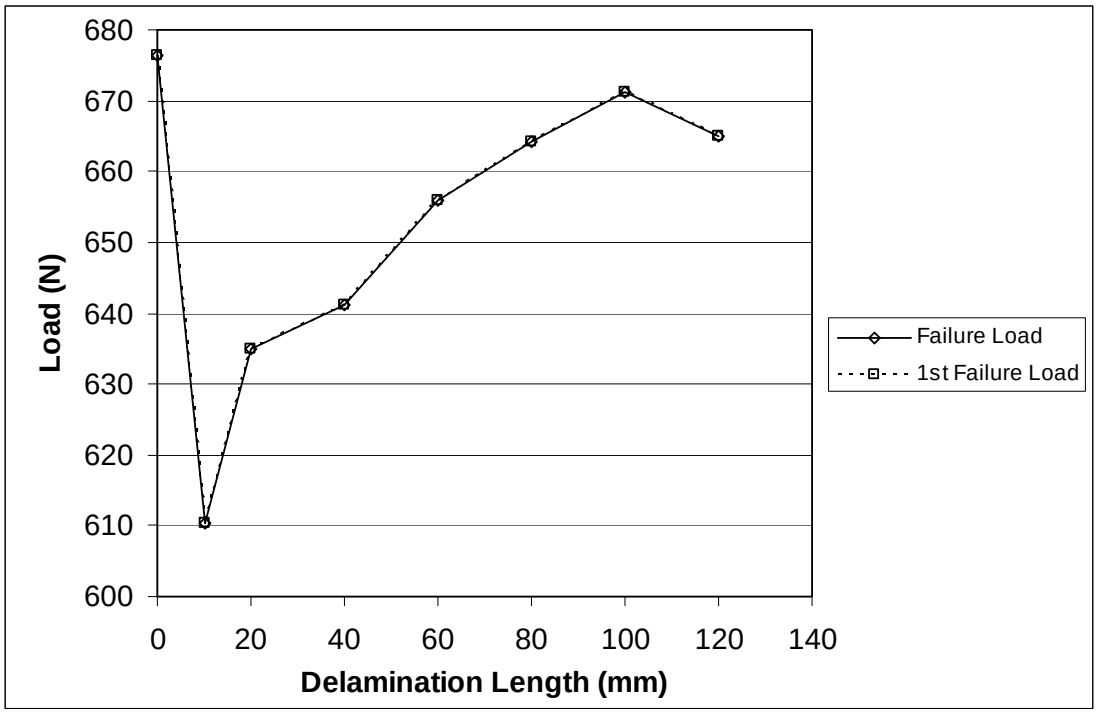

Figure 6. 20: Failure load of $(70°//-70°/-70°/70°)_t$ with several delamination length.

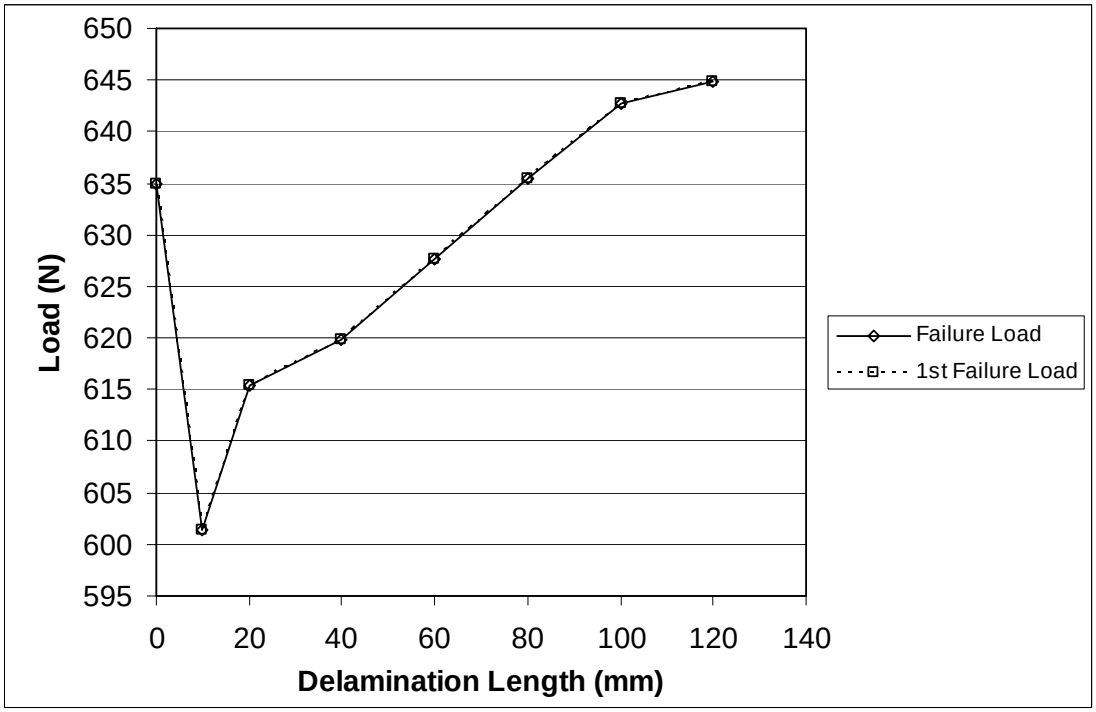

Figure 6. 21: Failure load of $(80°//-80°/-80°/80°)_t$ with several delamination length.

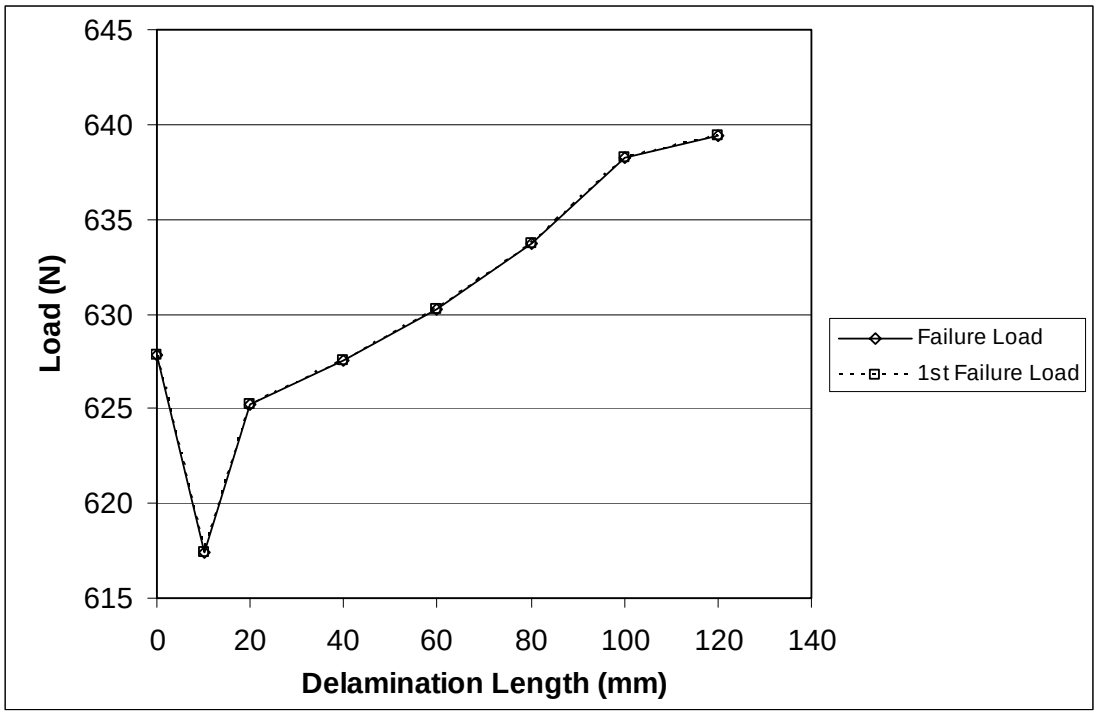

Figure 6. 22: Failure load of $(90°//90°/90°/90°)_t$ with several delamination length.

As can be seen in Figures 6.23 and 6.24, dimensionless variables 1st failure load divided by no delamination failure load and final failure load divided by no delamination failure load are made to compare 1st failure and final failure load of every lamination angle. From these figures, it can be seen that $(20°//-20°/-20°/20°)_t$ laminate is the most critical one which give the lowest percentage of both 1st failure and final failure load with no delamination failure load. Moreover, in comparison with experimental results, finite element results give very good prediction in comparison of 1st failure load with no delamination failure load. On the other hand, the prediction is not too good for comparison of final failure load with no delamination failure load, which gives bigger error that the previous comparison.

In conclusion, the twisting in $(\theta//-\theta/-\theta/\theta)_t$ laminates will cause the structure to sustain stress concentration and can be followed by degradation in the structure (1st failure) especially for $10° \le \theta < 60°$ and $DL \ge 10mm$. Furthermore, it will also reduce the total load that can be sustained (final failure). Moreover, the effect of delamination in other stacking sequences towards failure load are not as critical as in $(\theta//-\theta/-\theta/\theta)_t$ laminates (Table 6.2).

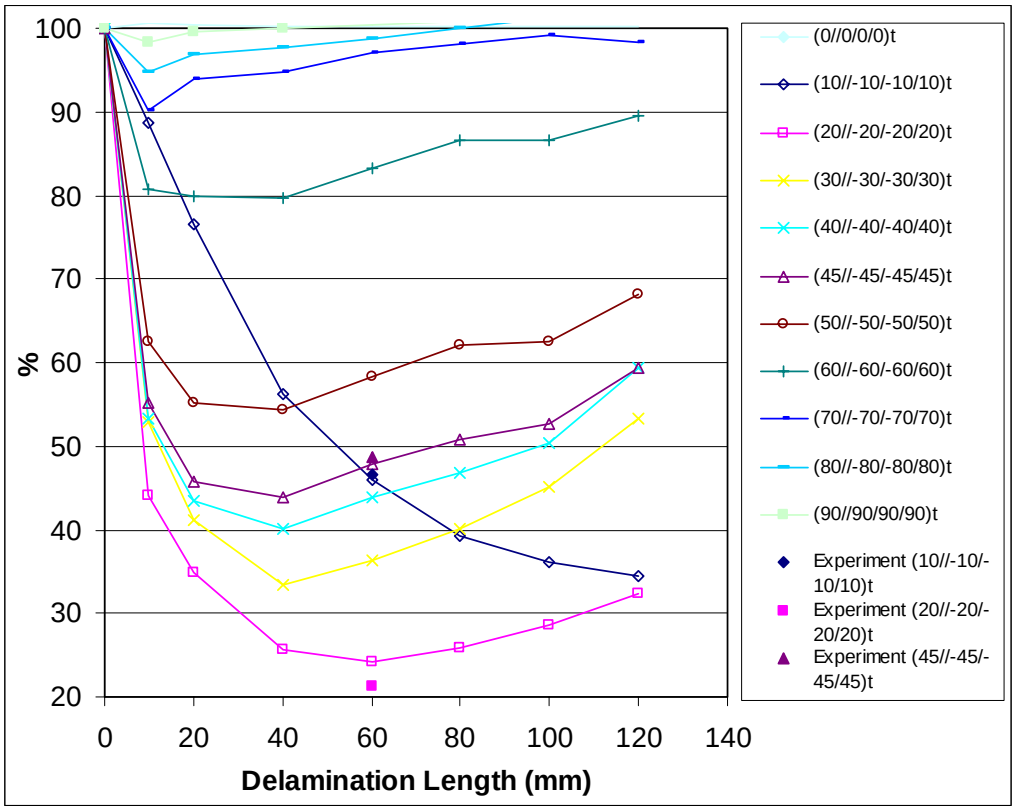

Figure 6. 23: 1st failure load/no delam failure load of $(\theta//-\theta/-\theta/\theta)_t$ laminates.

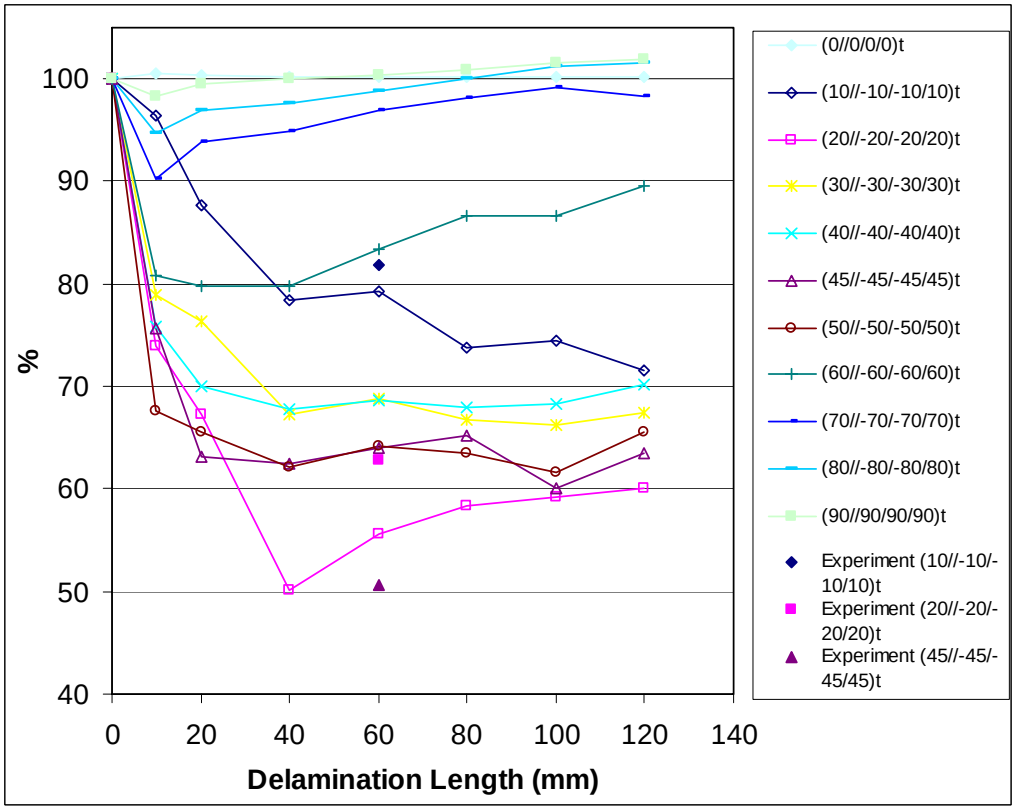

Figure 6. 24: Failure load / no delam failure load of $(\theta//-\theta/-\theta/\theta)_t$ laminates.

Table 6.2 Failure load list of other stacking sequences

Stacking Sequence	1 st failure (N)	last failure (N)
(90/0)s No delam	5441	9318
(0/90)s No delam	5441	9318
(90/0//0/90)t DL=60mm	5235	9129
(0/90//90/0)t DL=60mm	5304	9185
(90//0/0/90)t DL=60mm	5103.5	9269.8
(0//90/90/0)t DL=60mm	5325	8057
(10/-10//-10/10)t DL=60mm	11251	11251
(20/-20//-20/20)t DL=60mm	8327	8327
(30/-30//-30/30)t DL=60mm	3414	3414
(45/-45//-45/45)t DL=60mm	1649	1649
(60/-60//-60/60)t DL=60mm	811.8	811.8
(80/-80//-80/80)t DL=60mm	632.2	632.2

Chapter Seven

CONCLUSION AND FUTURE WORK

7.1 Conclusion

The conclusion is based on the results pertaining to laminate with a central delamination and subjected to tensile load. In summary, conclusions that can be deduced from the results presented in Chapters V and VI are:

1. Mid plane delamination tends to make the crack to propagate in mode I crack propagation.
2. Delamination between 1st and 2nd layers tends to cause mixed mode crack propagation problem.
3. The effect of delamination in composite structure will diminish when the thickness of the structure increases.
4. Delamination in $(90°/0°//0°/90°)_t$, $(0°/90°//90°/0°)_t$, $(\theta/-\theta//-\theta/\theta)_t$, $(90°//0°/0°/90°)_t$, $(0°//90°/90°/0°)_t$, $(45°//-45°/-45°/45°)_t$, $(60°//-60°/-60°/60°)_t$ and $(80°//-80°/-80°/80°)_t$ laminates are most likely will not propagate.
5. Delamination in $(10°//-10°/-10°/10°)_t$, $(20°//-20°/-20°/20°)_t$ and $(30°//-30°/-30°/30°)_t$ laminates have probability to propagate.
6. Twisting in $(\theta//-\theta/-\theta/\theta)_t$ laminates can cause the structure to sustain stress concentration and can be followed by degradation in the structure (1st failure) and will also reduce the total load that can be sustained (final failure) especially for $10° \le \theta < 60°$ and $DL \ge 10mm$.
7. The effect of delamination in composite structures can be critical depends on the structures stacking sequence, the position of delamination (in which layer delamination appear) and the delamination length.

7.2 Future Works

Future research can be focused on the following:

1. More experiment validation of the current results.

Some experimental validations have already been done, however these validations still not enough. More experimental validation need to be done to validate the current result.

2. Analytical model to predict the twisting angle of $(\theta//-\theta/-\theta/\theta)_t$ laminates.

   The prediction of twisting angle of $(\theta//-\theta/-\theta/\theta)_t$ laminates have been done using finite element model, however the experimental validation of this result is still not enough (the result of experimental validation is not in twisting angle directly). Thus we need some other way to validate the finite element result and it can be done with analytical model.

REFERENCES

1. *Ashby, M. F.,"Technology of the 1990s: Advanced Materials and Predictive Design," Philosophical Transactions of the Royal Society of London, A322, 393-407 (1987).*
2. Agarwal, B.D. and L.J. Broutman, *Analysis and Performance of Fiber Composites, 2nd edition.* 1990.
3. Gibson, R.F., *Principles of Composite Materials Mechanics.* McGraw-Hill, 1994.
4. Prombut, P., et al., *Delamination of multidirectional composite laminates at 0 degrees/theta degrees ply interfaces.* Engineering Fracture Mechanics, 2006. **73**(16): p. 2427-2442.
5. Czigany, T. and J. Kargerkocsis, *Comparison of the Failure Mode in Short and Long Glass-Fiber-Reinforced Injection-Molded Polypropylene Composites by Acoustic-Emission.* Polymer Bulletin, 1993. **31**(4): p. 495-501.
6. Ducept, F., D. Gamby, and P. Davies, *A mixed-mode failure criterion derived from tests on symmetric and asymmetric specimens.* Composites Science and Technology, 1999. **59**(4): p. 609-619.
7. Akbulut, H. and T. Ural, *An investigation on buckling of composite laminated plates with corner circular notches.* Journal of Thermoplastic Composite Materials, 2007. **20**(4): p. 371-387.
8. Shivakumar, K.N. and J.D. Whitcomb, *Buckling of a Sublaminate in a Quasi-Isotropic Composite Laminate.* Journal of Composite Materials, 1985. **19**(1): p. 2-18.
9. Nemeth, M.P., *Importance of Anisotropy on Buckling of Compression-Loaded Symmetrical Composite Plates.* Aiaa Journal, 1986. **24**(11): p. 1831-1835.
10. Luo, R.K., E.R. Green, and C.J. Morrison, *Impact damage analysis of composite plates.* International Journal of Impact Engineering, 1999. **22**(4): p. 435-447.
11. Tan, T.M. and C.T. Sun, *Use of Statical Indentation Laws in the Impact Analysis of Laminated Composite Plates.* Journal of Applied Mechanics-Transactions of the Asme, 1985. **52**(1): p. 6-12.

12. Sjoblom, P.O., J.T. Hartness, and T.M. Cordell, *On Low-Velocity Impact Testing of Composite-Materials.* Journal of Composite Materials, 1988. **22**(1): p. 30-52.
13. Kumar, R.L.V., et al., *Post impact compression strength (PICS) evaluation of glass/epoxy composite using a novel approach - Effect of delamination area.* Journal of Reinforced Plastics and Composites, 2007. **26**(11): p. 1101-1109.
14. Soutis, C. and P.T. Curtis, *Prediction of the post-impact compressive strength of CFRP laminated composites.* Composites Science and Technology, 1996. **56**(6): p. 677-684.
15. Xiong, Y., et al., *A Prediction Method for the Compressive Strength of Impact Damaged Composite Laminates.* Composite Structures, 1995. **30**(4): p. 357-367.
16. Chen, N.Z. and C.G. Soares, *Progressive failure analysis for prediction of post-buckling compressive strength of laminated composite plates and stiffened panels.* Journal of Reinforced Plastics and Composites, 2007. **26**(10): p. 1021-1042.
17. Chen, N.Z. and C.G. Soares, *Reliability assessment of post-buckling compressive strength of laminated composite plates and stiffened panels under axial compression.* International Journal of Solids and Structures, 2007. **44**(22-23): p. 7167-7182.
18. Kwon, Y.W., S.H. Yoon, and P.J. Sistare, *Compressive failure of carbon-foam sandwich composites with holes and/or partial delamination.* Composite Structures, 1997. **38**(1-4): p. 573-580.
19. Chang, F.K. and L.B. Lessard, *Damage Tolerance of Laminated Composites Containing an Open Hole and Subjected to Compressive Loadings .1. Analysis.* Journal of Composite Materials, 1991. **25**(1): p. 2-43.
20. Lessard, L.B. and F.K. Chang, *Damage Tolerance of Laminated Composites Containing an Open Hole and Subjected to Compressive Loadings .2. Experiment.* Journal of Composite Materials, 1991. **25**(1): p. 44-64.
21. Khamseh, A.R. and A.M. Waas, *Failure mechanisms of composite plates with a circular hole under remote biaxial planar compressive loads.* Journal of Engineering Materials and Technology-Transactions of the Asme, 1997. **119**(1): p. 56-64.

22. Yang, H.T.Y. and C.C. He, *3-Dimensional Finite-Element Analysis of Free-Edge Stresses and Delamination of Composite Laminates.* Journal of Composite Materials, 1994. **28**(15): p. 1394-1412.
23. Schellekens, J.C.J. and R. Deborst, *Free-Edge Delamination in Carbon-Epoxy Laminates - a Novel Numerical Experimental Approach.* Composite Structures, 1994. **28**(4): p. 357-373.
24. Lorriot, T., et al., *Onset of free-edge delamination in composite laminates under tensile loading.* Composites Part B-Engineering, 2003. **34**(5): p. 459-471.
25. Kutlu, Z. and F.K. Chang, *Composite Panels Containing Multiple through-the-Width Delaminations and Subjected to Compression .1. Analysis.* Composite Structures, 1995. **31**(4): p. 273-296.
26. Kutlu, Z. and F.K. Chang, *Composite Panels Containing Multiple through-the-Width Delaminations and Subjected to Compression .2. Experiments and Verification.* Composite Structures, 1995. **31**(4): p. 297-314.
27. Gillespie, J.W. and R.B. Pipes, *Compressive Strength of Composite Laminates with Interlaminar Defects.* Composite Structures, 1984. **2**(1): p. 49-69.
28. Short, G.J., F.J. Guild, and M.J. Pavier, *Delaminations in flat and curved composite laminates subjected to compressive load.* Composite Structures, 2002. **58**(2): p. 249-258.
29. Beilins, V., *Delamination of Composite Plates under Tensile Load.* Mechanics of Composite Materials, 1995. **31**(1): p. 34-38.
30. Swanson, S.R., *Introduction to Design and Analysis with Advanced Composite Materials.* Prentice-Hall, 1997.
31. *S. W. Tsai, "Strength Theories of Filamentary Structures," in R. T. Schwartz and H. S. Schwartz, Eds., Fundamental Aspects of Fiber Reinforced Plastic Composites, Interscience, New York, 1968, Chapter 1.*
32. *R. Hill, The Mathematical Theory of Plasticity, Oxford University Pres, Oxford, 1950.*
33. *Tsai, S. W. and Wu, E. M. (1971). A general theory of strength for anisotropic materials. Journal of Composite Materials. vol. 5, pp. 58-80.*
34. *Hashin, Z., 1980, "Failure Criteria for Unidirectional Fiber Composites," J. Appl. Mech. 47, 329-334.*

35. *Hashin, Z., and A. Rotem, "A Fatigue Criterion for Fiber-Reinforced Materials," Journal of Composite Materials, vol. 7, pp. 448–464, 1973.*
36. *Griffith, A.A. (1921). The Phenomena of Rupture and Flow in Solids, Philosophical Transaction of the Royal Society of London, A 221, pp. 163-197.*
37. *Griffith, A.A. (1924). The Theory of Rupture, Proceedings of the First International Conference of Applied Mechanics, Delft.*
38. *Irwin, G.R. (1948). Fracture Dynamics, Fraturing of Metals, American Society for Metals, Cleveland, ppp. 147-166.*
39. Kumar, P., *Elements of Fracture Mechanics, 1st ed.* Wheeler Publishing, 1999.
40. Rice, J.R., *A Path Independent Integral and Approximate Analysis of Strain Concentration by Notches and Cracks.* Journal of Applied Mechanics-Transactions of the Asme, 1968. **35**: p. 379-386.
41. *Erdogan, F. and Sih, G.C. (1963). On Crack Extension in Plates under Plane Loading and Transverse Shear, Transaction of ASME, Journal Of Basic Engineering, 85, pp. 519-527.*
42. *Sih, G.C. (1973). Method of Analysis and Solutions of Crack Problems, Mechanics of Fracture, Vol. I, Ed. G.C. Sih, Noordhoff, Leiden.*
43. *Sih, G.C. (1973). Some Basic Problems in Fracture Mechanics and New Concepts, Engineering Fracture Mechanics, 5, pp. 365-377.*
44. *Sih, G.C. (1974). Strain Energy Density Factor Applied to Mixed Mode Crack Problems, International Journal of Fracture, 10, No. 3, pp. 305-321.*
45. *K. L. Reifsnider, E. G. Henneke, W. W. Stinchcomb and J. L. Duke, Proc. Znt. Union of Theor. Appl. Mech., Blacksburg, Virginia, (1982). Pergamon Press, New York (1983) pp. 339-390.*
46. *C. K. H. Dharan, J. engng Maw. Technol. 100, 233-247 (1978).*
47. *Garg, 1988. A.C. Garg, Delamination-A damage model in composite structures. Engng Fracture Mech. 29 (1988), pp. 557–584.*
48. *C. T. Herakovich, J. compos. Mater. 15, 336-348 (1981).*
49. *N. J. Pagano and R. B. Pipes, Znr. J. Mech. Sci. 15, 679-688 (1973).*
50. *I. M. Daniel, R. E. Rowlands and J. B. Whiteside, Expl. Mech. 14, l-10 (1974).*
51. *D. 0. Stalnaker and W. W. Stinchcomb, ASTM STP 674, 620-641 (1979).*

52. *A. L. Highsmith, W. W. Stinchcomb and K. L. Reifsnider, ASTM STP 836, 194-216 (1984).*
53. *T. K. O'Brien, NASA-TM-84592 (1983).*
54. *C. T. Herakovich, Znt. J. Mech. Sci. 18, 129-134 (1976).*
55. *G. L. Farley and C. T. Herakovich, ASTM STP 658, 143-159 (1978).*
56. *F. W. Crossman and A. S. D. Wang, J. compos. Mater. 12, 2-18 (1978).*
57. *G. L. Farley and C. T. Herakovich, Two dimensional hygrothermal diffusion into a finite width composite laminate, VPI-E-77-20 (1977).*
58. *C. T. Herakovich and D. M. Wang, Expl Mech. 17,409-414 (1977).*
59. *M. W. Hyer, C. T. Herakovich, S. K. Milkovich and J. S. Short Jr, Composites 14, 276-280 (1983).*
60. *P. W. Hsu and C. T. Herakovich, J. compos. Mater. 11, 422-428 (1977).*
61. *J. G. Williams and M. D. Rhodes, ASTM STP 787,450-480 (1982).*
62. *M. D. Rhodes and J. G. Williams, NASA-TM 85748 (1984).*
63. *K. L. Reifsnider, E. G. Henneke, and W. W. Stinchcomb, Defect Property Relationship in Composite Materials, AFML-TR-76-81(1979).*
64. Spearing, S.M. and A.G. Evans, *The Role of Fiber Bridging in the Delamination Resistance of Fiber-Reinforced Composites.* Acta Metallurgica Et Materialia, 1992. **40**(9): p. 2191-2199.
65. Caprino, G., *The Use of Thin Dcb Specimens for Measuring Mode-1 Interlaminar Fracture-Toughness of Composite-Materials.* Composites Science and Technology, 1990. **39**(2): p. 147-158.
66. Devitt, D.F., R.A. Schapery, and W.L. Bradley, *A Method for Determining the Mode .1. Delamination Fracture-Toughness of Elastic and Viscoelastic Composite-Materials.* Journal of Composite Materials, 1980. **14**(OCT): p. 270-285.
67. Blackman, B.R.K., et al., *The failure of fibre composites and adhesively bonded fibre composites under high rates of test .1. Mode I loading - Experimental studies.* Journal of Materials Science, 1995. **30**(23): p. 5885-5900.
68. Smiley, A.J. and R.B. Pipes, *Rate Sensitivity of Mode-Ii Interlaminar Fracture-Toughness in Graphite Epoxy and Graphite Peek Composite-Materials.* Composites Science and Technology, 1987. **29**(1): p. 1-15.

69. Chatterjee, S.N., *Analysis of Test Specimens for Interlaminar Mode-Ii Fracture-Toughness .1. Elastic Laminates.* Journal of Composite Materials, 1991. **25**(5): p. 470-493.

70. Qiao, P.H., J.L. Wang, and J.F. Davalos, *Analysis of tapered ENF specimen and characterization of bonded interface fracture under Mode-II loading.* International Journal of Solids and Structures, 2003. **40**(8): p. 1865-1884.

71. Kinloch, A.J., et al., *THE MIXED-MODE DELAMINATION OF FIBER COMPOSITE-MATERIALS.* Composites Science and Technology, 1993. **47**(3): p. 225-237.

72. de Morais, A.B. and A.B. Pereira, *Mixed mode I+II interlaminar fracture of glass/epoxy multidirectional laminates - Part 1: Analysis.* Composites Science and Technology, 2006. **66**(13): p. 1889-1895.

73. Wilkinson, S.P., T.C. Ward, and J.E. McGrath, *Effect of Thermoplastic Modifier Variables on Toughening a Bismaleimide Matrix Resin for High-Performance Composite-Materials.* Polymer, 1993. **34**(4): p. 870-884.

74. Kim, J.K., et al., *FRACTURE-TOUGHNESS OF CFRP WITH MODIFIED EPOXY-RESIN MATRICES.* Composites Science and Technology, 1992. **43**(3): p. 283-297.

75. Laksimi, A., et al., *Mode-I Interlaminar Fracture of Symmetrical Cross-Ply Composites.* Composites Science and Technology, 1991. **41**(2): p. 147-164.

76. F. Ozdil, L.A.C., *Beam analysis of angle-ply laminate DCB specimens.* Composite Science and Technology, 1998. **59**: p. 305-315.

77. F. Ozdil, L.A.C.P.D., *Beam analysis of angle-ply lamiante end-notched flexure specimens.* Composite Science and Technology, 1998. **58**: p. 1929-1938.

78. A.B. Pereira, A.B.d.M., *Mixed mode I + II interlaminar fracture of glass/epoxy multidirectional laminates- Part 2: Experiments.* Composite Science and Technology, 2006. **66**: p. 1986-1902.

79. F. Ozdil, L.A.C., *Beam analysis of angle-ply laminate mixed-mode bending specimens.* Composite Science and Technology, 1999. **59**: p. 937-945.

80. *W. J. Johnson and P. D. Mangalgiri, J. Comp. Technol. Res. 9, 10 (1987).*

81. *R. Bordia, B. J. Dalgleish, P. G. Charalambides and A. G. Evans, J. Am. Ceram. Soc. 74, 2776 (1991).*

82. *G. Bao, B. Fan and A. G. Evans, Mech. Mater. 13, 59 (1992).*

83. Asp, L.E., *The effect of moisture and temperature on the interlaminar delamination toughness of a carbon/epoxy composite.* Composite Science and Technology, 1997. **58**: p. 967-977.

84. Morais, A.B.d., *Mode III interlaminar fracture of carbon/epoxy laminates using the edge crack torsion (ECT) test.* Composite Science and Technology, 2009. **69**: p. 670-676.

85. Dharmawan, F., *Mixed mode fracture toughness of GFRP compsites.* Composite Structures, 2006. **75**: p. 328-338.

APPENDIX I

FINITE ELEMENT INPUT PROGRAM LISTINGS

APPENDIX I.1 An example of a Finite Element full model input program listing for energy release rates calculation

```
*Heading
 (30//-30/-30/30)t; ml=0.3mm; ed=0.0001; bias=10; hen=15
** Job name: zzz3030c60b10he15p1 Model name: zc60b10he15cr5mm
*Preprint, echo=NO, model=NO, history=NO, contact=NO
**
** PARTS
**
*Part, name="load node"
*Node
      8,          80.,          0.,          0.
*End Part
**
*Part, name=zc60b10he15
*Node
      1,          70.,          0.,          0.
      2,          70.,          0.,       0.125
      3,          70.,        -10.,       0.125
      4,          70.,        -10.,          0.
      5,          30.,          0.,       0.125
*Element, type=C3D20R
   1,   469,   483,  4939,  4841,     1,     2,   400,   427, 12249, 12248, 12247, 12246,
```

2, 4841, 4939, 4940, 4842, 427, 400, 401, 426, 12247, 12260, 12259, 12258,
*Element, type=C3D15
10141, 296, 21, 43, 4499, 609, 4736, 46232, 15280, 46231, 46233, 44848, 46234, 38820, 14180, 44872
*Elset, elset=atasbawahzc60b10he15
1, 2, 3, 4, 5, 6, 7, 8, 9, 10, 11, 12, 13, 14, 15, 16
*Elset, elset=tengah22zc60b10he15
241, 242, 243, 244, 245, 246, 247, 248, 249, 250, 251, 252, 253, 254,
*Orientation, name=Ori-7
1., 0., 0., 0., 1., 0.
** Region: (fiberdux:Picked), (Material Orientation:atasbawahzc60b10he15)
*Elset, elset=_I1, internal
1, 2, 3, 4, 5, 6, 7, 8, 9, 10, 11, 12, 13, 14, 15, 16
** Section: fiberdux
*Solid Section, elset=_I1, orientation=Ori-7, material="fiberdux r913c-hta epoxy"
1.,
*Orientation, name=Ori-8
1., 0., 0., 0., 1., 0.
** Region: (fiberdux:Picked), (Material Orientation:tengah22zc60b10he15)
*Elset, elset=_I2, internal
241, 242, 243, 244, 245, 246, 247, 248, 249, 250, 251, 252, 253, 254,
** Section: fiberdux
*Solid Section, elset=_I2, orientation=Ori-8, material="fiberdux r913c-hta epoxy"
1.,
*End Part
**
**
** ASSEMBLY
**
*Assembly, name=Assembly
**

```
*Instance, name=zc60b10he15-1, part=zc60b10he15
*End Instance
**
*Instance, name="load node-1", part="load node"
*End Instance
**
*Nset, nset="load node", instance="load node-1"
 8,
*Nset, nset="end load", instance=zc60b10he15-1
    1,    2,    3,    4,   17,   18,   19,   20,   41,   44,   45,  393,  394,  395,  396,
400
*Nset, nset="end part", instance=zc60b10he15-1
    9,   10,   11,   12,   25,   28,   31,   32,  109,  112,  114,  115,  116,  117,
294,
*Surface, type=ELEMENT, name=ataszc60b10he15
_ataszc60b10he15_S4, S4
_ataszc60b10he15_S5, S5
*Elset, elset=_bawahzc60b10he15_S4, internal, instance=zc60b10he15-1, generate
 3136,  3315,     1
*Elset, elset=_bawahzc60b10he15_S5, internal, instance=zc60b10he15-1, generate
 6346,  6525,     1
*Surface, type=ELEMENT, name=bawahzc60b10he15
_bawahzc60b10he15_S4, S4
_bawahzc60b10he15_S5, S5
** Constraint: Constraint-1
*Equation
2
"end load", 1, 1.
"load node", 1, -1.
*Nset, nset=_PickedSet282-1_, internal, instance=zc60b10he15-1
 398,
*End Assembly
*Amplitude, name=tabular, time=TOTAL TIME
0., 0., 1., 1.
```

```
**
** MATERIALS
**
*Material, name="fiberdux r913c-hta epoxy"
*Elastic, type=ORTHOTROPIC
152456.,  4687.9,  12165.,  4687.9, 5649.68,  12165.,   5430.,   5430.
**
** INTERACTION PROPERTIES
**
*Surface Interaction, name=CONTACT
1.,
*Surface Behavior, pressure-overclosure=HARD
**
** INTERACTIONS
**
** Interaction: contact
*Contact Pair, interaction=CONTACT, small sliding, type=SURFACE TO
SURFACE, supplementary constraints=YES
bawahzc60b10he15, ataszc60b10he15
** ----------------------------------------------------------------
**
** STEP: under load
**
*Step, name="under load", inc=100000
*Static, stabilize=0.0001
0.0001, 1., 1e-100, 1.
**
** BOUNDARY CONDITIONS
**
** Name: end load Type: Displacement/Rotation
*Boundary, amplitude=tabular
"end load", 2, 2
"end load", 3, 3
"end load", 4, 4
```

```
"end load", 5, 5
"end load", 6, 6
** Name: end part Type: Symmetry/Antisymmetry/Encastre
*Boundary
"end part", ENCASTRE
** Name: load node Type: Displacement/Rotation
*Boundary, amplitude=tabular
"load node", 1, 1, 0.3
**
** OUTPUT REQUESTS
**
*Restart, write, frequency=0
**
** FIELD OUTPUT: F-Output-1
**
*Output, field, variable=PRESELECT
**
** HISTORY OUTPUT: H-Output-6
**
*Output, history
*Node Output, nset="load node"
RF1, U1
**
** HISTORY OUTPUT: H-Output-1
**
*Contour integral, crack name=H-Output-1_Crack-1, contours=6, crack tip nodes
_PickedSet282-1_, _PickedSet283-1_, -1., 0., 0.
**
** HISTORY OUTPUT: H-Output-2
**
*Contour integral, crack name=H-Output-2_Crack-2, contours=6, crack tip nodes
_PickedSet284-1_, _PickedSet285-1_, -0.923886, 0., 0.382669
**
** HISTORY OUTPUT: H-Output-3
```

```
**
*Contour integral, crack name=H-Output-3_Crack-3, contours=6, crack tip nodes
_PickedSet286-1_, _PickedSet287-1_, -0.70708, 0., 0.707134
**
** HISTORY OUTPUT: H-Output-4
**
*Contour integral, crack name=H-Output-4_Crack-4, contours=6, crack tip nodes
_PickedSet288-1_, _PickedSet289-1_, -0.382624, 0., 0.923904
**
** HISTORY OUTPUT: H-Output-5
**
*Contour integral, crack name=H-Output-5_Crack-5, contours=6, crack tip nodes
_PickedSet290-1_, _PickedSet291-1_, 0., 0., 1.
*End Step
```

APPENDIX I.2 An example of a Finite Element full model input program listing for failure load calculation

```
*Heading
** Job name: hashinfaildl60c3030p1 Model name: cont shell nc 2s dl60mm 2x5
2x2HS
*Preprint, echo=NO, model=NO, history=NO, contact=NO
**
** PARTS
**
*Part, name="cont shell wc 2s 2x5 2x2"
*Node
      1,          30.,          -10.,          0.375
      2,          30.,           10.,          0.375
      3,          70.,           10.,          0.375
      4,          70.,          -10.,          0.375
      5,          30.,          -10.,             0.
*Element, type=SC8R
```

```
 1,  57,   5,  88, 454,  25,   1,  56, 391
 2,  58,  57, 454, 455,  26,  25, 391, 392
 3,  59,  58, 455, 456,  27,  26, 392, 393
 4,  60,  59, 456, 457,  28,  27, 393, 394
 5,  61,  60, 457, 458,  29,  28, 394, 395
*Elset, elset=atasdl6022
 81,  82,  83,  84,  85,  86,  87,  88,  89,  90,  91,  92,  93,  94,  95,  96
 97,  98,  99, 100, 101, 102, 103, 104, 105, 106, 107, 108, 109, 110, 111, 112
113, 114, 115, 116, 117, 118, 119, 120, 121, 122, 123, 124, 125, 126, 127, 128
129, 130, 131, 132, 133, 134, 135, 136, 137, 138, 139, 140, 141, 142, 143, 144
*Elset, elset=bawahdl6022
  1,  2,  3,  4,  5,  6,  7,  8,  9,  10,  11,  12,  13,  14,  15,  16
 17,  18,  19,  20,  21,  22,  23,  24,  25,  26,  27,  28,  29,  30,  31,  32
 33,  34,  35,  36,  37,  38,  39,  40,  41,  42,  43,  44,  45,  46,  47,  48
 49,  50,  51,  52,  53,  54,  55,  56,  57,  58,  59,  60,  61,  62,
*Elset, elset=contatasdl6022, generate
 91,  370,   1
*Elset, elset=contbawahdl6022, generate
 471,  750,   1
*Elset, elset=_PickedSet7, internal, generate
  1,  920,   1
*Orientation, name=Ori-1
        1.,          0.,          0.,          0.,          1.,
** Section: composite2dbuatsibawah
*Shell Section, elset=bawahdl6022, composite, orientation=Ori-1, controls=EC-1
0.125, 3, "FIBERDUX LAMINA DATA FACESHEET", 30.
0.25, 3, "FIBERDUX LAMINA DATA FACESHEET", -30.
** Section: composite2dbuatsiatas
*Shell Section, elset=atasdl6022, composite, orientation=Ori-1, controls=EC-1
0.0625, 3, "FIBERDUX LAMINA DATA FACESHEET", 30.
0.0625, 3, "FIBERDUX LAMINA DATA FACESHEET", 30.
*End Part
**
*Part, name="load node-mesh-1"
```

```
*Node
      4,          80.,          0.,          0.
*End Part
**
**
** ASSEMBLY
**
*Assembly, name=Assembly
**
*Instance, name="cont shell wc 2s 2x5 2x2-1", part="cont shell wc 2s 2x5 2x2"
*End Instance
**
*Instance, name="load node-mesh-1-1", part="load node-mesh-1"
*End Instance
**
*Nset, nset="end load", instance="cont shell wc 2s 2x5 2x2-1"
   3,   4,   7,   8,  15,  16,  41,  42,  43,  44,  45,  46,  47,  48,  49,  73
  74,  75,  76,  77,  78,  79,  80,  81, 239, 240, 241, 242, 243, 244, 245, 246
 247,
*Nset, nset="end part", instance="cont shell wc 2s 2x5 2x2-1"
  19,  20,  21,  22,  23,  24, 329, 330, 331, 332, 333, 334, 335, 336, 337, 352
 353, 354, 355, 356, 357, 358, 359, 360, 375, 376, 377, 378, 379, 380, 381, 382
 383,
*Nset, nset="load node", instance="load node-mesh-1-1"
 4,
*Elset, elset=whole, instance="cont shell wc 2s 2x5 2x2-1", generate
   1,  920,    1
*Elset, elset=_atasdl6022_S1, internal, instance="cont shell wc 2s 2x5 2x2-1",
generate
  91,  370,    1
*Surface, type=ELEMENT, name=atasdl6022
_atasdl6022_S1, S1
*Elset, elset=_bawahdl6022_S2, internal, instance="cont shell wc 2s 2x5 2x2-1",
generate
```

```
 471,  750,    1
*Surface, type=ELEMENT, name=bawahdl6022
_bawahdl6022_S2, S2
** Constraint: Constraint-1
*Equation
2
"end load", 1, 1.
"load node", 1, -1.
*End Assembly
**
** ELEMENT CONTROLS
**
*Section Controls, name=EC-1, ELEMENT DELETION=YES
1., 1., 1.
*Amplitude, name=tabular, time=TOTAL TIME
0., 0., 1., 1.
**
** MATERIALS
**
*Material, name="FIBERDUX LAMINA DATA FACESHEET"
*Damage Initiation, criterion=HASHIN
1900., 1550.,  65.5,  140., 101.2, 101.2
*Damage Evolution, type=ENERGY
 1e-08, 1e-08, 1e-09, 1e-09
*Density
 1.1e-09,
*Elastic, type=LAMINA
150000., 9500., 0.263, 5430., 5430., 3260.
*Material, name="fiberdux lamina tsai hill wu"
*Density
 1.1e-09,
*Elastic, type=LAMINA
150000., 9500., 0.263, 5430., 5430., 3260.
*Fail Strain
```

```
 0.17,  -0.07,   0.05, -0.013,   0.11
*Fail Stress
1900.,-1550.,  65.5, -140., 101.2,    0.,    0.
**
** INTERACTION PROPERTIES
**
*Surface Interaction, name=CONTACT
1.,
*Surface Behavior, pressure-overclosure=HARD
**
** BOUNDARY CONDITIONS
**
** Name: constraint Type: Symmetry/Antisymmetry/Encastre
*Boundary
"end part", ENCASTRE
** ----------------------------------------------------------------
**
** STEP: under load
**
*Step, name="under load", nlgeom=YES, inc=100000
*Static, stabilize, factor=0.01
0.01, 1., 1e-100, 0.01
**
** BOUNDARY CONDITIONS
**
** Name: displacement Type: Displacement/Rotation
*Boundary, amplitude=tabular
"load node", 1, 1, 0.767
** Name: load constraint Type: Displacement/Rotation
*Boundary
"end load", 2, 2
"end load", 3, 3
"end load", 4, 4
"end load", 5, 5
```

```
"end load", 6, 6
**
** OUTPUT REQUESTS
**
*Restart, write, frequency=0
**
** FIELD OUTPUT: F-Output-1
**
*Output, field
*Node Output
CF, RF, U
*Element Output, directions=YES
CFAILURE, DMICRT, LE, PE, PEEQ, PEMAG, S, STATUS
*Contact Output
CDISP, CSTRESS
**
** HISTORY OUTPUT: H-Output-1
**
*Output, history
*Node Output, nset="load node"
RF1, U1
*End Step
```

APPENDIX II

ANISOTROPIC, ORTHOTROPIC, ISOTROPIC AND COMPOSITE CONSTITUTIVE EQUATIONS

APPENDIX II.1 Anisotropic constitutive equation

They are nine stress components in a general three dimensional state of stress (Figure II.1) and normally each of those components is represented by σ_{ij} notation. Along with each stress components, there is a strain component ε_{ij}. The components with $i = j$ are the normal components and the components with $i \neq j$ are the shear components.

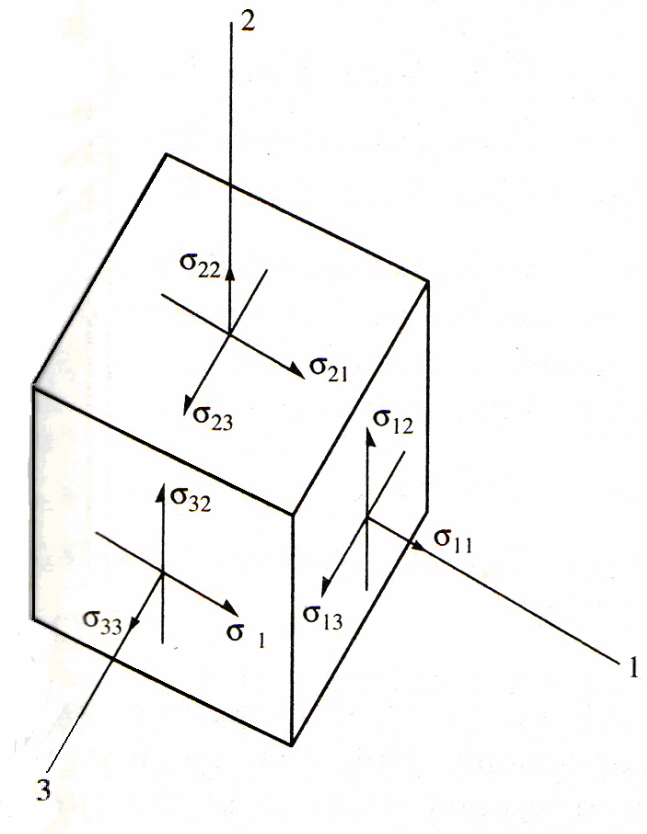

Figure II. 1: Three dimensional state of stress [3].

In generalized anisotropic Hooke's law each stress component is a function of those nine strain components. At a point in the material, the most general stress strain relationship can be expressed by following equation

$$\begin{Bmatrix} \sigma_{11} \\ \sigma_{22} \\ \sigma_{33} \\ \sigma_{23} \\ \sigma_{31} \\ \sigma_{12} \\ \sigma_{32} \\ \sigma_{13} \\ \sigma_{21} \end{Bmatrix} = \begin{bmatrix} C_{1111} & C_{1122} & C_{1133} & C_{1123} & C_{1131} & C_{1112} & C_{1132} & C_{1113} & C_{1121} \\ C_{2211} & C_{2222} & C_{2233} & C_{2223} & C_{2231} & C_{2212} & C_{2232} & C_{2213} & C_{2221} \\ C_{3311} & C_{3322} & C_{3333} & C_{3323} & C_{3331} & C_{3312} & C_{3332} & C_{3313} & C_{3321} \\ C_{2311} & C_{2322} & C_{2333} & C_{2323} & C_{2331} & C_{2312} & C_{2332} & C_{2313} & C_{2321} \\ C_{3111} & C_{3122} & C_{3133} & C_{3123} & C_{3131} & C_{3112} & C_{3132} & C_{3113} & C_{3121} \\ C_{1211} & C_{1222} & C_{1233} & C_{1223} & C_{1231} & C_{1212} & C_{1232} & C_{1213} & C_{1221} \\ C_{3211} & C_{3222} & C_{3233} & C_{3223} & C_{3231} & C_{3212} & C_{3232} & C_{3213} & C_{3221} \\ C_{1311} & C_{1322} & C_{1333} & C_{1323} & C_{1331} & C_{1312} & C_{1332} & C_{1313} & C_{1321} \\ C_{2111} & C_{2122} & C_{2133} & C_{2123} & C_{2131} & C_{2112} & C_{2132} & C_{2113} & C_{2121} \end{bmatrix} \begin{Bmatrix} \varepsilon_{11} \\ \varepsilon_{22} \\ \varepsilon_{33} \\ \varepsilon_{23} \\ \varepsilon_{31} \\ \varepsilon_{12} \\ \varepsilon_{32} \\ \varepsilon_{13} \\ \varepsilon_{21} \end{Bmatrix} \quad \text{(II.1).}$$

$[C]$ is elastic constant matrix that have 81 components. It has been known that stress and strain are symmetric and elastic constant must be symmetric too. As a result only 36 nonzero components that can be considered into account now. For simplicity, we can decrease the number of subscript in the elastic constant matrix components, stress components and strain components. The changes of stress and strain subscript can be seen in the equation below

$$\begin{aligned} &\sigma_{11} = \sigma_1 && \sigma_{22} = \sigma_2 && \sigma_{33} = \sigma_3 \\ &\sigma_{23} = \sigma_{32} = \sigma_4 && \sigma_{13} = \sigma_{31} = \sigma_5 && \sigma_{12} = \sigma_{21} = \sigma_6 \\ &\varepsilon_{11} = \varepsilon_1 && \varepsilon_{22} = \varepsilon_2 && \varepsilon_{33} = \varepsilon_3 \\ &\varepsilon_{23} = \varepsilon_{32} = \varepsilon_4 && \varepsilon_{23} = \varepsilon_{32} = \varepsilon_4 && \varepsilon_{23} = \varepsilon_{32} = \varepsilon_4 \end{aligned} \quad \text{(II.2).}$$

and elastic constant matrix $[C]$ can be written as

$$C_{ij} = \begin{bmatrix} C_{11} & C_{12} & C_{13} & C_{14} & C_{15} & C_{16} \\ C_{12} & C_{22} & C_{23} & C_{24} & C_{25} & C_{26} \\ C_{13} & C_{23} & C_{33} & C_{34} & C_{35} & C_{36} \\ C_{14} & C_{24} & C_{34} & C_{44} & C_{45} & C_{46} \\ C_{15} & C_{25} & C_{35} & C_{45} & C_{55} & C_{56} \\ C_{16} & C_{26} & C_{36} & C_{46} & C_{56} & C_{66} \end{bmatrix} \quad \text{(II.3).}$$

Equation (II.3) normally known as stiffness matrix for anisotropic material.

APPENDIX II.2 3D orthotropic constitutive equation

The other type of symmetry is material property symmetry. Material property symmetry also can reduce the stiffness matrix components, because the material property at certain distance from one side of symmetry plane is just the same as material property at same distance from the other side of symmetry plane. The easiest example is unidirectional composite lamina. Unidirectional composite lamina has three planes of material property symmetry, and those planes are perpendicular to each other (Figure II.2) so normally we call it as orthotropic material. Different from anisotropic material properties that do not depend on coordinate system, orthotropic material properties depend on coordinate system. Furthermore, they are two coordinate systems that normally been used along orthotropic material, principal and non principal coordinates systems (Figure II.2). For convenience orthotropic material properties normally are stated along with principal coordinate system. Stiffness matrix for orthotropic material associated with principal coordinate system is of the form

$$C_{ij} = \begin{bmatrix} C_{11} & C_{12} & C_{13} & 0 & 0 & 0 \\ C_{12} & C_{22} & C_{23} & 0 & 0 & 0 \\ C_{13} & C_{23} & C_{33} & 0 & 0 & 0 \\ 0 & 0 & 0 & C_{44} & 0 & 0 \\ 0 & 0 & 0 & 0 & C_{55} & 0 \\ 0 & 0 & 0 & 0 & 0 & C_{66} \end{bmatrix} \quad \text{(II.4).}$$

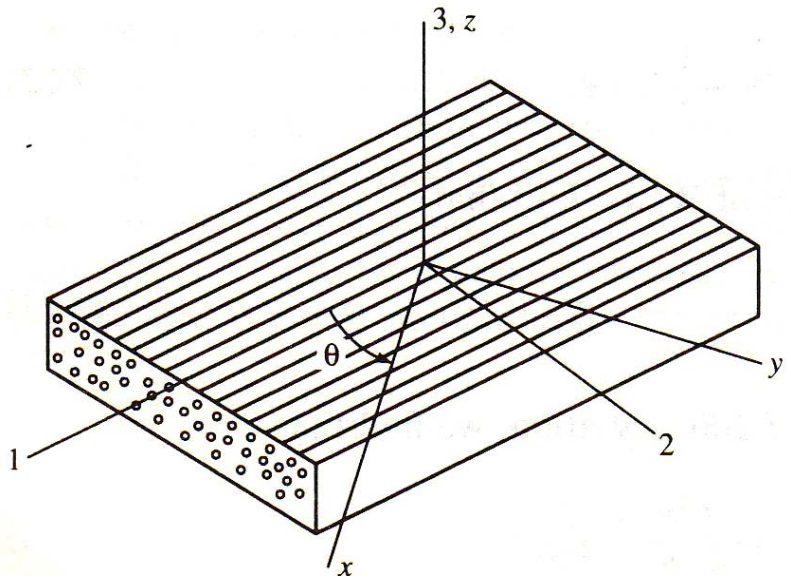

Figure II. 2: Orthotropic lamina with principal and non principal coordinate systems [3].

Moreover, we need to get the value of stiffness matrix components. The easiest way to get it is assuming only one stress that is exist and the other stresses are zero, so every strain can be expressed in that active stress. If it is assumed that only normal stress in 1st direction (σ_1) exist and the other stress components are assumed equal to zero, the strain components can be stated in σ_1 as

$$\varepsilon_1 = \frac{\sigma_1}{E_1}$$

$$\varepsilon_2 = -\nu_{12}\varepsilon_1 = -\frac{\nu_{12}\sigma_1}{E_1}$$

$$\varepsilon_3 = -\nu_{13}\varepsilon_1 = -\frac{\nu_{13}\sigma_1}{E_1} \qquad \text{(II.5).}$$

$$\gamma_{12} = \gamma_{23} = \gamma_{13} = 0$$

When it is assumed all of stress components equal to zero except σ_2, the strain components can be expressed as

$$\varepsilon_2 = \frac{\sigma_2}{E_2}$$

$$\varepsilon_1 = -\nu_{21}\varepsilon_2 = -\frac{\nu_{21}\sigma_2}{E_2}$$

$$\varepsilon_3 = -\nu_{23}\varepsilon_2 = -\frac{\nu_{23}\sigma_2}{E_2} \qquad \text{(II.6)}$$

$$\gamma_{12} = \gamma_{23} = \gamma_{13} = 0$$

Furthermore if the only existed stress is σ_3, the strain components will be of the form

$$\varepsilon_3 = \frac{\sigma_3}{E_3}$$

$$\varepsilon_1 = -\nu_{31}\varepsilon_3 = -\frac{\nu_{31}\sigma_3}{E_3}$$

$$\varepsilon_2 = -\nu_{32}\varepsilon_3 = -\frac{\nu_{32}\sigma_3}{E_3} \qquad \text{(II.7).}$$

$$\gamma_{12} = \gamma_{23} = \gamma_{13} = 0$$

Unlike normal strain, shear strain in certain direction depends only on shear stress and shear modulus in the same direction, so it can be stated as

$$\gamma_{12} = \frac{\tau_{12}}{G_{12}}$$

$$\gamma_{23} = \frac{\tau_{23}}{G_{23}} \qquad \text{(II.8).}$$

$$\gamma_{13} = \frac{\tau_{13}}{G_{13}}$$

In the end we already got the value of every component in equation II.4, so the stress strain relationship for 3D orthotropic material associated with principal coordinate can be written as

$$\begin{Bmatrix} \varepsilon_1 \\ \varepsilon_2 \\ \varepsilon_3 \\ \gamma_{23} \\ \gamma_{31} \\ \gamma_{12} \end{Bmatrix} = \begin{bmatrix} 1/E_1 & -\nu_{21}/E_2 & -\nu_{31}/E_3 & 0 & 0 & 0 \\ -\nu_{12}/E_1 & 1/E_2 & -\nu_{32}/E_3 & 0 & 0 & 0 \\ -\nu_{13}/E_1 & -\nu_{23}/E_2 & 1/E_3 & 0 & 0 & 0 \\ 0 & 0 & 0 & 1/G_{23} & 0 & 0 \\ 0 & 0 & 0 & 0 & 1/G_{31} & 0 \\ 0 & 0 & 0 & 0 & 0 & 1/G_{12} \end{bmatrix} \begin{Bmatrix} \sigma_1 \\ \sigma_2 \\ \sigma_3 \\ \tau_{23} \\ \tau_{31} \\ \tau_{12} \end{Bmatrix} \qquad \text{(II.9).}$$

Further simplification as stated below

$$E_1 = E_2 = E_3 = E$$

$$G_{12} = G_{23} = G_{13} = G$$

$$\nu_{12} = \nu_{23} = \nu_{13} = \nu \qquad \text{(II.10)}$$

$$G = \frac{E}{2(1+\nu)}$$

reduce the independent engineering constant become two and we normally call it as isotropic material.

APPENDIX II.3 2D orthotropic constitutive equation

3D orthotropic can be simplified into 2D problem, using plane stress assumption. Because of plane stress assumption σ_3, τ_{23}, and τ_{31} are equal to zero, so the stress strain relation become

$$\begin{Bmatrix} \sigma_1 \\ \sigma_2 \\ \tau_{12} \end{Bmatrix} = \begin{bmatrix} Q_{11} & Q_{12} & 0 \\ Q_{12} & Q_{22} & 0 \\ 0 & 0 & 2Q_{66} \end{bmatrix} \begin{Bmatrix} \varepsilon_1 \\ \varepsilon_2 \\ \gamma_{12}/2 \end{Bmatrix} \qquad \text{(II.11)}$$

where

$$Q_{11} = \frac{E_1}{1-\nu_{12}\nu_{21}}$$

$$Q_{12} = \frac{\nu_{12}E_2}{1-\nu_{12}\nu_{21}}$$

$$Q_{22} = \frac{E_2}{1-\nu_{12}\nu_{21}} \qquad \text{(II.12).}$$

$$Q_{66} = G_{12}$$

2D orthotropic stress strain relationship is more convenience than 3D orthotropic stress strain relationship. Furthermore, it still visible to represent composite lamina stress strain relationship, because composite normally lamina has very thin thickness and for that case we can use plain stress assumption. To be noted, this 2D orthotropic stress strain relationship still uses principal coordinate system.

APPENDIX II.4 Coordinates transformation

Equation II.12 shows us the stress strain relationship for 2D orthotropic material using principal coordinate system. This stress strain relationship will be different if we use non principal coordinate system, and it will be discussed here.

Consider direction 1 and 2 in the Figure II.3 as local coordinate system and

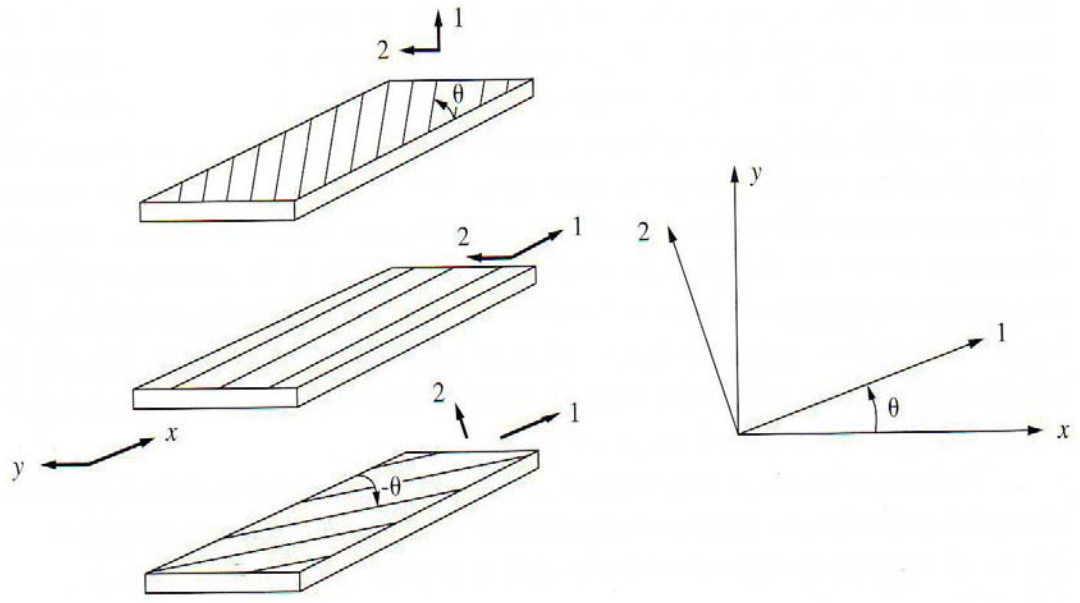

Figure II. 3: Unidirectional plies with a local 1,2 fiber coordinate system and a global x,y coordinate system [30].

they also refer to fiber direction and transverse to fiber direction (principal coordinate system). Furthermore, x and y direction in the same picture represent the global coordinate system. The stress transformation from global to local coordinate system is given by

$$\begin{Bmatrix}\sigma_1\\ \sigma_2\\ \tau_{12}\end{Bmatrix}=[T]\begin{Bmatrix}\sigma_x\\ \sigma_y\\ \tau_{xy}\end{Bmatrix} \tag{II.13}$$

where the transformation matrix

$$[T]=\begin{bmatrix}\cos^2\theta & \sin^2\theta & 2\sin\theta\cos\theta\\ \sin^2\theta & \cos^2\theta & -2\sin\theta\cos\theta\\ -\sin\theta\cos\theta & \sin\theta\cos\theta & \cos^2\theta-\sin^2\theta\end{bmatrix} \tag{II.14}.$$

The transformation is almost the same for the strain components, but be cautious of shear strain component. We must differentiate engineering shear strain and shear strain, with shear strain is half of engineering shear strain. The easiest way to do that is using a matrix R witch is of the form

$$[R]=\begin{bmatrix}1 & 0 & 0\\ 0 & 1 & 0\\ 0 & 0 & 2\end{bmatrix} \tag{II.15}.$$

In addition, the relation between engineering and tensor strain can be stated as

$$\begin{Bmatrix}\varepsilon_1\\ \varepsilon_2\\ \gamma_{12}\end{Bmatrix}=[R]\begin{Bmatrix}\varepsilon_1\\ \varepsilon_2\\ \gamma_{12}/2\end{Bmatrix} \tag{II.16}.$$

As a result, the strain transformation from global to local coordinate system can be written as

$$\begin{Bmatrix}\varepsilon_1\\ \varepsilon_2\\ \gamma_{12}\end{Bmatrix}=[R]\begin{Bmatrix}\varepsilon_1\\ \varepsilon_2\\ \gamma_{12}/2\end{Bmatrix}=[R][T]\begin{Bmatrix}\varepsilon_x\\ \varepsilon_y\\ \gamma_{xy}/2\end{Bmatrix}=[R][T][R^{-1}]\begin{Bmatrix}\varepsilon_x\\ \varepsilon_y\\ \gamma_{xy}\end{Bmatrix} \tag{II.17}.$$

The stress strain relationship using principal coordinate system can be expressed as

$$\begin{Bmatrix}\sigma_1\\ \sigma_2\\ \tau_{12}\end{Bmatrix}=[Q]\begin{Bmatrix}\varepsilon_1\\ \varepsilon_2\\ \gamma_{12}\end{Bmatrix}=[Q][R]\begin{Bmatrix}\varepsilon_1\\ \varepsilon_2\\ \gamma_{12}/2\end{Bmatrix} \tag{II.18}$$

Combining equation II.13, II.16, II.17 and II.18

$$\begin{Bmatrix}\sigma_x\\ \sigma_y\\ \tau_{xy}\end{Bmatrix}=\left[T^{-1}\right]\begin{Bmatrix}\sigma_1\\ \sigma_2\\ \tau_{12}\end{Bmatrix}=\left[T^{-1}\right][Q][R]\begin{Bmatrix}\varepsilon_1\\ \varepsilon_2\\ \gamma_{12}/2\end{Bmatrix}=\left[T^{-1}\right][Q][R][T]\begin{Bmatrix}\varepsilon_x\\ \varepsilon_y\\ \gamma_{xy}/2\end{Bmatrix} \quad \text{(II.19).}$$

In the end, stress strain relationship for 2D orthotropic material using non principal coordinate system is of the form

$$\begin{Bmatrix}\sigma_x\\ \sigma_y\\ \tau_{xy}\end{Bmatrix}=\left[T^{-1}\right][Q][R][T]\left[R^{-1}\right]\begin{Bmatrix}\varepsilon_x\\ \varepsilon_y\\ \gamma_{xy}\end{Bmatrix}=\left[\overline{Q}\right]\begin{Bmatrix}\varepsilon_x\\ \varepsilon_y\\ \gamma_{xy}\end{Bmatrix} \quad \text{(II.20)}$$

where

$$\left[\overline{Q}\right]=\left[T^{-1}\right][Q][R][T]\left[R^{-1}\right] \quad \text{(II.21).}$$

APPENDIX II.5 Composite laminate constitutive equation

Several laminas stacked together into one are called as laminate. Consequently laminate properties are affected by the properties of each lamina from which it is arranged. The derivation of laminate properties from its laminas properties will be given in this subchapter.

For this problem, it is assumed that individual laminas are perfectly bonded together, normal to the center line remain normal after deformation (through the thickness shear deformations are neglected), and the only cause of z displacement is bending. u , v and w respectively are the displacements in the x, y and z. The relation between displacement u and v with center line displacement u_0 and v_0 (Figure II.4) can be stated as

$$u(x,y,z)=u_0(x,y)-z\frac{\partial w(x,y)}{\partial x}$$

$$v(x,y,z)=v_0(x,y)-z\frac{\partial w(x,y)}{\partial y} \quad \text{(II.22)}$$

and it is well known that in plane normal and shear strain can be written as

$$\varepsilon_x=\frac{\partial u}{\partial x}$$

$$\varepsilon_y=\frac{\partial v}{\partial y} \quad \text{(II.23).}$$

$$\gamma_y=\frac{\partial v}{\partial x}+\frac{\partial u}{\partial y}$$

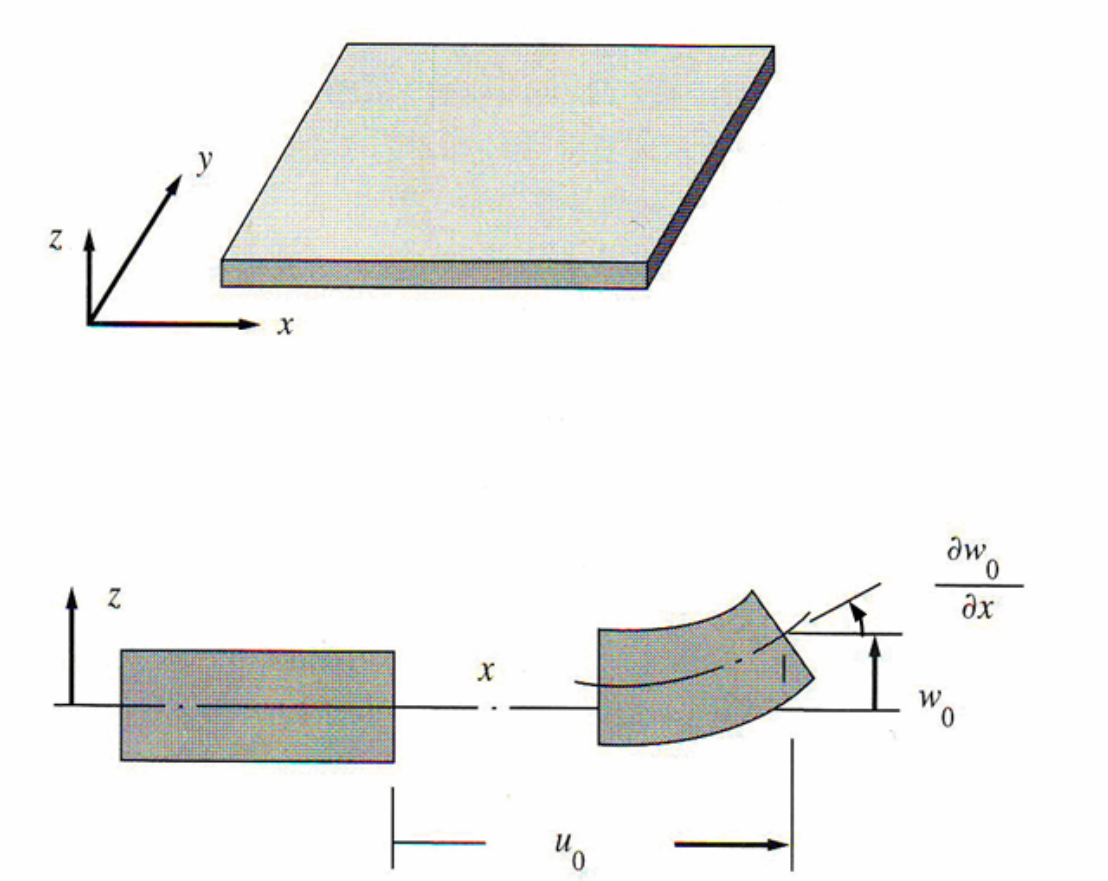

Figure II. 4: Illustration of extension and bending plate deformation [30].

By substituting equation II.22 into equation II.23, we can get

$$\begin{Bmatrix} \varepsilon_x \\ \varepsilon_y \\ \gamma_{xy} \end{Bmatrix} = \begin{Bmatrix} \frac{\partial u_0}{\partial x} \\ \frac{\partial v_0}{\partial y} \\ \frac{\partial v_0}{\partial x} + \frac{\partial u_0}{\partial v} \end{Bmatrix} + z \begin{Bmatrix} -\frac{\partial^2 w}{\partial x^2} \\ -\frac{\partial^2 w}{\partial y^2} \\ -2\frac{\partial^2 w}{\partial x \partial y} \end{Bmatrix} \qquad \text{(II.24).}$$

Furthermore the center line strains and curvature can be defined as

$$\begin{Bmatrix} \varepsilon_x^0 \\ \varepsilon_y^0 \\ \gamma_{xy}^0 \end{Bmatrix} = \begin{Bmatrix} \frac{\partial u_0}{\partial x} \\ \frac{\partial v_0}{\partial y} \\ \frac{\partial v_0}{\partial x} + \frac{\partial u_0}{\partial v} \end{Bmatrix} \qquad \text{(II.25)}$$

and

$$\begin{Bmatrix} \kappa_x \\ \kappa_y \\ \kappa_{xy} \end{Bmatrix} = z \begin{Bmatrix} -\dfrac{\partial^2 w}{\partial x^2} \\ -\dfrac{\partial^2 w}{\partial y^2} \\ -2\dfrac{\partial^2 w}{\partial x \partial y} \end{Bmatrix} \tag{II.26}.$$

Finally, by substituting equation II.26 and II.25 into II.24, the strains can be written as

$$\begin{Bmatrix} \varepsilon_x \\ \varepsilon_y \\ \gamma_{xy} \end{Bmatrix} = \begin{Bmatrix} \varepsilon_x^0 \\ \varepsilon_y^0 \\ \gamma_{xy}^0 \end{Bmatrix} + z \begin{Bmatrix} \kappa_x \\ \kappa_y \\ \kappa_{xy} \end{Bmatrix} \tag{II.27}.$$

After strains-center line strains and curvatures relationship has been found, stress-force and moment relationship need to be found too. Figure 2.1 show the notation for location of ply interfaces. Based on the same figure, the relation between stress of each ply and the total force and the total moment can be derived as

$$\begin{Bmatrix} N_x \\ N_y \\ N_{xy} \end{Bmatrix} = \sum_{k=1}^{N} \int_{h_{k-1}}^{h_k} \begin{Bmatrix} \sigma_x \\ \sigma_y \\ \tau_{xy} \end{Bmatrix} dz \tag{II.28}$$

and

$$\begin{Bmatrix} M_x \\ M_y \\ M_{xy} \end{Bmatrix} = \sum_{k=1}^{N} \int_{h_{k-1}}^{h_k} \begin{Bmatrix} \sigma_x \\ \sigma_y \\ \tau_{xy} \end{Bmatrix} z dz \tag{II.29}.$$

Finally the last step, the relation between total force and moment with strains need to be found. This relation is well known as *A*, *B* and *D* matrices. To get this relationship, first we need substitute equation II.20 into equation II.28 and II.29, thus the result can be written as

$$\begin{Bmatrix} N_x \\ N_y \\ N_{xy} \end{Bmatrix} = \sum_{k=1}^{N} \int_{h_{k-1}}^{h_k} \overline{Q_k} \begin{Bmatrix} \varepsilon_x \\ \varepsilon_y \\ \gamma_{xy} \end{Bmatrix} dz = \sum_{k=1}^{N} \int_{h_{k-1}}^{h_k} \overline{Q_k} \begin{Bmatrix} \varepsilon_x^0 \\ \varepsilon_y^0 \\ \gamma_{xy}^0 \end{Bmatrix} dz + \sum_{k=1}^{N} \int_{h_{k-1}}^{h_k} \overline{Q_k} \begin{Bmatrix} \kappa_x \\ \kappa_y \\ \kappa_{xy} \end{Bmatrix} z dz \tag{II.30}$$

and

$$\begin{Bmatrix} M_x \\ M_y \\ M_{xy} \end{Bmatrix} = \sum_{k=1}^{N} \int_{h_{k-1}}^{h_k} \overline{Q_k} \begin{Bmatrix} \varepsilon_x \\ \varepsilon_y \\ \gamma_{xy} \end{Bmatrix} z dz = \sum_{k=1}^{N} \int_{h_{k-1}}^{h_k} \overline{Q_k} \begin{Bmatrix} \varepsilon_x^0 \\ \varepsilon_y^0 \\ \gamma_{xy}^0 \end{Bmatrix} z dz + \sum_{k=1}^{N} \int_{h_{k-1}}^{h_k} \overline{Q_k} \begin{Bmatrix} \kappa_x \\ \kappa_y \\ \kappa_{xy} \end{Bmatrix} z^2 dz \tag{II.31}.$$

Because constant material properties can be assumed over each ply, so

$$\int_{h_{k-1}}^{h_k} dz = h_k - h_{k-1}$$

$$\int_{h_{k-1}}^{h_k} z dz = \frac{h_k^2 - h_{k-1}^2}{2} \qquad \text{(II.32).}$$

$$\int_{h_{k-1}}^{h_k} z^2 dz = \frac{h_k^3 - h_{k-1}^3}{3}$$

Finally, we can write the relation of force and moment with strains and curvature as

$$\begin{Bmatrix} N \\ M \end{Bmatrix} = \begin{bmatrix} A & B \\ B & D \end{bmatrix} \begin{Bmatrix} \varepsilon^0 \\ \kappa \end{Bmatrix} \qquad \text{(II.33)}$$

where

$$A_{ij} = \sum_{k=1}^{N} \left(\overline{Q_{ij}}\right)_k (h_k - h_{k-1})$$

$$B_{ij} = \sum_{k=1}^{N} \left(\overline{Q_{ij}}\right)_k \frac{h_k^2 - h_{k-1}^2}{2} \qquad \text{(II.34).}$$

$$D_{ij} = \sum_{k=1}^{N} \left(\overline{Q_{ij}}\right)_k \frac{h_k^3 - h_{k-1}^3}{3}$$